The Dissertation Committee for Chu Ong Ting
certifies that this is the approved version of the following dissertation:

Suppression of Radiation Damping in Electromagnetic Waveguide, Signature of Quantum Decoherence in the Field Bath

Committee:

Ilya Prigogine, Supervisor

Tomio Petrosky, Supervisor

George Sudarshan

Linda Reichl

Dean Driebe

Roger Broucke

Suppression of Radiation Damping in Electromagnetic Waveguide, Signature of Quantum Decoherence in the Field Bath

by

Chu Ong Ting, B.S.

DISSERTATION

Presented to the Faculty of the Graduate School of

The University of Texas at Austin

in Partial Fulfillment

of the Requirements

for the Degree of

DOCTOR OF PHILOSOPHY

THE UNIVERSITY OF TEXAS AT AUSTIN

May 2003

This dissertation is dedicated to my Lord and Savior, Jesus Christ,
for whose glory are all things, to my wife for her help and encouragement,
to my little son, for his heavenly given smiles and to my parents,
brother and sisters, who define the meaning of a family.

Acknowledgments

I would like to thank Prof. Prigogine and Dr. Petrosky for their continuous interest, encouragement and help in this work, especially Dr. Petrosky has been teaching me things more than Physics itself. I would also like to thank Dr. Driebe who first introduced me to the world of physics research in non-equilibrium statistical dynamics. I am gratitude to Prof. Sudarshan , and Prof. Broucke for giving me many nice comments on this work. Of course I also thank all my committee members for their generous encouragement, and patience.

I owe a debt to all the members of the Center for Studies in Statistical mechanics and Complex Systems, who create such a great pleasure for me to work with them together. Especially thanks go to Dr. G. Ordonez, Dr. S. Kim, and Mr. B. A. Tay who helped me on many technical problems. I am grateful to our secretary, Annie Harding for helping me on countless tedious paperwork.

Finally, I give thanks to all my coworkers at Austin Chinese Christian Campus Fellowship who have always been supportive to me and refreshing my spiritual life. Among those I would like to mention Pastor Hsu and Haymama for their unconditional loves to the students.

Suppression of Radiation Damping in Electromagnetic Waveguide, Signature of Quantum Decoherence in the Field Bath

Publication No. _____

Chu Ong Ting, Ph.D.
The University of Texas at Austin, 2003

Supervisors: Ilya Prigogine
Tomio Petrosky

Recent development of spectral analysis of the Liouville-von Neumann equation has revealed the fact that irreversibility is a rigorous dynamical property of Poincaré non-integrable systems with an infinite degrees of freedom interacting among each other through resonance coupling. In the present work we discuss this role of resonance in some examples of matter-field coupling systems for both classical and quantum mechanics: the one is a classical motion of a charged particle in electromagnetic waveguide, and the other is the decoherence problem of quantum matter-field interacting systems.

In the first part of this dissertation, we study an accelerated motion of a charged classical dipole molecule with frequency ω_1 inside the rectangular waveguide. If the particle is in free space, it is well known that its accelerated motion will eventually stop by radiating the field through the resonance interaction. This result is the so-called radiation damping. For the case in the waveguide, there are two possible situations, due to the existence of the cut-off frequency ω_c of the waveguide. Under the cut-off frequency electromagnetic wave cannot propagate inside the

waveguide. The stability of the dipole depends on the relation between ω_1 and ω_c. For $\omega_1 < \omega_c$, the dipole cannot resonate with the field. This corresponds to the Poincaré integrable system. For this case the dipole keeps its accelerated motion without emitting the radiating field. Therefore the radiation damping of the dipole molecules is suppressed inside the waveguide under the absence of resonance interaction. The motion of this steady state somewhat resembles a quantum ground state. We show that this steady state is dressed by electromagnetic field. The overlap of the dressing field leads to a force analogous to van der Waals force in quantum mechanics. The critical frequency determined by $\omega_1 = \omega_c$ gives a critical size of the waveguide. For heavy molecules, such as HCl, this is of order 10^{-5}m. We show that the size of the dressing field is the same order of the size of the waveguide. Hence we have a macroscopic size of the dressing in the waveguide.

For $\omega_1 > \omega_c$, the dipole can resonate with the field, and the system becomes non-integrable in the sense of Poincaré. As a result, the accelerated motion eventually stop by emitting the resonance field. This corresponds to the problem of classical radiation damping. We show that there is non-negligible deviation of exponential decay in a short time scale of the order $t \sim 1/\omega_1$. This corresponds to the quantum Zeno effect, well known in quantum unstable systems. After this period, the dipole decays exponentially in time by emitting the resonance field. We found by choosing ω_c very close to ω_1, we can increase the decay rate 10^5 times faster than the case where the dipole is in the free space, at the same time the emitted field travel 10^{-4} times slower than the speed of light. This is again a consequence of the existence of the cut-off frequency in the waveguide. Indeed, the cut-off frequency leads to a non-linear dispersion relation for the electromagnetic field. To some extent, the electromagnetic field is sticky inside the waveguide. Due to the large decay rate and slower speed of light, the size of the wavepacket emitted by the dipole is

significantly small (about 10cm for HCl). This is even smaller than the quantum case in free space, where the wavepacket of the field emitted by the decay of electron in hydrogen atom is about 1m.

In the second part of this dissertation, we study a quantum matter-field coupled system. We focus our attention on the problem of quantum decoherence in a system of a particle coupled with a field, the Hamiltonian of which has a similar structure to the problem of classical radiation damping mentioned above.

We apply the complex spectral representation of the Liouville-von Neumann operator that gives a rigorous approach to the irreversible processes. We focus our attention on the time evolution of the field, which is commonly neglected in phenomenological approaches to the decoherence problem. We found a signature of decoherence in the field which has a characteristic time dependence proportional to t that comes from the secular effect between the particle and the field through the resonance interaction that breaks time-symmetry.

Table of Contents

List of Tables

List of Figures

Chapter 1

Introduction

The fundamental laws of dynamics, be they classical or quantum are time reversible. However the experience in our daily life tells us that almost all of the realities are time irreversible. These could be either microscopic such as the spontaneous emission of excited atom, or macroscopic such as self-organization of the biological cell to the evolution of the universe. In fact the irreversibility phenomena has been widely studied in diverse fields, see [1], [2].

It is important to understand the origin of these irreversible phenomena from the fundamental dynamical point of view. In this dissertation we shall limit our scopes of studies of irreversibility within the framework of the microscopic dynamics.

The essential ingredient of irreversibility is the existence of the continuous spectrum in the Hamiltonian and the resonance interaction. For example, let us consider a matter-field interacting system where a discrete spectrum ω_1 of the matter coupled with the continuous spectrum $\omega_{\mathbf{k}}$ of the field, with a coupling constant λ. In the perturbation series which attempts to diagonalize the Hamiltonian, one encounters a diverging denominator, such as $1/(\omega_{\mathbf{k}} - \omega_1)$ (so-called small denominator problem) at the resonance point $\omega_{\mathbf{k}} = \omega_1$. According to the Poincaré theorem [3], [4], it is impossible to obtain the invariants of motion which are analytic in term of λ at λ=0. This leads to the Poincaré definition of non-integrable systems, where the invariants of motion are destroyed due to the resonance interaction.

In this dissertation we shall study this essential role played by resonance in

the matter-field interaction of both classical and quantum systems. We shall concentrate two interesting subjects, classical radiation damping in the electromagnetic waveguide and quantum decoherence. As we shall see later this two apparently different problems may be described by the a common type of Hamiltonian, that is the Friedrichs model with resonance interaction which has been well investigated in quantum mechanics [5–10].

In the classical regime, we study the problem of classical radiation damping of a dipole inside the rectangular electromagnetic waveguide. The traditional approach to this problem presented in the literatures [11], [12] gives us the time irreversible equation for the radiation damping such as the well-known Lorentz-Abraham equation. However it leads to well-known unphysical phenomena such as self-accelerated and pre-accelerated solutions. To derive the Lorentz-Abraham equation, the reaction of field to the particle has not been consistently taken into account in the Larmor formula [11]. The difficulty comes from the fact that the perturbative approach to deal with the reaction process is impossible since the system is non-integrable in the sense of Poincaré.

The resonance singularity appears when the frequency of the particle coincides with the spectrum of the field. This degeneracy can be removed if the spectrum of the field is discrete. This is the case when the particle is located inside a closed cavity with perfect reflective walls of the field. For this case the system is integrable, and the particle may keep its accelerated motion inside the cavity. This may be understood as the field bouncing back and forth inside the cavity may re-excite the particle. In contrast if the particle is located in open space without boundaries, the spectrum of the field is continuous. Then the system is non-integrable. The resonance effects coming from the degeneracy of the frequencies of the particle and the field leads to a physical effect as a damping of accelerated motion of the particle

(the radiation damping). Then the particle eventually stop by emitting the field.

The advantage of the Friedrich type of the Hamiltonian system which we shall consider here is that we can diagonalize the Hamiltonian without using any approximation. As a result, we can deal with the reaction process mentioned above, even the system is non-integrable. As we shall see, there is no self-accelerated solution, and the evolution is causal in our solution.

In this of dissertation we shall present in some sense an intermediate situation between the closed cavity and the entirely open space. We shall consider the situation where a classical dipole is located inside a rectangular waveguide with two open ends in z direction and boundary walls in x and y direction (see Figure 2.1).

Due to the reflecting walls, we have infinite branches of continuous spectrum each of which has lower bound given by the boundary conditions. These lower bound frequencies are known as the "cut-off" frequencies, below which the field cannot propagate inside the waveguide [11]. Suppose the frequency ω_1 of the dipole is below the lowest frequency ω_c among the cut-off frequencies, then the dipole cannot resonate since the denominator $\omega_{\mathbf{k}} - \omega_1 \geq \omega_c - \omega_1 > 0$ never vanishes. Hence we have an integrable system. In spite of the fact that the waveguide has open ends, the dipole may keep its accelerated motion without emitting the resonance field. In other words, there is a suppression of radiation damping. This situation is somewhat resemblance to a quantum ground state.

On the contrary if $\omega_1 > \omega_c$ in such a way that the discrete spectrum ω_1 of the dipole is embedded inside the continuum far enough from the critical frequency ω_c, then the system becomes non-integrable, and the accelerated motion eventually stop by emitting the resonance field.

Therefore the motion of a charged particle inside the waveguide has an interesting parallelism to the quantum stable and unstable atom system. Thanks to

this parallelism, one may expect that many interesting concepts established in the problem of the stable and unstable atom in quantum mechanics such as the dressing of the field around the ground state, and spontaneous emission of the field from excited particles may be applicable to analyze our classical matter-field coupling system. We shall show indeed this will be the case. For example, the quantum ground state of the atom is dressed by a photon cloud. The overlap of this photon cloud leads to van der Waals force. In our classical system at integrable case, we shall show the stable steady state is dressed by classical electromagnetic field. The overlap of the dressing field leads to a classical force which is analogous to van der Waals force in quantum mechanics. The dressing field has the same size as the waveguide. For the case where the size $b \sim 10^{-5}$m as shown in Figure 2.1, the size of the dressing field is about 10^4 larger than the classical dipole itself. Therefore it leads to macroscopically long range force.

For the classical unstable case, we shall show that there are also many parallelism to quantum unstable case. For the unstable atom in quantum mechanics, it is well known that the time evolution consists of three different periods [13]. In a short time period, we have a deviation of the exponential decay of the excited bare state (i.e., the well-known quantum Zeno process [14], which is a non-Markovian process associated with a memory effect to the initial condition). In the intermediate time period, the Markovian process described by the exponential decay dominates. In the long time period, we have again the deviation from the exponential decay (the so-called long-time tail). We shall show in our classical system with non-integrable case, the radiation damping of the dipole also carries these features. As far as the author knows, these deviation from the exponential decay in classical systems has not been explicitly studied in the traditional approach of radiation damping [11], [12].

For the exponential decay, the decay process in classical system in the free space is known to be extremely slow compared with that in quantum systems. For example, a classical HCl dipole decays in 10^{-2}s while the spontaneous decay of electron in hydrogen atom is 10^{-9}s. However inside the waveguide, we are able to increase the decay rate γ of classical radiation damping. For example, we can make γ 10^5 faster than that in the free space for a suitable choice of the geometry and the size of the waveguide. It turns out the decay time of HCl dipole inside the waveguide can be reduced to 10^{-7}s which is much closer to the quantum regime. Therefore the waveguide can act in both ways that either suppresses the damping, or enhances it. There is another remarkable effect due to the waveguide. Since the the emitted resonance field carries an effective mass, we can reduce the the group velocity 10^4 slower than the speed of light, again with a suitable size of the waveguide. As a result, the wavepacket of emitted resonance field become about 10cm for HCl dipole. This is surprisingly shorter than the quantum case, where the wavelength of the field emitted by the decay of electron in hydrogen atom in free space is about 1m.

It is relatively easier to realize all these interesting phenomena in classical regime than in quantum regime. As we shall show the critical size of the waveguide for the stability of motion for classical dipole such as HCl, is about $b_c \equiv \pi c/\omega_1 \sim 10^{-5}$m. This is much larger than the quantum case of lighter mass electrons in atom, which is $b_c \sim 10^{-7}$m. Modern nano-technology may allows to build such moderately large size of waveguide for classical systems.

In the second part of this dissertation, we shall discuss quantum matter-field interacting systems. The system we consider here is the quantum version of Friedrichs model. Comparing with the classical Friedrichs model considered in the first part of our dissertation, there is no the case of classical radiation damping inside the waveguide, there is no boundary of walls here. Therefore the discrete

spectrum is always embedded in the continuous spectrum, i.e. the system is always non-integrable due to the resonance.

This type of system has been repeatedly analyzed in the context of quantum decoherence [15–19]. However all these arguments have a common phenomenological element, namely the field surrounding the particle has already in thermal equilibrium. Moreover, all assumed that the field as a thermal bath is so large that one can neglect the time evolution of the field.

This hypothesis is correct as far as we are interested in the non-local quantities, such as the distribution of the energy in each mode. However if we are interested in the local quantities such as the spatial structure of the dressing cloud which surrounds the particle, we can not neglect the time evolution of the field. Indeed we have shown in Figure 5.4 that there is a non-negligible dressing cloud of field appears around the particle as well as a non-negligible propagation of the field that does not die out in time.

To study the evolution of the system, we use the complex spectral representation of the Liouville-von Neumann operator for density matrices outside the Hilbert space. In those quantum system with broken time symmetry such as unstable particle, the need to extend the wave function outside the Hilbert space was recognized some years ago by various physicists and mathematicians including Sudarshan, Chiu and Gorini [20], Böhm and Gadella [21], and Kumicak and Brändas [22]. The physical motivation was to include the decaying state as an uniquely specified object in the spectral decomposition of the Hamiltonian.

However, to analyze the quantum decoherence, not only we have to go outside Hilbert space, but also turn ourselves to the density matrix description. Since our formulation is based on exact dynamics without any phenomenological assumption, we are able to start from arbitrary initial conditions including the case in which

surrounding field is far from equilibrium. Indeed we show the decoherence for both the particle and the field starting with a pure state of the whole system.

For a weakly coupled case we derive the Pauli type of master equation which breaks time symmetry. We then obtain the relaxation time which gives an estimation of the decoherence time scale of the particle. We also show there is a secular term appeared in the time evolution of the field. Under the thermodynamic limit, we show this non-negligible resonance effect leads to the decoherence in the field. As far as authors' knowledge, the decoherence of the field had not been discussed before.

We point out the decoherence time scale obtained under $\lambda^2 t$ approximation should be bounded below by the time scale of memory effect. We then go beyond the $\lambda^2 t$ approximation to calculate the memory effect. By applying this correction to the Markov approximation, we show the prediction of quantum Zeno effect in our theory [23], [24]. We want to emphasize that estimation of contributions from the memory effect is still a controversial subject. Our complex spectral representation of the Liouvillian offers a systematic way to calculate the contribution from memory effect.

This dissertation is organized as follows. We first explore the resonance effect in a classical system, which is a dipole molecule inside a rectangular waveguide. In Chapter 2, we explicitly specify our system and show the Hamiltonian could be mapped into classical Friedrichs model. We then analyze the stability condition of the motion of the particle. This is based on the location of the discrete spectrum with respect to the continuous spectrum. It turns out there are two possible outcomes, stable and unstable.

In Chapter 3 we study the integrable case. We diagonalize the Hamiltonian using the Bogoliubov transformation, which gives us a set of new normal modes for particle and field. We show the new normal modes of particle consists of the

non-vanished accelerated motion of the dipole and the electromagnetic dressing. We then investigate the structure of the dressing and the transition from the bare dipole to this dressed steady state. The classical van der Waals force due to the overlapped dressings of two dipole molecules is studied in the last section.

In Chapter 4, we study the non-integrable case. In this case we show on the level of diagonalization of Hamiltonian that there is no new normal mode for the particle. Therefore we lose the one-to-one correspondence between the perturbed spectrum and unperturbed spectrum according to Poincaré resonance. We show the accelerated motion will stop due to the resonance effect. With the careful separation of the pole contribution and the branch point contribution, we show that the pole contribution gives exponential decay while the branch point contribution gives power law decay. In the very short time scale, we show our result recovers the Zeno effect which had not been considered in traditional approach of classical radiation damping. We then analyze the emitted field, and found there exists a resonance field which is absent in the integrable case.

In Chapter 5 we study the problem of quantum decoherence in the terms of density matrices. The time evolution of the density matrix is governed by the Liouville-von Neumann equation. We then apply the complex spectral representation of the Liouville-von Neumann operator to this problem. We first obtain the Pauli type of master equation which breaks time symmetry under Markovian approximation ($\lambda^2 t$). Later we calculate the non-Markovian contribution and show the recovery of quantum Zeno effect by going beyond this $\lambda^2 t$ approximation. In the last section we compare our theoretical predictions with the numerical simulation.

Part I

Suppression of Radiation Damping in Electromagnetic Waveguide

Chapter 2

Hamiltonian of the waveguide

2.1 Motivation

In the first part of this dissertation we shall study a motion of classical dipole molecule interacting with electromagnetic field inside the waveguide. This leads to the problem of classical radiation damping.

The traditional approach of studying matter-field interaction is solving approximately the coupled Maxwell equations and the Lorentz equation. One tries to obtain a closed equation of motion by decoupled this set of differential equations under various approximation schemes. This leads to the well-known Lorentz-Abraham equation which gives the irreversible damping motion of the particle [11].

However, it is well known the Lorentz-Abraham equation has many unphysical aspects such as self-accelerated and pre-accelerated solutions, due to the approximations made in the derivation of such a broken time symmetry equation from time reversible theory. It also shows a strictly exponential decay of the canonical variable associated to the unstable particle, which contradicts the exact equations of motion. In quantum mechanics, the deviation from purely exponential decay is especially significant in a short time scale (the so-called "quantum Zeno" period [14]). The corresponding Zeno period also exists in classical unstable systems. There have been several attempts to improve the classical Lorentz-Abraham equation [25], [26], however all results have failed to predict the existence of the Zeno period.

The difficulties of this problem come from the fact that this matter-field

interacting system is generally non-integrable in the sense of Poincaré, due to the resonance denominators. When the frequency spectrum of the matter is embedded in the continuous spectrum of the field, there appears division by zero in the formal solutions. Hence to deal with the problem of radiation damping, we have to consistently take care of this resonance singularity.

In the following we shall give an brief overview of our approach of this problem. Our basic idea of solving this problem is to employ the well-established formalism in quantum mechanics for the spontaneous emission of excited atoms. As we shall show in coming section that the Hamiltonian could be reduced to classical version of Friedrichs model which describes a particle(dipole molecule) with a discrete spectrum coupled bi-linearly with the field with continuous spectrum. This is an exact soluble model that could be diagonalized by Bogoliubov transformation.

The stability of the particle is determined by the location of its spectrum ω_1 with respect to the continuous spectrum. For the case the discrete spectrum is outside the continuum there is no resonance. We have a set of perturbed normal modes for the particle and the field, and the motion of particle remains. On the contrary, if the discrete spectrum is embedded within the continuum, then the perturbed normal mode of particle is destroyed by the existence of resonance and the motion of particle ceases. Due to the boundary effect of the waveguide, we have the continuous spectrum bounded below by a non-zero, positive cut-off frequency $\omega_c \propto 1/b$ where b is the size[1] of the rectangular waveguide. The critical size of the waveguide b_c is defined as the largest size of the waveguide such that the motion of the particle is stable, i.e. $b_c = \pi c/\omega_1$ from the stability condition. The oscillation frequency of the dipole molecules is fixed by nature, which is generally in the range

[1]More precisely, it is the height of the waveguide due to our assumption made later that height is greater than the width

of $10^{13} - 10^{14}$Hz. Therefore we have the corresponding critical size of the waveguide $b_c \sim 10^{-5} - 10^{-4}$m which could be easily produced by current technology. .

As we will see in Chapter 3, there are many new elements which had only been previously realized in the quantum system, appears in our classical waveguide because of the existence of perturbed normal mode, which is essentially a dressed stable state in classical regime. Moreover we see in Chapter 4 that the description of radiation damping based on our approach does not have any unphysical solutions. In contrast to the traditional approach our result is valid at all times. We not only have exponential decay component in the unstable particle, but also have the deviation of exponential decay during the very short Zeno period and the very long time tail period, which is consistent with the dynamics.

Since the size of the waveguide is feasible under current technology, it should be possible to realize our theoretical result in the real experiment.

2.2 Mapping to the Friedrichs model

In this section we shall explicitly formulate the Hamiltonian of a dipole molecule inside a rectangular waveguide. As we shall see, the Hamiltonian could be mapped into a generalized version of the Friedrichs model originally introduced in quantum mechanics. This model has been used extensively in the literature [27] for studying the matter-field interacting system.

In the first part of this dissertation we restrict our interest to the classical version of this model. We shall later discuss about the differences between quantum and classical version of this model and its interpretation.

We consider a classical dipoles located inside a rectangular electromagnetic waveguide. Figure 2.1 gives an illustration of our system. The waveguide lies along

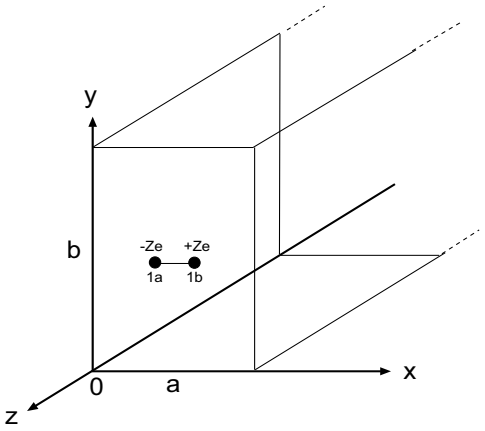

Figure 2.1: The illustration of our Hamiltonian system, which is a dipole in a rectangular waveguide made of perfect conductor. The width of the waveguide is a and the height is b with the restriction $b > a$. We assume the length $L \gg b > a$ such that "fringing effect" is ignored.

the z axis, with the length L is much more greater than the width a and the height b, therefore the "fringing effect" is neglected inside the waveguide under this consideration. Without loss of generality we assume the $b > a$. To avoid unnecessary complication we assume the waveguide is a perfect conductor that there is no energy loss through the walls. The dipole molecule consists of two opposite charged atoms

Table 2.1: Molecular processes and corresponding electromagnetic spectrums

Types of motion	Energy/Molecule(eV)	Frequency(Hz)
Rotation of polyatomic molecule	$4 \times 10^{-6} \sim 4 \times 10^{-4}$	$10^{9} \sim 10^{11}$
Rotation of small molecule	$4 \times 10^{-4} \sim 4 \times 10^{-2}$	$10^{11} \sim 10^{13}$
Vibration of flexible bond	$4 \times 10^{-2} \sim 4 \times 10^{-1}$	$10^{13} \sim 10^{14}$
Electronic transition	$4 \times 10^{-1} \sim 4 \times 10^{1}$	$10^{14} \sim 10^{16}$

located at r_a $(-Ze)$and r_b $(+Ze)$ respectively. In general these dipole molecules could have different types of motion based on their excitation energy. In Table 2.1 [28] we show some possible motions of several common molecules and their corre-

sponding excitation energies and frequencies. The last column denotes the domain of the frequency associated with the motion. Here we are especially interested in the vibration regime where the dipole molecules could be treated as a simple harmonic oscillator with the oscillation frequency ω_1 falls in the range $10^{13} \sim 10^{14}$Hz. To have better physical idea of the dipole molecules we are referring to, we shows several possibilities of the dipole molecules and their vibration frequencies in Table 2.2 [28]. We consider the vibration amplitude is the same order as the molecule size, i.e., 1nm. In this case, the actions correspond to these heavy molecules are $10^3 - 10^4\hbar$, which fall in the regime of classical mechanics. Under these considerations, the total

Table 2.2: The vibrational frequencies of diatomic molecules

Molecules	Frequency (Hz)	Critical Size b_c (m)
HCl	8.64×10^{13}	1.09×10^{-5}
CO	6.48×10^{13}	1.45×10^{-5}
NaCl	1.10×10^{13}	8.58×10^{-5}
KBr	8.73×10^{12}	1.08×10^{-4}

Hamiltonian of our system is given by

$$\begin{aligned} H &= \frac{1}{2m_a}\left(\mathbf{p}_a + Ze\frac{\mathbf{A}(\mathbf{r}_a)}{c}\right)^2 + \frac{1}{2m_b}\left(\mathbf{p}_b - Ze\frac{\mathbf{A}(\mathbf{r}_b)}{c}\right)^2 + \frac{1}{2}\mu_1\omega_1^2|\mathbf{r_b} - \mathbf{r_a}|^2 \\ &\quad + \frac{1}{8\pi}\int d^3r\left(\frac{1}{c^2}\left|\frac{\partial\mathbf{A}(\mathbf{r})}{\partial t}\right|^2 + |\vec{\bigtriangledown} \times \mathbf{A}(\mathbf{r})|^2\right) \end{aligned} \tag{2-1}$$

with the reduced mass $\mu_1 = m_a m_b/(m_a + m_b)$. Here we use the boldface for vectors. The expansion of the first two terms at the right hand side of Eq. (2-1) gives the kinetic energy of the dipole, the interaction between the dipole and the field, and the direct field-field interaction. The waveguide boundary effect is contained in the form of the vector potential which we shall show in Eq. (2-10), and Eq. (2-11). The complete set of canonical conjugate pairs of variables in this system are

$(\mathbf{p}_a, \mathbf{r}_a)$, $(\mathbf{p}_b, \mathbf{r}_b)$, and $(\mathbf{A}(\mathbf{r}), \partial\mathbf{A}(\mathbf{r})/\partial t)$. By introducing the new canonical pairs for the dipole,

$$\begin{aligned}
\mathbf{R}_1 &= \frac{m_a\mathbf{r}_a + m_b\mathbf{r}_b}{m_a + m_b} && (2\text{-}2)\\
\mathbf{P}_1 &= \mathbf{p}_a + \mathbf{p}_b && (2\text{-}3)\\
\mathbf{r}_1 &= \mathbf{r}_b - \mathbf{r}_a && (2\text{-}4)\\
\mathbf{p}_1 &= \mu\left(\frac{\mathbf{p}_b}{m_b} - \frac{\mathbf{p}_a}{m_a}\right) && (2\text{-}5)
\end{aligned}$$

We rewrite the Hamiltonian in terms of these new variables

$$\begin{aligned}
H &= \frac{\mathbf{P}_1^2}{2M} + \frac{\mathbf{p}_1^2}{2\mu_1} + \frac{1}{2}\omega_1^2\mathbf{r}_1^2 + \frac{1}{8\pi}\int d^3r\left(\frac{1}{c^2}\left|\frac{\partial\mathbf{A}(\mathbf{r})}{\partial t}\right|^2 + |\vec{\bigtriangledown}\times\mathbf{A}(\mathbf{r})|^2\right)\\
&\quad -\frac{Ze}{\mu_1 c}\mathbf{p_1}\cdot\mathbf{A}(\mathbf{R}) + \frac{Z^2e^2}{2\mu_1 c^2}\mathbf{A}^2(\mathbf{R}) \qquad (2\text{-}6)
\end{aligned}$$

with the total mass of the dipole $M \equiv m_a + m_b$. In the above expression, we have applied the so-called "dipole approximation" that approximate the field acting on the center of mass of the dipole. As far as we are interested in the scale which is much greater than the size of the dipole molecule, this approximation gives reliable result [29].

We assume that the dipole molecule is initially located at the center of the waveguide. Moreover we shall drop the motion of center of mass under the hypothesis that the forces acting on the center of mass $\mathbf{R}_1$ are negligible. In Section 3.4 we shall show that this hypothesis gives a good approximation. The field-field interaction is in the order of $O(e^2/\mu_1 c^2)$, which will be neglected as it is a higher order term compared with the dipole-field interaction.

In general, Hamiltonian in Eq. (2-6) generates a nonlinear set of equations of motion due to the rotational motion of the dipole molecule. One can eliminate this nonlinearity by restricting our interest to a special class of initial conditions, that the

dipole oscillates parallel to one the walls of the waveguide. Under this restriction, the rotation mode of the dipole will never be excited due to the geometrical symmetry of the system. The great advantage of this setting is that the Hamiltonian is reduced to a bi-linear form which is exactly solvable. As we shall see, we find many non-trivial results even under this restricted setting.

In the following we consider the case where the dipole oscillates in x direction (thus $\mathbf{r}_1$ becomes x_1). The extension to other directions is straightforward. Let us introduce the unperturbed normal coordinate of the dipoles defined by

$$q_1 = \sqrt{\frac{\mu\omega_1}{2}}(x_1 + i\frac{p_1}{\mu\omega_1}) \tag{2-7}$$

The inverse transformation is given by

$$x_1 = \sqrt{\frac{1}{2\mu_1\omega_1}}(q_1 + q_1^*) \quad , \quad p_1 = -i\sqrt{\frac{\mu_1\omega_1}{2}}(q_1 - q_1^*) \tag{2-8}$$

For electromagnetic field in the waveguide, it is well-known that the vector potential can be decomposed into TE modes (Transverse Electric field modes) and TM modes (Transverse Magnetic field modes), i.e. $\mathbf{A}(\mathbf{r},t) = \mathbf{A}_{TE}(\mathbf{r},t) + \mathbf{A}_{TM}(\mathbf{r},t)$ [11]. By solving the sourceless Maxwell equations inside the rectangular waveguide with subjected to the the boundary conditions on a perfect conductor and by choosing the Coulomb gauge, we obtain the explicit form of the vector potential written in these orthogonal basis

$$\begin{aligned}
\mathbf{A}_{TE}(\mathbf{r},t) &= \int' d\mathbf{k}\sqrt{\frac{2\Delta_{mn}}{\pi^2 c}}\frac{C_{mn}}{\sqrt{\omega_{\mathbf{k}}}}\left[-\frac{n\pi}{b}W_{1,mn}(\mathbf{r})\hat{e}_x + \frac{m\pi}{a}W_{2,mn}(\mathbf{r})\hat{e}_y\right] && \text{(2-9)}\\
&\quad \times q_{E,\mathbf{k}}(t)e^{ikz} + c.c && \text{(2-10)}
\end{aligned}$$

$$\begin{aligned}
\mathbf{A}_{TM}(\mathbf{r},t) &= \int' d\mathbf{k}\sqrt{\frac{2c}{\pi^2}}\frac{C_{mn}}{\sqrt{\omega_{\mathbf{k}}^3}}\left[i\frac{km\pi}{a}W_{1,mn}(\mathbf{r})\hat{e}_x + i\frac{kn\pi}{b}W_{2,mn}(\mathbf{r})\hat{e}_y\right.\\
&\quad \left. + \alpha_{mn}^2 W_{3,mn}(\mathbf{r})\hat{e}_z\right] q_{M,\mathbf{k}}(t)e^{ikz} + c.c && \text{(2-11)}
\end{aligned}$$

with the constant factor Δ_{mn} and C_{mn} defined as

$$\Delta_{mn} = \begin{cases} 1 & m, n \neq 0 \\ \frac{1}{2} & \min(m, n) = 0 \end{cases} \tag{2-12}$$

$$C_{mn} = \sqrt{\frac{2\pi^2 c^3}{ab\alpha_{mn}^2}} \tag{2-13}$$

The functions $W_{i,mn}(\mathbf{r})$ depend only on x and y and are given by

$$W_{1,mn}(\mathbf{r}) = \cos(\frac{m\pi x}{a}) \sin(\frac{n\pi y}{b}) \tag{2-14a}$$

$$W_{2,mn}(\mathbf{r}) = \sin(\frac{m\pi x}{a}) \cos(\frac{n\pi y}{b}) \tag{2-14b}$$

$$W_{3,mn}(\mathbf{r}) = \sin(\frac{m\pi x}{a}) \sin(\frac{n\pi y}{b}) \tag{2-14c}$$

$$\tag{2-14d}$$

The dispersion relation is given by

$$\omega_{\mathbf{k}} = c\sqrt{\alpha_{mn}^2 + k^2} \tag{2-15}$$

where α_{mn} is defined by

$$\alpha_{mn} \equiv \sqrt{\frac{m\pi}{a}^2 + \frac{n\pi}{b}^2} \tag{2-16}$$

The derivation of these orthogonal basis from is presented in Appendix A.

Here we have the vector potential expanded in TE and TM wave. The wave vector $\mathbf{k} = (\frac{m\pi}{a}, \frac{n\pi}{b}, k)$ is discrete in x and y direction due to the confinement of the waveguide. The discrete pair (m, n) ranges over all integers from 0 to ∞ excluding $\{0, 0\}$, while the k is continuous from $-\infty$ to ∞. The integration notation with prime $\int' d\mathbf{k}$ is the abbreviation of $\sum_{m,n}^{\infty} \int_{-\infty}^{\infty} dk$.

With the implementation of the complete basis of the field together with the normal coordinate of the dipole molecule in Eq. (2-7), as well as the approximations

mentioned above, we have the Hamiltonian formulated in terms of the normal modes q_α for $\alpha = \{1, (\sigma, \mathbf{k})\}$ with σ =E and M (TE and TM modes, respectively),

$$\begin{aligned} H &= H_0 + \lambda V \\ &= \omega_1 q_1^* q_1 + \sum_{\sigma=E,M} \int' d\mathbf{k} \omega_\mathbf{k} q_{\sigma,\mathbf{k}}^* q_{\sigma,\mathbf{k}} \\ &\quad + \lambda \int' d\mathbf{k} (V_{\sigma,\mathbf{k}}(\mathbf{R}) q_{\sigma,\mathbf{k}} - V_{\sigma,\mathbf{k}}^*(\mathbf{R}) q_{\sigma,\mathbf{k}}^*)(q_1 - q_1^*) \end{aligned} \tag{2-17}$$

with the dimensionless coupling constant λ defined as

$$\lambda \equiv \sqrt{\frac{(Ze)^2}{(\mu_1 c^2)(c/\omega_1)}} \tag{2-18}$$

For a typical dipole such as HCl, we have $\lambda \approx 10^{-6} \ll 1$. The interaction potential of each mode is given by

$$V_{E,\mathbf{k}}(\mathbf{R}) = -i\frac{n}{b}\sqrt{\frac{\Delta_{mn}}{\omega_\mathbf{k}}} C_{mn} W_{1,mn}(\mathbf{R}) e^{ikR_z} \tag{2-19a}$$

$$V_{M,\mathbf{k}}(\mathbf{R}) = -\frac{mck}{a\sqrt{\omega_\mathbf{k}^3}} C_{mn} W_{1,mn}(\mathbf{R}) e^{ikR_z} \tag{2-19b}$$

As a function of k, both $V_{E,\mathbf{k}}(\mathbf{R})$ and $V_{M,\mathbf{k}}(\mathbf{R})$ have the branch points at $k = \pm i\alpha_{mn}$ and there is no pole in the complex plane of k. Since our dipole oscillates in the x direction, only $W_{1,mn}(\mathbf{R})$ the x component of the vector potential $\mathbf{A}(\mathbf{r})$ is involved in the particle-field interaction. The canonical variables q_α are related to the angle-action variables (ϕ_α, J_α) through the relation $q_\alpha = \sqrt{J_\alpha} e^{i\phi_\alpha}$. They satisfy the canonical relations

$$\{q_\alpha, q_\beta^*\}_{PB} = -i\delta_{\alpha\beta} \tag{2-20}$$

$$\{q_\alpha, q_\beta\}_{PB} = 0 \tag{2-21}$$

where $\{\ ,\}_{PB}$ is the poisson bracket with respect to a set of canonical variables, and $\delta_{\alpha,\beta}$ denotes Kronecker delta for the discrete spectrum, and Dirac delta for the continuous spectrum.

Our classical Hamiltonian in Eq. (2-17) corresponds to the well-known Friedrichs model with virtual processes in quantum mechanics. We have a "particle"[2] with discrete spectrum ω_1 bi-linearly coupled with the fields whose spectrums $\omega_{\mathbf{k}}$ are continuous.

The spectrums of unperturbed Hamiltonian H_0 consist of one discrete spectrum ω_1 and infinite sets of continuous spectrums. Each (m, n) mode gives a continuous spectrum bounded from below at $c\alpha_{mn}$. These lower bound frequencies $c\alpha_{mn}$ form a set of cut-off frequencies in this waveguide in the sense that for electromagnetic wave with frequency ω_k, only those modes whose cut-off frequency $c\alpha_{mn} < \omega_k$ will propagate inside the waveguide, while the others with $c\alpha_{mn} > \omega_k$ will become evanescent wave and die out quickly. Among these branches of continuum, TE_{01} has the smallest value of the cut-off frequency, i.e.,

$$\omega_c \equiv \frac{\pi c}{b} \tag{2-22}$$

As we shall see below it corresponds to the critical frequency of our system that determines the stability of the motion. In Figure 2.2 we plot the unperturbed spectrum of our system. The horizontal axis corresponds to the frequency, starting from 0 to ∞. There are infinite branches of the continuum as (m, n) could be arbitrary large[3], but here we only show four lowest modes. The TE_{11} mode overlaps with TM_{11} mode, and the continuous spectrum is bounded below by ω_c, which corresponds to TE_{01} under the setting $b > a$.

The frequency region outside the continuous spectrum is shown by dashed line. The discrete spectrum of the particle could be either outside these continuum, or be embedded inside the continuum (but far enough from ω_c) as both are shown

[2]We shall use the words particle or dipole molecule interchangeably throughout this dissertation.
[3]For TE_{mn} wave, one of the (m, n) can be zero, while for TM_{mn} wave, both $m \neq 0$ and $n \neq 0$.

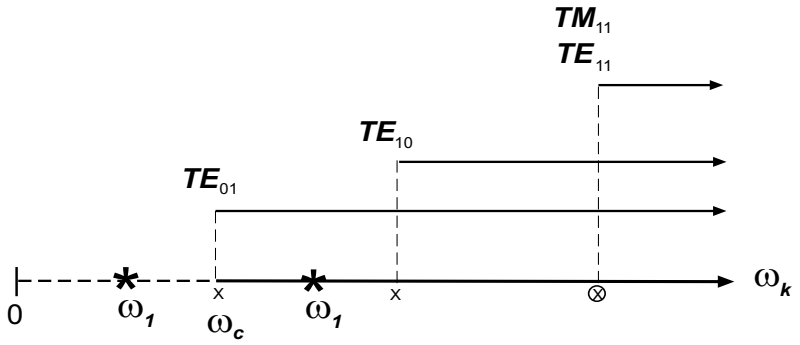

Figure 2.2: The unperturbed spectrum of the waveguide system. We show both possible locations of ω_1 in this diagram. Note $\times$ denotes the TE branches, and $\otimes$ denotes the overlapped TE and TM branches. ω_c is the lower bound of TE_{01} mode. The dashed line indicates the region which is not overlapped by continuous branches.

in Figure 2.2. The outcomes of these two possibilities are totally different that the first one ($\omega_1 < \omega_c$) leads to a stable particle oscillates with perturbed frequency and amplitude, while the latter ($\omega_1 > \omega_c$) contain the resonance between the particle and the field which leads to the decay of an unstable particle. Hence the lowest cut-off frequency ω_c acts as the critical frequency of our system which determines the stability of the particle.

Notice the oscillation frequency ω_1 (see Table 2.2) is given by nature which can not be controlled by experiment. On the other hand, the critical frequency ω_c in Eq. (2-22) is inversely proportional to the size of the waveguide b which is a control parameter in experiment. This indicates by making the size of the waveguide smaller than the wavelength correspond with the ω_1 (which is the critical size b_c shown in Table 2.2), the dipole cannot resonance with the waveguide. Hence the dipole will be stabilized and keeps its accelerated motion. This is analog to the quantum ground state.

Chapter 3

Existence of the steady motion

3.1 Diagonalization of the Hamiltonian

In this chapter we shall focus ourselves in the case $\omega_1 < \omega_c$ where the stable motion maintained. We first find a new set of dressed normal modes which diagonalize Hamiltonian.

Since our Hamiltonian in Eq. (2-17) is bi-linear, one can diagonalize as Eq. (3-1) by a linear transformation of the normal modes. This corresponds to the familiar Bogoliubov transformation in quantum mechanics. As we shall see the dressed particle mode consists of the bare particle mode dressed by electromagnetic field. We shall explicitly analyze the electromagnetic field associated with the dressed particle mode in Section 3.2.

We then investigate the time evolution of the bare particle mode and its radiated field in Section 3.3.1 and Section 3.3.2, respectively.

In Section 3.4 we calculate the force coming from the walls acting on the center of mass of the dipole molecule. we shall see that the force on the center of mass of the dipole molecule is negligible as mentioned in the previous section. This force is the result of the overlapping between dressing field and waveguide boundary. In quantum mechanics, it is called as Casimir-Polder force.

In the last section of this chapter, we investigate force due to two overlapped dressed particle modes. We first generalize our Hamiltonian of one dipole inside the waveguide to the case of two dipoles. We are interested in the integrable case where

there exists two dressed stable particle modes. Then we calculate the forces between them which is coming from overlapped dressing field. It is corresponding to the van der Waals forces in quantum mechanics.

Now let us diagonalize the Hamiltonian (2-17). By a linear transformation of the normal modes, we have

$$H = \tilde{\omega}_1 Q_1^* Q_1 + \sum_\sigma \int' d\mathbf{k}\ \omega_{\mathbf{k}} Q_{\sigma,\mathbf{k}}^* Q_{\sigma,\mathbf{k}} \tag{3-1}$$

Here the "Bogoliubov" transformation is given by,

$$\begin{aligned} Q_1 &= N_1 \left[\frac{\omega_1 + \tilde{\omega}_1}{2\omega_1} q_1 + \frac{\omega_1 - \tilde{\omega}_1}{2\omega_1} q_1^* + \lambda \sum_\sigma \int' d\mathbf{k} \left(\frac{V_{\sigma,\mathbf{k}}(\mathbf{R})}{\omega_{\mathbf{k}} - \tilde{\omega}_1} q_{\sigma',\mathbf{k}} \right.\right. \\ &\quad \left.\left. + \frac{V_{\sigma,\mathbf{k}}^*(\mathbf{R})}{\omega_{\mathbf{k}} + \tilde{\omega}_1} q_{\sigma,\mathbf{k}}^* \right) \right] \end{aligned} \tag{3-2a}$$

$$\begin{aligned} Q_{\sigma,\mathbf{k}} &= q_{\sigma,\mathbf{k}} - \frac{2\lambda\omega_1 V_{\sigma,\mathbf{k}}^*(\mathbf{R})}{\xi_1^+(\omega_{\mathbf{k}})} \left[\frac{\omega_{\mathbf{k}} + \omega_1}{2\omega_1} q_1 - \frac{\omega_{\mathbf{k}} - \omega_1}{2\omega_1} q_1^* \right. \\ &\quad \left. + \lambda \sum_{\sigma'} \int' d\mathbf{l} \left(\frac{V_{\sigma',\mathbf{l}}(\mathbf{R})}{\omega_{\mathbf{l}} - \omega_{\mathbf{k}} - i\epsilon} q_{\sigma',\mathbf{k}} + \frac{V_{\sigma',\mathbf{l}}^*(\mathbf{R})}{\omega_{\mathbf{l}} + \omega_{\mathbf{k}}} q_{\sigma',\mathbf{l}}^* \right) \right] \end{aligned} \tag{3-2b}$$

$$\begin{aligned} q_1 &= N_1 \left[\frac{\tilde{\omega}_1 + \omega_1}{2\omega_1} Q_1 + \frac{\tilde{\omega}_1 - \omega_1}{2\omega_1} Q_1^* \right] \\ &\quad - \lambda \sum_{\sigma'} \int' d\mathbf{l} \left[\frac{(\omega_{\mathbf{l}} + \omega_1) V_{\sigma',\mathbf{l}}(\mathbf{R})}{\xi_1^-(\omega_{\mathbf{l}})} Q_{\sigma',\mathbf{l}} + \frac{(\omega_{\mathbf{l}} - \omega_1) V_{\sigma',\mathbf{l}}^*(\mathbf{R})}{\xi_1^+(\omega_{\mathbf{l}})} Q_{\sigma',\mathbf{l}}^* \right] \end{aligned} \tag{3-3a}$$

$$\begin{aligned} q_{\sigma,\mathbf{k}} &= Q_{\sigma,\mathbf{k}} - \lambda N_1 V_{\sigma,\mathbf{k}}^*(\mathbf{R}) \left[\frac{Q_1}{\tilde{\omega}_1 - \omega_{\mathbf{k}}} + \frac{Q_1^*}{\tilde{\omega}_1 + \omega_{\mathbf{k}}} \right] + 2\lambda^2 \omega_1 V_{\sigma,\mathbf{k}}^*(\mathbf{R}) \\ &\quad \times \sum_{\sigma'} \int' d\mathbf{l} \left[\frac{V_{\sigma',\mathbf{l}}(\mathbf{R}) Q_{\sigma,\mathbf{l}}}{\xi_1^-(\omega_{\mathbf{l}})(\omega_{\mathbf{l}} - \omega_{\mathbf{k}} - i\epsilon)} + \frac{V_{\sigma',l}^*(\mathbf{R}) Q_{\sigma',l}^*}{\xi_1^+(\omega_{\mathbf{l}})(\omega_{\mathbf{l}} + \omega_{\mathbf{k}})} \right] \end{aligned} \tag{3-3b}$$

where ϵ is a positive infinitesimal number. Hereafter, We abbreviate the limiting notation $\epsilon \to 0^+$ to avoid heavy notation. The function ξ_1 is defined by

$$\xi_1(z) \equiv z^2 - \omega_1^2 - 4\lambda^2\omega_1 \sum_\sigma \int' d\mathbf{k} \frac{\omega_\mathbf{k} |V_{\sigma,\mathbf{k}}(\mathbf{R})|^2}{z^2 - \omega_k^2} \tag{3-4}$$

with

$$\xi_1^\pm(\omega_\mathbf{k}) \equiv \xi_1(\omega_\mathbf{k} \pm i\epsilon) \tag{3-5}$$

The normalization factor is given by

$$N_1 \equiv \left[\frac{\tilde{\omega}_1}{\omega_1} \frac{d\xi_1(z)}{dz^2}\bigg|_{z=\tilde{\omega}_1} \right]^{-\frac{1}{2}} \tag{3-6}$$

$\tilde{\omega}_1$ is the shifted frequency associated to Q_1, and is given by the solution of the transcendental equation

$$\xi_1(\tilde{\omega}_1) = 0 \tag{3-7}$$

These new normal modes form a canonical pairs,

$$\{Q_\alpha, Q_\beta^*\}_{PB} = -i\delta_{\alpha\beta} \tag{3-8}$$

$$\{Q_\alpha, Q_\beta\}_{PB} = 0 \tag{3-9}$$

The new object Q_1 consists of the bare particle mode dressed by the field modes. As we shall show in next section that the dressing of the particle mode has two important features. First it decays exponentially in z direction which is different from the usual power law decayed dressing in open space [29]. This exponential decaying dressing is due to the fact that the field in the waveguide has an "effective mass" which is given by cut-off frequency α_{mn} from the dispersion relation in Eq. (2-15). Therefore higher TE or TM modes of the field corresponds to the situation with heavier mass than those lower modes. Second interesting result of our dressing is that its size is macroscopic as it is the same order as the size of the waveguide so that it might be relatively easy to detect the macroscopic dressing experimentally.

In the expression of the Bogoliubov transformation in Eq. (3-2a) we have denominators proportional to $\omega_{\mathbf{k}} - \tilde{\omega}_1$. In this chapter our consideration to the case where $\omega_1 < \omega_c$ so that this denominator never vanish. In other words, there is no resonance between the particle and the field in the stable case. This implies that our system is integrable in the sense of Poincaré.

Since the Hamiltonian is diagonalized in Eq. (3-1), the time evolution of $Q_1(t)$, and $Q_{\sigma,\mathbf{k}}(t)$ are given by

$$Q_1(t) = Q_1(0)e^{-i\tilde{\omega}_1 t} \quad , Q_{\sigma,\mathbf{k}}(t) = Q_{\sigma,\mathbf{k}}(0)e^{-i\omega_{\mathbf{k}} t} \tag{3-10}$$

If we expand Eq. (3-7) up to $\mathrm{O}(\lambda^2)$, we obtain

$$\tilde{\omega}_1 \approx \omega_1 - 2\lambda^2 \int dl \frac{\omega_{\mathbf{l}} \, |V_{\sigma,\mathbf{l}}(\mathbf{R})|^2}{\omega_k^2 - \omega_1^2} < \omega_1 \tag{3-11}$$

This shows that the dressed particle oscillates in a smaller frequency $\tilde{\omega}_1$, independent from our initial preparation. For the continuous spectrums, it remain unchanged under the interaction.

3.2 Dressed particle mode

Here we shall investigate the dressed particle mode Q_1, which consist of the bare particle mode $q_{\sigma,\mathbf{k}}$ and the field modes $q_{\sigma,\mathbf{k}}$. We first calculate the time evolution of $q_1(t)$ associated with Q_1. Putting

$$Q_{\sigma,\mathbf{k}}(0) = 0 \tag{3-12}$$

in Eq. (3-3a) and using Eq. (3-10), we have

$$\begin{aligned} q_1(t) &= N_1 \left(\frac{\tilde{\omega}_1 + \omega_1}{2\omega_1} Q_1(t) + \frac{\tilde{\omega}_1 - \omega_1}{2\omega_1} Q_1^*(t) \right) \\ &= N_1 Q_1(0) \left(\frac{\tilde{\omega}_1}{\omega_1} \cos(\tilde{\omega}_1 t) - i \sin(\tilde{\omega}_1 t) \right) \end{aligned} \tag{3-13}$$

where we have assumed the initial condition $Q_1(0)$ be real. One could verify for general case where $Q_1(0)$ is complex, the result is the same with the only change of phase in time, i.e. t becomes $(t+t_0)$ with t_0 as initial phase.

Eq. (3-13) shows $q_1(t)$ associated with $Q_1(t)$ oscillates in time with a new perturbed frequency obtained from the transcendental equation in Eq. (3-7).

Next we calculate the field mode $q_{\sigma,\mathbf{k}}(t)$ associated with Q_1. Using the same initial condition as Eq. (3-12) in Eq. (3-3b) with the time evolution given in Eq. (3-10), we obtain for real $Q_1(0)$,

$$\begin{aligned} q_{\sigma,\mathbf{k}}(t) &= -\lambda N_1 V^*_{\sigma,\mathbf{k}}(\mathbf{R})\left(\frac{Q_1(t)}{\tilde{\omega}_1-\omega_{\mathbf{k}}}+\frac{Q_1^*(t)}{\tilde{\omega}_1+\omega_{\mathbf{k}}}\right) \\ &= 2\lambda N_1 Q_1(0) V^*_{\sigma,\mathbf{k}}(\mathbf{R})\left(\frac{\tilde{\omega}_1\cos(\tilde{\omega}_1 t)-i\omega_{\mathbf{k}}\sin(\tilde{\omega}_1 t)}{\omega_{\mathbf{k}}^2-\tilde{\omega}_1^2}\right) \end{aligned} \tag{3-14}$$

For complex $Q_1(0)$, we can again obtain the same expression of Eq. (3-14) except that t is replaced by $t+t_0$. By substituting the time evolution of all $q_{\sigma,\mathbf{k}}$ modes into Eq. (2-10), this gives the vector potential of TE wave associated to the dressed particle mode Q_1,

$$\begin{aligned} \mathbf{A}_{TE}(\mathbf{r},t) &= 2\lambda N_1 Q_1(0)\sum_{mn}\frac{n}{b}\sqrt{\frac{2\Delta_{mn}^2}{\pi^2 c}}C_{mn}^2 W_{1,mn}(\mathbf{R})\Big(-\frac{n\pi}{b}W_{1,mn}(\mathbf{r})\hat{e}_x \\ &\quad +\frac{m\pi}{a}W_{2,mn}(\mathbf{r})\hat{e}_y\Big)\int_{-\infty}^{\infty}dk\left[\frac{\omega_{\mathbf{k}}\sin(\tilde{\omega}_1 t)+i\tilde{\omega}_1\cos(\tilde{\omega}_1 t)}{\omega_{\mathbf{k}}(\omega_{\mathbf{k}}^2-\tilde{\omega}_1^2)}e^{ikz}+c.c\right] \end{aligned} \tag{3-15}$$

The $\cos(\tilde{\omega}_1 t)$ is cancelled out with its complex conjugate part that only the $\sin(\tilde{\omega}_1 t)$ remain. The integration over k can be performed explicitly [30], which gives up to $O(\lambda)$,

$$\begin{aligned} \mathbf{A}_{TE}(\mathbf{r},t) &\approx 4\sqrt{2}\lambda Q_1(0)\sin(\tilde{\omega}_1 t)\sum_{mn}\frac{n\Delta_{mn}}{bc^2\sqrt{c}\sqrt{\alpha_{mn}^2-(\frac{\omega_1}{c})^2}}C_{mn}^2 W_{1,mn}(\mathbf{R}) \\ &\quad\times\left[-\frac{n\pi}{b}W_{1,mn}(\mathbf{r})\hat{e}_x+\frac{m\pi}{a}W_{2,mn}(\mathbf{r})\hat{e}_y\right]e^{-\sqrt{\alpha_{mn}^2-\left(\frac{\omega_1}{c}\right)^2}|z|} \end{aligned} \tag{3-16}$$

Similarly, by substituting $q_{\sigma,\mathbf{k}}(t)$ from Eq. (3-14) into Eq. (2-11), we have the vector potential of TM wave. Up to $O(\lambda)$,

$$\begin{aligned}\mathbf{A}_{TM}(\mathbf{r},t) \approx & -4\sqrt{2}\lambda Q_1(0)\sin(\tilde{\omega}_1 t)\sum_{mn}\frac{m}{a\omega_1^2\sqrt{c}}C_{mn}^2 W_{1,mn}(\mathbf{R}) \\ & \times\Bigg\{\left(\frac{m\pi}{a}W_{1,mn}(\mathbf{r})\hat{e}_x+\frac{n\pi}{b}W_{2,mn}(\mathbf{r})\hat{e}_y\right) \\ & \times\left(\alpha_{mn}e^{-\alpha_{mn}|z|}-\sqrt{\alpha_{mn}^2-(\frac{\omega_1}{c})^2}e^{-\sqrt{\alpha_{mn}^2-\left(\frac{\omega_1}{c}\right)^2}|z|}\right) \\ & +\mathrm{sgn}(z)\alpha_{mn}^2 W_{3,mn}(\mathbf{r})\hat{e}_z\left(e^{-\sqrt{\alpha_{mn}^2-\left(\frac{\omega_1}{c}\right)^2}|z|}-e^{-\alpha_{mn}|z|}\right)\Bigg\} \quad (3\text{-}17)\end{aligned}$$

with the $\mathrm{sgn}(z)$ is defined as

$$\mathrm{sgn}(z)=\begin{cases}1 & , \quad z>0\\ -1 & , \quad z<0\end{cases} \quad (3\text{-}18)$$

In Eq. (3-16) and Eq. (3-17) we see the vector potential of the field associated with Q_1 stays around the dipole without propagation. It is the analogy of the dressing cloud in the quantum ground state. Note that the dressings of both TE and TM waves decay *exponentially* in z direction. This is the result of the existence of effective mass (see Eq. (2-15)) for the field inside waveguide. In open space in quantum mechanics, the dressing cloud of the ground state obeys power law decay since the photon has no mass [29].

The size of our classical dressing cloud is in the order of $1/\sqrt{\alpha_{mn}^2-(\omega_1/c)^2}$ for given (m,n) mode. For smaller m and n, the dressing is larger in size. For the case $b>a$, the largest dressing corresponds to the TE_{01} mode whose size is $c/\sqrt{\omega_c^2-\omega_1^2}>b/\pi$. This is the same order as the size of the waveguide, which is macroscopic as compares with the size of the dipole. For example, a HCl dipole with size about 10^{-9}m located in the waveguide with $b=10^{-5}\mathrm{m}<b_c$, we have the dressing ten thousands times larger than the dipole molecule. Moreover, since

the critical frequency ω_c is inversely proportional to the size of the waveguide (see Eq. (2-22)), we may obtain extremely large dressing cloud by adjusting the the size of the waveguide such that $\omega_c \approx \omega_1$.

In Figure 3.1 to Figure 3.3, we show the dressing field obtained in the above calculation. For all the figures in the waveguide problem, we have chosen a unit system where the unit of length is b, the unit of time is b/c, the unit of mass is μ_1, the unit of q_1 is $\sqrt{\mu_1 bc}$ and the unit of vector potential is $\sqrt{\mu_1 c^2/b}$.

In order to exaggerate the effect of interaction, here we have chosen large value of λ as $\lambda = 0.1$, $\omega_1 = 2.5$, $a = 0.5$ for all these figures. The center of mass of the dipole is located at the center of the waveguide where $R_x = a/2$, $R_y = b/2$, $R_z = 0$. As a result the vector potential is vanish for all $m =$ odd and $n =$ even due to the symmetry of function $W_{1,mn}(\mathbf{R})$ defined in Eq. (2-14d). Since we are mainly interested in the exponential profile of the dressing, which is the same for all three components of the vector potential, we show only x component of the vector potential.

In Figure 3.1, we show the z direction profile of the x component amplitude of the $\mathbf{A}_{TE_{mn}}(a/2, b/2, z)$ of the dressing without including the oscillating factor $\sin\tilde{\omega}_1 t$. The first three dominant modes $(m, n) = (0, 1)$, $(0, 3)$, and $(0, 5)$ are plotted in the figure. The larger the n, the thicker the line. As predicted in Eq. (3-16), one can see that the size of the largest dressing (TE_{01} mode) is greater than the size of waveguide ($b = 1$). Also, higher modes of (m, n) gives smaller contribution.

In Figure 3.2, we show the corresponding profile in Figure 3.1 for first three dominant modes in TM wave, which is TM_{21}, TM_{23}, and TM_{25} in this case. The thicker line corresponds with the higher mode. Here we have TM_{21} as the leading mode in TM wave. Different from $A_{TE_{mn}}$ which is always negative value, $A_{TM_{mn}}$

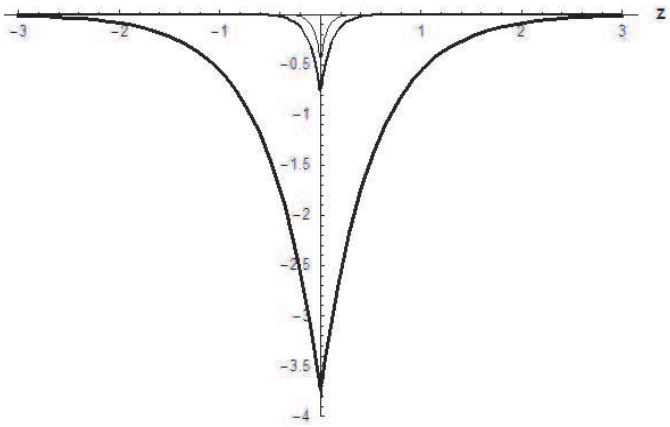

Figure 3.1: The profile of the x component of $A_{TE_{01}}$, $A_{TE_{03}}$, and $A_{TE_{05}}$. The higher the mode, the thicker the line. The horizontal axis is the distance from the particle in z direction while the vertical axis is the x component of the $\mathbf{A}_{TE}(R_x, R_y, z)$ without the oscillating factor $\sin\tilde{\omega}_1 t$.

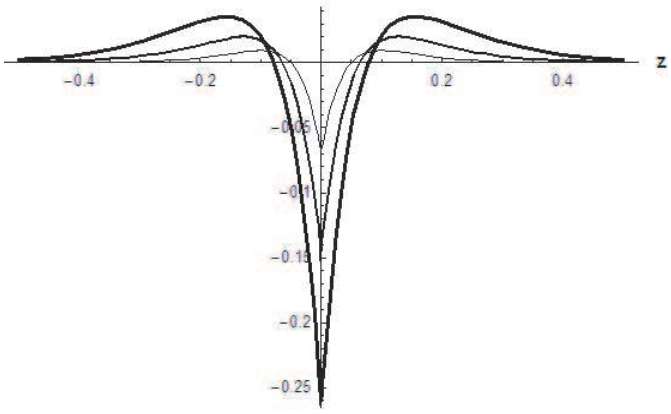

Figure 3.2: The profile of the x component of $A_{TM_{21}}$, $A_{TM_{23}}$, and $A_{TM_{25}}$. The higher the mode, the thicker the line. The horizontal axis is the distance from the particle in z direction while the vertical axis is the x component of the $\mathbf{A}_{TM}(a/2, b/2, z)$ without the oscillating factor $\sin\tilde{\omega}_1 t$.

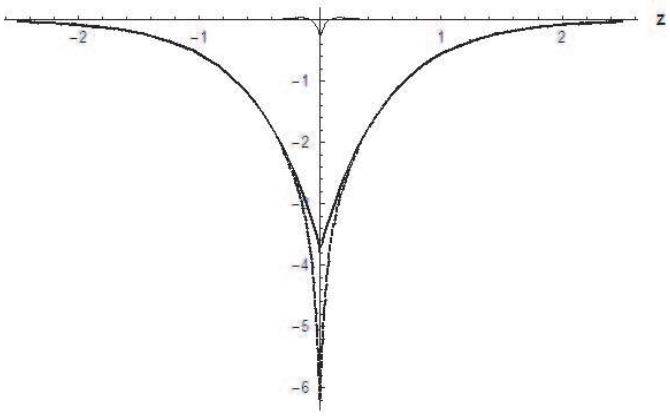

Figure 3.3: The profile of the leading mode in TE and TM wave. The thin line is TM_{21} mode while the thick line is TE_{01} mode.

have both positive and negative value since it consists of the competition of two exponential decaying terms with opposite signs as shown in Eq. (3-17).

In Figure 3.3 we compare the dressings of the leading modes of TE and TM waves which are $\mathbf{A}_{TE_{01}}(a/2, b/2, z)$ and $\mathbf{A}_{TM_{21}}(a/2, b/2, z)$ shown in Figure 3.1 and Figure 3.2, respectively. The thick line is TE_{01} mode, while the thin line is TM_{21} mode. It shows TE_{01} mode is order of magnitude larger than TM_{21} mode.

As a summary, we found that the dressing field surrounding the particle mode in Q_1 is macroscopic in size which is larger than the cross section of the waveguide. The largest size corresponds to the dominant TE_{01} mode.

3.3 Time evolution of the original variables

3.3.1 Time evolution of the $q_{\sigma,\mathbf{k}}(t)$

In this section we shall investigate the time evolution of $q_1(t)$ for the initial condition given by,

$$q_{\sigma,\mathbf{k}}(0) = 0 \qquad , \qquad p_1(0) = 0 \tag{3-19}$$

The value of $q_1(0)$ is real for Eq. (3-19). Substituting the initial condition Eq. (3-19) into Eq. (3-2a) and Eq. (3-2b) we obtain

$$Q_1(t) = N_1 q_1(0) e^{-i\tilde{\omega}_1 t} \tag{3-20}$$

$$Q_{\sigma,\mathbf{k}}(t) = -2\lambda\omega_1 q_1(0) \frac{V^*_{\sigma,\mathbf{k}}(\mathbf{R})}{\xi_1^+(\omega_\mathbf{k})} e^{-i\omega_\mathbf{k} t} \tag{3-21}$$

where we have used Eq. (3-10). By applying the inverse transformation Eq. (3-3a), we have

$$q_1(t) = q_{1S}(t) + q_{1Z}(t) \tag{3-22}$$

Here $q_{1S}(t)$ is non-decaying component (or stable component) of $q_1(t)$ and is given by

$$q_{1S}(t) = N_1^2 q_1(0) \left[\frac{\tilde{\omega}_1}{\omega_1} \cos(\tilde{\omega}_1 t) - i \sin(\tilde{\omega}_1 t) \right] \tag{3-23}$$

The explicit form of N_1 and $\tilde{\omega}_1$ are presented in Appendix B. By comparing Eq. (3-23) with Eq. (3-13), one can see $q_{1S}(t)$ is corresponds to the dressed particle mode $Q_1(t)$.

The $q_{1Z}(t)$ is defined as

$$\begin{aligned} q_{1Z}(t) &= 4\lambda^2\omega_1 q_1(0) \sum_{\sigma,m,n} \int_0^\infty dk \frac{|V_{\sigma,\mathbf{k}}(\mathbf{R})|^2}{|\xi_1^+(\omega_\mathbf{k})|^2} \left[(\omega_\mathbf{k} + \omega_1) e^{-i\omega_\mathbf{k} t} + (\omega_\mathbf{k} - \omega_1) e^{i\omega_\mathbf{k} t} \right] \\ &\approx 4\lambda^2\omega_1 q_1(0) \sum_{mn} C^2_{mn} W^2_{1,mn}(\mathbf{R}) \int_0^\infty dk \left[\frac{n^2\Delta_{mn}}{b^2\omega_\mathbf{k}} + \frac{m^2c^2k^2}{a^2\omega_\mathbf{k}^3} \right] \\ &\quad \times \left[\frac{(\omega_\mathbf{k} + \omega_1) e^{-i\omega_\mathbf{k} t} + (\omega_\mathbf{k} - \omega_1) e^{i\omega_\mathbf{k} t}}{(\omega_\mathbf{k}^2 - \omega_1^2)^2} \right] \end{aligned} \tag{3-24}$$

To obtain the last line, we have used Eq. (2-19a), and Eq. (2-19b). The terms proportional to Δ_{mn} are coming from TE wave while the terms proportional $1/\omega_\mathbf{k}^3$ are coming from TM wave. Among these terms, the dominant contribution is TE_{01} mode.

In the above expression we have approximated $\xi_1^+(\omega_\mathbf{k})$ defined in Eq. (3-5) by neglecting higher order term in λ, as $\lambda \ll 1$. For the stable case $\omega_1 < \omega_c$, $\xi_1^+(\omega_\mathbf{k})$

does not vanish for all $\omega_{\mathbf{k}}$. For this case, one can evaluate the integration in Eq. (3-24) by using the stationary phase approximation. Under this approximation, we have [31]

$$\int_0^\infty dk \frac{(\omega_{\mathbf{k}} \pm \omega_1) e^{\mp i\omega_{\mathbf{k}} t}}{\omega_{\mathbf{k}}(\omega_{\mathbf{k}}^2 - \omega_1^2)^2} \approx \sqrt{\frac{\pi\alpha_{mn}}{2ct}} \frac{(\alpha_{mn} \pm \frac{\omega_1}{c}) e^{\mp i(ct\alpha_{mn} + \frac{\pi}{4})}}{c^4 \alpha_{mn}(\alpha_{mn}^2 - (\frac{\omega_1}{c})^2)^2} \tag{3-25}$$

$$\int_0^\infty dk \frac{c^2 k^2 (\omega_{\mathbf{k}} \pm \omega_1) e^{\mp i\omega_{\mathbf{k}} t}}{\omega_{\mathbf{k}}^3(\omega_{\mathbf{k}}^2 - \omega_1^2)^2} \approx \frac{\sqrt{\pi}}{4} \left(\frac{2\alpha_{mn}}{ct}\right)^{\frac{3}{2}} \frac{(\alpha_{mn} \pm \frac{\omega_1}{c}) e^{\mp i(ct\alpha_{mn} + \frac{\pi}{4})}}{c^4 \alpha_{mn}^3(\alpha_{mn}^2 - (\frac{\omega_1}{c})^2)^2} \tag{3-26}$$

for $\omega_1 t \gg 1$. Substituting them into Eq. (3-24), we obtain

$$\begin{aligned} q_{1Z}(t) \approx\ & 4\lambda^2 \omega_1 q_1(0) \sum_{mn} \sqrt{\frac{2\pi\alpha_{mn}}{ct}}\, C_{mn}^2 W_{1,mn}^2(\mathbf{R}) \\ & \times \left\{ \frac{n^2 \Delta_{mn}}{b^2 c^4} \left[\frac{\alpha_{mn} \cos(\alpha_{mn} ct + \frac{\pi}{4}) - i(\frac{\omega_1}{c}) \sin(\alpha_{mn} ct + \frac{\pi}{4})}{\alpha_{mn}(\alpha_{mn}^2 - (\frac{\omega_1}{c})^2)^2} \right] \right. \\ & \left. + \frac{m^2\sqrt{\pi}}{a^2 c^4 \alpha_{mn} ct} \left[\frac{\alpha_{mn} \cos(\alpha_{mn} ct + \frac{3\pi}{4}) - i(\frac{\omega_1}{c}) \sin(\alpha_{mn} ct + \frac{3\pi}{4})}{\alpha_{mn}(\alpha_{mn}^2 - (\frac{\omega_1}{c})^2)^2} \right] \right\} \end{aligned} \tag{3-27}$$

where the first contribution of order $1/\sqrt{\omega_1 t}$ comes from TE wave, while the second contribution of order $1/\sqrt{\omega_1^3 t^3}$ comes from TM wave. For $\omega_1 t \gg 1$, the TE wave contribution dominates.

As we shall see in Section 4.2, this power law decaying component is closely related to the "Zeno" effect ($q_{1b}(t)$ term in Eq. (4-12)) that corresponds to a deviation from exponential decay for unstable particle mode, which has been well investigated in quantum mechanics [7], [14].

For $\omega_1 t \gg 1$, $q_1(t)$ approaches to $q_{1S}(t)$. In Figure 3.4, we show the time evolution of $|q_{1Z}(t)|^2$ given by Eq. (3-24) (solid line) and the stationary phase approximation given in Eq. (3-27) (dashed line). We use the same parameters and unit as in the last section with $q_1(0) = 1$. Since TE_{01} dominates, we take only this dominant mode proportional Δ_{01} in plotting $|q_{1Z}(t)|^2$. The integration in Eq. (3-24) is performed numerically. For $\omega_1 t \gg 1$ we see the stationary phase approximation

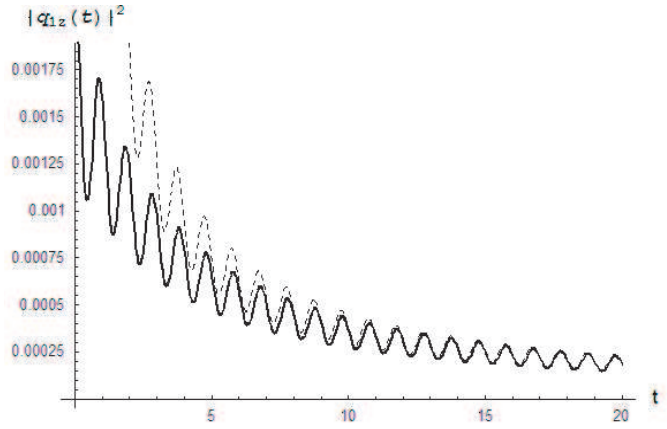

Figure 3.4: Comparison of $|q_{1z}(t)|^2$ from numerical integration and result from Stationary phase approximation. The solid line is the $|q_{1z}(t)|^2$ calculated through exact numerical integration while the dashed line is the prediction from stationary phase approximation.

gives very good prediction. In Figure 3.5, we show the our theoretical result of a trajectory of $x_1(t)$ and $p_1(t)$ in phase space for $0 \leq t \leq 30$ (see Eq. (2-7)). The integration in Eq. (3-24) of $q_{1Z}(t)$ was calculated numerically. Here we take the dominant TE_{01} mode in the calculation of $q_{1Z}(t)$. Similar when we evaluate the value of N_1 and $\tilde{\omega}_1$ given in Appendix B, we keep only TE_{01} mode. At $t = 0$ we have $x_1(0) = 0.9$ and $p_1(0) = 0$. As time goes on, the particle approaches to a steady solution which has a smaller amplitude than the initial amplitude.

3.3.2 Time evolution of the field

In previous section, we see the approaching to steady solution of $q_1(t)$ from the initial condition in Eq. (3-19). In this section we are interested in the time evolution of the field modes $q_{\sigma,\mathbf{k}}(t)$ corresponds with the same initial condition in Eq. (3-19).

In Eq. (3-20) and Eq. (3-21) we have the time evolution of $Q_1(t)$, and $Q_{\sigma,\mathbf{k}}(t)$ under the initial condition Eq. (3-19) without any bare field. By substituting them

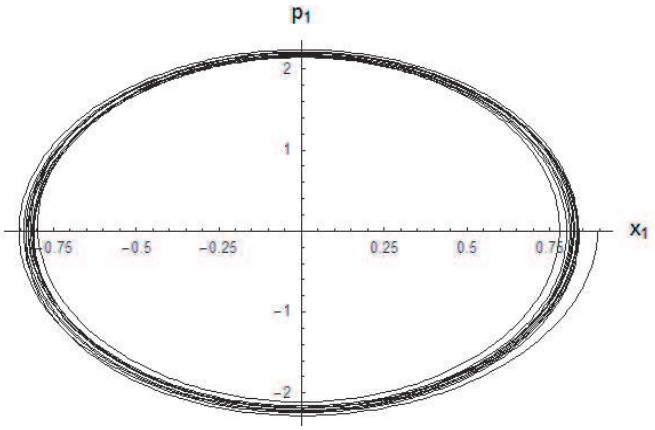

Figure 3.5: Time evolution of stable particle in phase space. We start from $p_1(0) = 0$, $q_1(0) = 1$, and evolve it up to $t = 60$.

into the inverse transformation of the field mode in Eq. (3-3b), we have $q_{\sigma,\mathbf{k}}(t)$ up to λ

$$q_{\sigma,\mathbf{k}}(t) \approx -\lambda q_1(0) V^*_{\sigma,\mathbf{k}}(\mathbf{R}) \left[\frac{e^{-i\tilde{\omega}_1 t}}{\omega_1 - \omega_{\mathbf{k}}} + \frac{e^{i\tilde{\omega}_1 t}}{\omega_1 + \omega_{\mathbf{k}}} \right] - 2\lambda \frac{\omega_1 q_1(0) V^*_{\sigma,\mathbf{k}}(\mathbf{R}) e^{-i\omega_{\mathbf{k}} t}}{\omega^2_{\mathbf{k}} - \omega^2_1} \quad (3\text{-}28)$$

where the $\xi^+_1(\omega_{\mathbf{k}})$ has been again approximated as Eq. (3-5) by neglecting higher order term in λ. Eq. (3-28) gives $q_{\sigma,\mathbf{k}}(0) = 0$ as it should be. Since the TE mode dominates as shown in the previous section, we shall calculate only this mode. Substituting Eq. (3-28) into Eq. (2-10),

$$\mathbf{A}_{TE}(\mathbf{r}, t) = \mathbf{A}_{TE,C}(\mathbf{r}, t) + \mathbf{A}_{TE,Z}(\mathbf{r}, t) \quad (3\text{-}29)$$

with the definition

$$\begin{aligned}\mathbf{A}_{TE,C}(\mathbf{r},t) &= 4\lambda q_1(0)\sum_{mn}\frac{n}{b}\sqrt{\frac{2\Delta_{mn}^2}{\pi^2 c}}C_{mn}^2 W_{1,mn}(\mathbf{R})\left(\frac{-n\pi}{b}W_{1,mn}(\mathbf{r})\hat{e}_x\right.\\ &\left.+\frac{m\pi}{a}W_{2,mn}(\mathbf{r})\hat{e}_y\right)\int_0^\infty dk\left[\frac{\omega_{\mathbf{k}}\sin(\tilde{\omega}_1 t)}{\omega_{\mathbf{k}}(\omega_{\mathbf{k}}^2-\omega_1^2)}e^{ikz}+e^{-ikz}\right]\\ &= 4\sqrt{2}\lambda q_1(0)\sin(\tilde{\omega}_1 t)\sum_{mn}\frac{n\Delta_{mn}}{bc^2\sqrt{c}\sqrt{\alpha_{mn}^2-(\frac{\omega_1}{c})^2}}C_{mn}^2 W_{1,mn}(\mathbf{R})\\ &\times\left[-\frac{n\pi}{b}W_{1,mn}(\mathbf{r})\hat{e}_x+\frac{m\pi}{a}W_{2,mn}(\mathbf{r})\hat{e}_y\right]e^{-\sqrt{\alpha_{mn}^2-\left(\frac{\omega_1}{c}\right)^2}|z|} \qquad (3\text{-}30)\end{aligned}$$

and

$$\begin{aligned}\mathbf{A}_{TE,Z}(\mathbf{r},t) &= -2\lambda q_1(0)\omega_1\sum_{mn}\frac{n}{b}\sqrt{\frac{2\Delta_{mn}^2}{\pi^2 c}}C_{mn}^2 W_{1,mn}(\mathbf{R})\left(\frac{-n\pi}{b}W_{1,mn}(\mathbf{r})\hat{e}_x\right.\\ &\left.+\frac{m\pi}{a}W_{2,mn}(\mathbf{r})\hat{e}_y\right)\int_0^\infty dk\left[i\frac{e^{i(kz-\omega_{\mathbf{k}}t)}+e^{-i(kz+\omega_{\mathbf{k}}t)}}{\omega_{\mathbf{k}}(\omega_{\mathbf{k}}^2-\omega_1^2)}+c.c\right] \qquad (3\text{-}31)\end{aligned}$$

The $\mathbf{A}_{TE,C}(\mathbf{r},t)$ corresponds to the "dressing cloud" calculated for Eq. (3-12) at Eq. (3-16). As shown in Section 3.2, this cloud stays around the dipole.

In contrast, the vector potential $\mathbf{A}_{TE,Z}(\mathbf{r},t)$ given in Eq. (3-31) consist of two travelling waves, with the $\exp(ikz-i\omega_{\mathbf{k}}t)$ to positive direction of z and $\exp(-ikz-i\omega_{\mathbf{k}}t)$ to negative direction of z, respectively. Again the subscript "Z" stands for the "Zeno field", as it is related to Zeno effect mentioned in the previous subsection.

Due to the dispersion relation in Eq. (2-15) the Zeno field has an effective mass α_{mn}, with the the phase velocity given by

$$v_p \equiv \frac{\omega_{\mathbf{k}}}{k} = c\frac{\sqrt{\alpha_{mn}^2+k^2}}{k} \qquad (3\text{-}32)$$

As we shall see later this leads to the spreading of wavepacket in Zeno field. The integration in Eq. (3-31) can be performed explicitly for $|z|>ct$ (outside lightcone)

as [30],

$$\int_0^\infty dk \left(\frac{e^{i(kz-\omega_{\mathbf{k}}t)} + e^{-i(kz+\omega_{\mathbf{k}}t)}}{\omega_{\mathbf{k}}(\omega_{\mathbf{k}}^2 - \omega_1^2)} + c.c \right) = 2\pi i \frac{\sin\omega_1 t}{\omega_1 c^2 \sqrt{\alpha_{mn}^2 - (\frac{\omega_1}{c})^2}} e^{-\sqrt{\alpha_{mn}^2 - (\frac{\omega_1}{c})^2}|z|} \tag{3-33}$$

which gives

$$\mathbf{A}_{TE,Z}(\mathbf{r},t) = -\mathbf{A}_{TE,C}(\mathbf{r},t) \qquad \text{for} \qquad |z| > ct \tag{3-34}$$

Hence Zeno field cancels the dressing cloud outside the lightcone, i.e. we have

$$\mathbf{A}_{TE}(\mathbf{r},t) = 0 \qquad \text{for} \qquad |z| > ct \tag{3-35}$$

Inside the light cone we again apply the stationary phase approximation. In this approximation we have [31][1]

$$\int_0^\infty dk \frac{e^{i(kz-\omega_{\mathbf{k}}t)} + e^{-i(kz+\omega_{\mathbf{k}}t)}}{\omega_{\mathbf{k}}(\omega_{\mathbf{k}}^2 - \omega_1^2)} \approx \sqrt{\frac{\pi}{2ct}} \frac{e^{-i(\alpha_{mn}ct(1-\frac{z^2}{2c^2t^2})+\frac{\pi}{4})}}{c^3\sqrt{\alpha_{mn}}(\alpha_{mn}^2 - (\frac{\omega_1}{c})^2)} \tag{3-36}$$

where we neglected the higher order terms of $|z|/ct$. Using this in Eq. (3-31), we obtain

$$\begin{aligned} \mathbf{A}_{TE,Z}(\mathbf{r},t) \quad \approx \quad & -4\sqrt{2}\lambda q_1(0) \frac{\omega_1}{bc^4\sqrt{\pi t}} \sum_{m,n} \frac{n\Delta_{mn} C_{mn}^2 W_{1,mn}(\mathbf{R})}{\sqrt{\alpha_{mn}}(\alpha_{mn}^2 - (\frac{\omega_1}{c})^2)} \left[\frac{-n\pi}{b} W_{1,mn}(\mathbf{r})\hat{e}_x \right. \\ & \left. + \frac{m\pi}{a} W_{2,mn}(\mathbf{r})\hat{e}_y \right] \sin\left(\alpha_{mn}ct(1 - \frac{z^2}{2c^2t^2}) + \frac{\pi}{4} \right) \end{aligned} \tag{3-37}$$

In Figs. 3.6–3.9, we show the x-component of the vector potential of the TE_{01} emitted from the bare particle mode from several points of view. We choose the same parameters as in Section 3.3.1 that $\lambda = 0.1$, $\omega_1 = 2.5$, $a = 0.5$.

In Figure 3.6 we compare the Zeno field obtained from stationary phase approximation with the Zeno field obtained from Eq. (3-31) with the integration performed numerically. We plot the x component vector potential $\mathbf{A}_{TE_{01}}(a/2, b/2, 0, t)$

[1] For the case $z = 0$ the result is the twice of the right hand side of Eq. (3-36)

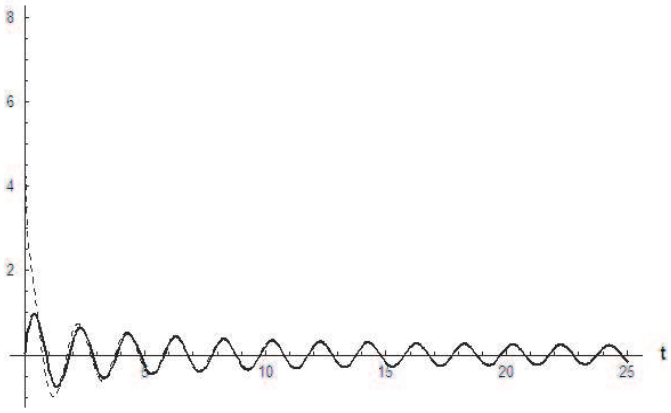

Figure 3.6: Stationary phase approximation of the Zeno field. We compare the x-component of the $\mathbf{A}_{TE_{01},Z}(a/2, b/2, 0, t)$ as a function of time at the center of mass of the dipole. The solid line corresponds to Eq. (3-31) with the integration performed numerically, and the dashed line corresponds to the stationary phase approximation given in Eq. (3-37).

as a function of time at the center of mass of the dipole molecule. The solid line is given by numerical integration of the form in Eq. (3-31) while the dashed line is the stationary phase approximation given by Eq. (3-37). As we see the stationary phase approximation again gives good approximation at the larger time scale $\omega_1 t \gg 1$. This shows the Zeno field of TE wave decay as $1/\sqrt{t}$ given in Eq. (3-37). These time scale is the same as the transition time of $q_1(t)$ for TE mode discussed in previous section. While the $q_1(t)$ is approaching to its steady solution $q_{1s}(t)$, the Zeno field is separated from the dressing field.

In Figure 3.7 we show z direction profile of the x component vector potential $\mathbf{A}_{TE_{01}}(a/2, b/2, z, t)$ for both Zeno field and dressing cloud at short time $t = 1.5$. The thin line is the dressing field, while the dashed lines are left and right moving Zeno field. The thick line is the total vector potential given by the summation of all three components shown in the figure.

The dressing cloud given in Eq. (3-30) stays around the dipole. There are

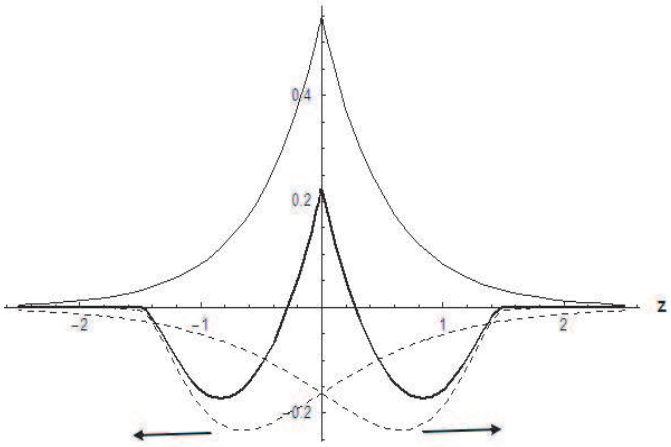

Figure 3.7: Decomposition of the emitted field. We show the z direction profile of x component of $\mathbf{A}_{TE_{01},C}(a/2, b/2, z, t)$ (thin line) and $\mathbf{A}_{TE_{01},Z}(a/2, b/2, z, t)$ (dashed lines) at $t = 1.5$. The two dashed lines correspond to the left moving and right moving terms in the $\mathbf{A}_{TE_{01},Z}(a/2, b/2, z, t)$. The thick line is the additional of the dashed lines and thin line, which gives the total vector potential of TE_{01}.

two moving Zeno fields, one is moving to left with $\exp[i(kz - \omega_{\mathbf{k}}t)]$ and the other is moving to right with $\exp[-i(kz - \omega_{\mathbf{k}}t)]$ shown in Eq. (3-31). The integration in Eq. (3-31) is performed numerically.

In Figure 3.8, we magnify Figure 3.7 near the light cone($z = 1.5$). We see the Zeno field (dashed line) cancels out exactly with the dressing field(thin line) outside light cone ($z = 1.5$). Therefore the total emitted fields (thick line) from the bare particle mode obeys causality.

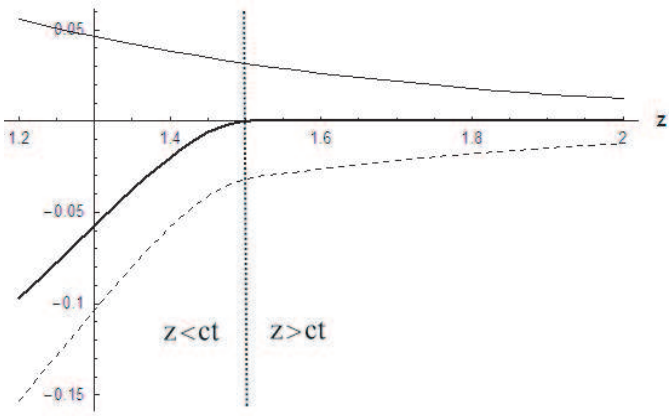

Figure 3.8: The causality of emitted field. We magnify Figure 3.7 near the light cone($z = 1.5$). The Zeno field (dashed line) cancels out with the dressing cloud (thin line) outside the lightcone. The thick line is the summation of both fields.

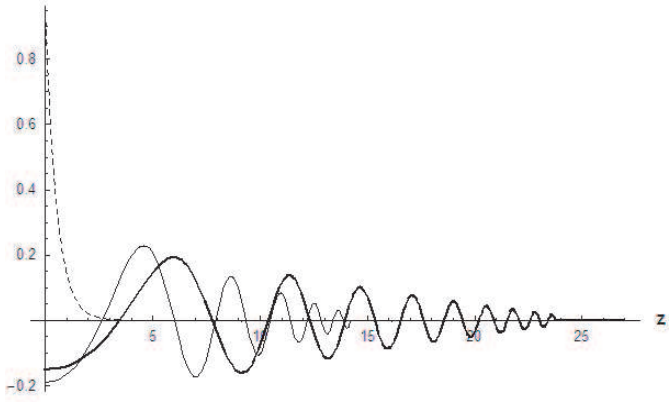

Figure 3.9: Propagation of Zeno field. We plot the x component of $\mathbf{A}_{TE_{01},Z}(a/2, b/2, z, t)$ as function of z at two different times, $t = 15$(thin line), and $t = 25$(thick line). For comparison, we show the amplitude of the dressing cloud $\mathbf{A}_{TE_{01},C}(a/2, b/2, z, t)$ (dashed line) without the oscillating factor $\sin(\tilde{\omega}_1 t)$.

In Figure 3.9 we visualize the separation of the Zeno field from the dressing field in space. We show the z direction profile of the x component vector potential

$\mathbf{A}_{TE_{01}}(a/2, b/2, z, t)$ of Zeno field at $t = 15$ (thin solid line) and $t = 25$ (thick solid line). The dashed line is the amplitude of the steady dressing cloud in Eq. (3-16) without the $\sin(\tilde{\omega}_1 t)$ factor. As time goes on, the Zeno field moves away from the dipole located at $z = 0$, The time scale of the separation of dressing field and Zeno field is given by $O(1/\sqrt{t})$ as has been shown in Eq. (3-37). Because of the existence of effective mass due to the cut-off frequency, we have a non-linear dispersion relation that leads to the spreading of the travelling Zeno field as shown in Figure 3.9.

In summary, we have shown that starting from the initial bare particle given in Eq. (3-19), we obtain a steady accelerated motion of the dipole dressed by the electromagnetic cloud.

3.4 Forces from the wall

In the previous section we saw that the steady state of the dipole molecules is dressed by the electromagnetic field. As we shall see in this section, the overlapping of this dressing field and the boundary of the waveguide will induce forces acting on the center of mass of the dipole molecule.

By taking the derivative of our Hamiltonian in Eq. (2-17) with respect to the center of mass of the dipole molecules, we have the force

$$\begin{aligned}
\mathbf{F} &= -\frac{\partial H}{\partial R_x}\hat{e}_x - \frac{\partial H}{\partial R_y}\hat{e}_y \\
&= -\lambda \sum_{\sigma} \int' dk \left[\left(\frac{\partial V_{\sigma,\mathbf{k}}(\mathbf{R})}{\partial R_x} q_{\sigma,l}(t) - \frac{\partial V^*_{\sigma,\mathbf{k}}(\mathbf{R})}{\partial R_x} q^*_{\sigma,k}(t) \right) \hat{e}_x \right. \\
&\quad \left. + \left(\frac{\partial V_{\sigma,\mathbf{k}}(\mathbf{R})}{\partial R_y} q_{\sigma,l}(t) - \frac{\partial V^*_{\sigma,\mathbf{k}}(\mathbf{R})}{\partial R_y} q^*_{\sigma,k}(t) \right) \hat{e}_y \right] [q_1(t) - q_1^*(t)] \qquad (3\text{-}38)
\end{aligned}$$

where the z component forces is absent because the waveguide is symmetry in z direction. To obtain the force associated to the dressing, we choose the dressed particle mode Q_1 given in Eq. (3-12) as our initial condition. Hence we have the

$q_1(t)$ and $q_{\sigma,\mathbf{k}}(t)$ given in Eq. (3-13) and Eq. (3-14), respectively. Substituting them into Eq. (3-38), we have the leading term in λ as

$$\mathbf{F} \approx 8\lambda^2 Q_1^2(0)\sin^2(\tilde{\omega}_1 t)\sum_{\sigma}\int' d\mathbf{k}\frac{\omega_{\mathbf{k}}V_{\sigma,\mathbf{k}}(\mathbf{R})}{\omega_{\mathbf{k}}^2-\omega_1^2}\left[\frac{\partial V^*_{\sigma,\mathbf{k}}(\mathbf{R})}{\partial R_x}\hat{e}_x+\frac{\partial V^*_{\sigma,\mathbf{k}}(\mathbf{R})}{\partial R_y}\hat{e}_y\right] \quad (3\text{-}39)$$

By substituting the interaction given in Eq. (2-19a) and Eq. (2-19b), we can carry out the integration of k explicitly. The forces associated with the dressing of TE and TM waves are then given by

$$\begin{aligned}\mathbf{F}_{TE} &= -8\pi\lambda^2 Q_1^2(0)\sin^2(\tilde{\omega}_1 t)\sum_{mn}(\frac{n}{bc})^2\frac{\Delta_{mn}C_{mn}^2 W_{1,mn}(\mathbf{R})}{\sqrt{\alpha_{mn}^2-(\frac{\omega_1}{c})^2}}\\ &\times \left\{\frac{m\pi}{a}\sin(\frac{m\pi R_{1x}}{a})\sin(\frac{n\pi R_{1y}}{b})\hat{e}_x-\frac{n\pi}{b}\cos(\frac{m\pi R_{1x}}{a})\cos(\frac{n\pi R_{1y}}{b})\hat{e}_y\right\} \quad (3\text{-}40)\end{aligned}$$

$$\begin{aligned}\mathbf{F}_{TM} &= -8\pi\lambda^2 Q_1^2(0)\sin^2(\tilde{\omega}_1 t)\sum_{mn}(\frac{m}{a\omega_1})^2 C_{mn}^2 W_{1,mn}(\mathbf{R})\\ &\times\left(\alpha_{mn}-\sqrt{\alpha_{mn}^2-(\frac{\omega_1}{c})^2}\right)\left\{\frac{m\pi}{a}\sin(\frac{m\pi R_{1x}}{a})\sin(\frac{n\pi R_{1y}}{b})\hat{e}_x\right.\\ &\left.-\frac{n\pi}{b}\cos(\frac{m\pi R_{1x}}{a})\cos(\frac{n\pi R_{1y}}{b})\hat{e}_y\right\} \quad (3\text{-}41)\end{aligned}$$

This shows that the force acting on the particle from the walls is in the order of λ^2, which is extremely small. For example we have $\lambda^2 \sim 10^{-12}$ for HCl. Therefore we can neglect these forces as anticipated in Section 2.2.

In Figure 3.10 we show the vector field of the total force inside the waveguide , by summing the contribution from TE wave in Eq. (3-40) and TM wave in Eq. (3-41) up to (m,n)=$(2,2)$. Here $R_x = 0.25$ and $R_y = 0.5$ is the center of the waveguide. We choose again the parameters $\lambda = 0.1$, $\omega_1 = 2.5$, $a = 0.5$. The length of the arrows indicates the the magnitude of the force. At the center of the waveguide the force become minimum. We see two stable points around at $R_x = 0.5$ and $R_y = 0.32$ or $R_y = 0.68$. These forces are coming from the overlapping of the dressed field

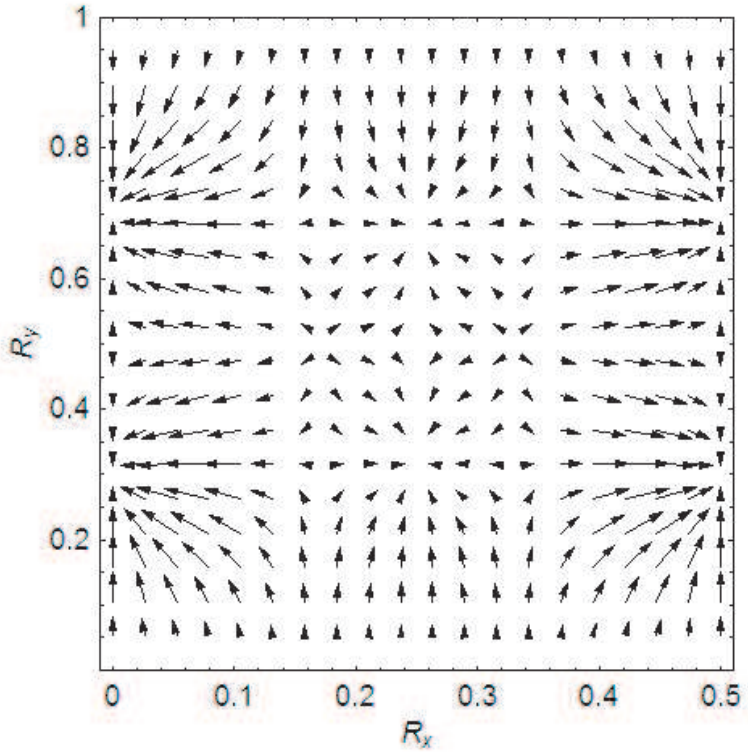

Figure 3.10: Forces due to the waveguide boundary. We show the vector field of the force inside the waveguide. The length of the arrow indicates the magnitude of the force.

with the walls. In quantum mechanics the similar force coming from the overlap of the dressing field in ground state and the wall is known as the Casimir-Polder force [29].

3.5 Extension to two dipoles system

3.5.1 Hamiltonian of two dipoles inside waveguide

In this section we are interested in the forces due to two overlapped dressing fields. In quantum mechanics, the force induced by overlapped dressings are called

van der Waals force. In our steady classical dressed particle in integrable case, we have the classical van der Waals force in the waveguide analogous to quantum systems [29].

We first generalize our Hamiltonian to the case of two dipole molecules inside the waveguide. By following the same procedure in Section 2.2, we have the Hamiltonian of two dipole case given by

$$\begin{aligned} H &= \omega_1 q_1^* q_1 + \omega_2 q_2^* q_2 + \sum_{\sigma=E,M} \int' d\mathbf{k} \omega_{\mathbf{k}} q_{\sigma,\mathbf{k}}^* q_{\sigma,\mathbf{k}} \\ &\quad + \lambda_1 \int' d\mathbf{k} (V_{\sigma,\mathbf{k}}(\mathbf{R}_1) q_{\sigma,\mathbf{k}} - V_{\sigma,\mathbf{k}}^*(\mathbf{R}_1) q_{\sigma,\mathbf{k}}^*)(q_1 - q_1^*) \\ &\quad + \lambda_2 \int' d\mathbf{k} (V_{\sigma,\mathbf{k}}(\mathbf{R}_2) q_{\sigma,\mathbf{k}} - V_{\sigma,\mathbf{k}}^*(\mathbf{R}_2) q_{\sigma,\mathbf{k}}^*)(q_2 - q_2^*) \end{aligned} \tag{3-42}$$

with the dimensionless coupling constants λ_1, λ_2 are defined as

$$\lambda_1 \equiv \sqrt{\frac{(Z_1 e)^2}{(\mu_1 c^2)(c/\omega_1)}} \quad , \quad \lambda_2 \equiv \sqrt{\frac{(Z_2 e)^2}{(\mu_2 c^2)(c/\omega_2)}} \tag{3-43}$$

Here we have two discrete spectrums coupled with infinite branches of continuum with the interaction $V_{\sigma,\mathbf{k}}(\mathbf{R})$ defined in Eq. (2-19a) and Eq. (2-19b). The position of the center of mass of each dipole molecule are given by $\mathbf{R}_1$, and $\mathbf{R}_2$ respectively.

The stability condition of the two particle modes is given by the location of their discrete spectrums with respect to the continuum, which is similar to the one dipole case. Here we are interested in the integrable case by restricting $\omega_1 < \omega_2 < \omega_c$. In this regime, the accelerated motion of both dipole molecules is maintained.

By applying linear transformation which diagonalize the Hamiltonian, we have

$$H = \tilde{\omega}_1 Q_1^* Q_1 + \tilde{\omega}_2 Q_2^* Q_2 + \sum_{\sigma} \int' d\mathbf{k} \ \omega_{\mathbf{k}} Q_{\sigma,\mathbf{k}}^* Q_{\sigma,\mathbf{k}} \tag{3-44}$$

The explicit forms of these new normal modes Q_1, Q_2, $Q_{\sigma,\mathbf{k}}$ and the shifted frequencies $\tilde{\omega}_1$ and $\tilde{\omega}_2$ are given in Appendix D. Their time evolutions are given by

$$Q_1(t) = Q_1(0)e^{-i\tilde{\omega}_1 t} \quad , \quad Q_2(t) = Q_2(0)e^{-i\tilde{\omega}_2 t} \quad , \quad Q_{\sigma,\mathbf{k}}(t) = Q_{\sigma,\mathbf{k}}(0)e^{-i\omega_{\mathbf{k}} t} \quad (3\text{-}45)$$

3.5.2 Forces from the overlapped dressings

In this section we shall calculate the classical van der Waals force analogous to quantum systems [29]. It is originated from the overlapped dressings. One can carry out the same procedure in Section 3.2 with $O(\lambda^2)$ approximation, and obtain the vector potential associated to the dressing of the Q_1 and Q_2 are given by Eq. (3-16) and Eq. (3-17) with the modification of the position of the center of mass. For instance, we have the vector potential of TE wave associated to the dressings of each dressed steady state given to λ order by

$$\begin{aligned} \mathbf{A}_{1,TE}(\mathbf{r},t) &\approx 4\sqrt{2}\lambda_1 Q_1(0)\sin(\tilde{\omega}_1 t)\sum_{mn}\frac{n\Delta_{mn}}{bc^2\sqrt{c}\sqrt{\alpha_{mn}^2-(\frac{\omega_1}{c})^2}}C_{mn}^2 W_{1,mn}(\mathbf{R}_1) \\ &\times \left[-\frac{n\pi}{b}W_{1,mn}(\mathbf{r})\hat{e}_x+\frac{m\pi}{a}W_{2,mn}(\mathbf{r})\hat{e}_y\right]e^{-\sqrt{\alpha_{mn}^2-\left(\frac{\omega_1}{c}\right)^2}|z-R_{1z}|} \quad (3\text{-}46) \end{aligned}$$

$$\begin{aligned} \mathbf{A}_{2,TE}(\mathbf{r},t) &\approx 4\sqrt{2}\lambda_2 Q_2(0)\sin(\tilde{\omega}_2 t)\sum_{mn}\frac{n\Delta_{mn}}{bc^2\sqrt{c}\sqrt{\alpha_{mn}^2-(\frac{\omega_2}{c})^2}}C_{mn}^2 W_{1,mn}(\mathbf{R}_2) \\ &\times \left[-\frac{n\pi}{b}W_{1,mn}(\mathbf{r})\hat{e}_x+\frac{m\pi}{a}W_{2,mn}(\mathbf{r})\hat{e}_y\right]e^{-\sqrt{\alpha_{mn}^2-(\frac{\omega_2}{c})^2}|z-R_{2z}|} \quad (3\text{-}47) \end{aligned}$$

In Figure 3.11 we plot the z direction profile of the x component vector potential $\mathbf{A}_{TE_{01}}(a/2, b/2, z)$ associated with each dressing given in Eq. (3-46) and Eq. (3-47). Here the parameters are given $\lambda_1 = \lambda_2 = 0.1$, $\mu_1 = 2\mu_2 = 1$, and $\omega_1 = 2\omega_2 = 2.5$. The center of mass of each particle are given by $R_{1x} = R_{2x} = a/2$, $R_{1y} = R_{2y} = b/2$ and $R_{1z} = -R_{2z} = -0.5$. In the figure, the dashed line is the dressing of each dressed state and the solid line is the sum of them.

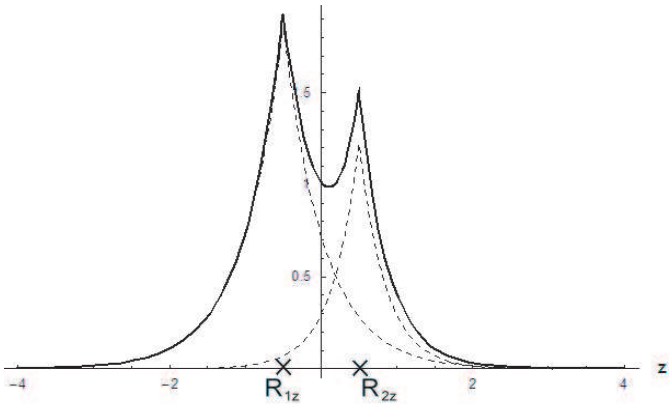

Figure 3.11: Overlap dressings of two dipoles. We plot the TE_{01} modes of the dressings of both dipoles. The dashed lines correspond to the dressing of each dipole while the solid line is the sum of them. The particles are located at $z = -0.5$, and $z = 0.5$.

In the following we calculate the forces acting on the center of mass of dipole 1 due to the overlap dressing shown in Figure 3.11. By taking the derivative of the Hamiltonian in Eq. (3-42) with respect to $\mathbf{R}_1$, we have

$$\begin{aligned} \mathbf{F}_1 &= -\frac{\partial H}{\partial \mathbf{R}_1} \\ &= -\lambda_1 \sum_{\sigma} \int' d\mathbf{k} \left(\frac{\partial V_{\sigma,\mathbf{k}}(\mathbf{R}_1)}{\partial \mathbf{R}_1} q_{\sigma,\mathbf{k}}(t) - \frac{\partial V^*_{\sigma,\mathbf{k}}(\mathbf{R}_1)}{\partial \mathbf{R}_1} q^*_{\sigma,\mathbf{k}}(t) \right) (q_1(t) - q_1^*(t)) \end{aligned} \quad (3\text{-}48)$$

To calculate the force associated to the dressed steady states Q_1, and Q_2, we let

$$Q_{\sigma,\mathbf{k}}(0) = 0 \quad (3\text{-}49)$$

Substituting Eq. (3-49), and Eq. (3-45) into the inverse transformation of $q_1(t)$, $q_{\sigma,\mathbf{k}}(t)$ given in Eq. (D-18) and Eq. (D-20) respectively, we have the leading order of $q_1(t)$ and $q_{\sigma,\mathbf{k}}(t)$ in λ as

$$q_1(t) \approx q_1(0) e^{-i\tilde{\omega}_1 t} \quad (3\text{-}50)$$

$$
\begin{aligned}
q_{\sigma,\mathbf{k}}(t) &\approx -\lambda_1 V^*_{\sigma,\mathbf{k}}(\mathbf{R}_1) Q_1(0) \left(\frac{e^{-i\tilde{\omega}_1 t}}{\omega_1 - \omega_{\mathbf{k}}} + \frac{e^{i\tilde{\omega}_1 t}}{\omega_1 + \omega_{\mathbf{k}}} \right) \\
&\quad -\lambda_2 V^*_{\sigma,\mathbf{k}}(\mathbf{R}_2) Q_2(0) \left(\frac{e^{-i\tilde{\omega}_2 t}}{\omega_2 - \omega_{\mathbf{k}}} + \frac{e^{i\tilde{\omega}_2 t}}{\omega_2 + \omega_{\mathbf{k}}} \right) \qquad (3\text{-}51)
\end{aligned}
$$

Substituting Eq. (3-50) and the first line of the right hand side of Eq. (3-50) into Eq. (3-48), one can see it has the same form as Eq. (3-39). This is the force acting on the center of mass of dipole 1 from the boundary, which has been studied in Section 3.4.

Here we are interesting in the forces due to the overlapped dressings. Substituting Eq. (3-50) and the second term with $Q_2(0)$ in Eq. (3-50), into Eq. (3-48), we have the force associated with the overlapped dressings,

$$
\begin{aligned}
\mathbf{F}_1^{od} &= -2\lambda_1\lambda_2 Q_1(0) Q_2(0) \sin(\tilde{\omega}_1 t) \sum_\sigma \int' d\mathbf{k} \\
&\times \left[i V^*_{\sigma,\mathbf{k}}(\mathbf{R}_2) \frac{\partial V_{\sigma,\mathbf{k}}(\mathbf{R}_1)}{\partial \mathbf{R}_1} \left(\frac{e^{-i\tilde{\omega}_2 t}}{\tilde{\omega}_2 - \omega_{\mathbf{k}}} + \frac{e^{i\tilde{\omega}_2 t}}{\tilde{\omega}_2 + \omega_{\mathbf{k}}} \right) + c.c \right] \qquad (3\text{-}52)
\end{aligned}
$$

where the superscript "od" denotes the force associated with overlapped dressing. With the interaction given in Eq. (2-19a) and Eq. (2-19b), we can carry out the integration explicitly. The x, and y components are given by

$$
\begin{aligned}
\mathbf{F}_1^{od}|_{x,y} &= -8\lambda_1\lambda_2 q_1(0) q_2(0) \sin\tilde{\omega}_1 t \sin\tilde{\omega}_2 t \sum_{mn} \pi C^2_{mn} W_{1,mn}(\mathbf{R}_2) \\
&\times \left\{ \frac{m\pi}{a} \sin(\frac{m\pi R_{1x}}{a}) \sin(\frac{n\pi R_{1y}}{b}) \hat{e}_x - \frac{n\pi}{b} \cos(\frac{m\pi R_{1x}}{a}) \cos(\frac{n\pi R_{1y}}{b}) \hat{e}_y \right\} \\
&\times \left\{ \Delta_{mn} (\frac{n}{bc})^2 \frac{e^{-\sqrt{\alpha^2_{mn} - (\frac{\omega_2}{c})^2}|R_{z_{12}}|}}{\sqrt{\alpha^2_{mn} - (\frac{\omega_2}{c})^2}} + (\frac{m}{a\omega_1})^2 \Big[\alpha_{mn} e^{-\alpha_{mn}|R_{z_{12}}|} \right. \\
&\left. - \sqrt{\alpha^2_{mn} - (\frac{\omega_2}{c})^2} e^{-\sqrt{\alpha^2_{mn} - (\frac{\omega_2}{c})^2}|R_{z_{12}}|} \Big] \right\} \qquad (3\text{-}53)
\end{aligned}
$$

while the z component is given by

$$\begin{aligned}\mathbf{F}_1^{od}|_z &= -8\lambda_1\lambda_2 q_1(0)q_2(0)\mathrm{sgn}(R_{z_{12}})\sin\tilde{\omega}_1 t\sin\tilde{\omega}_2 t\sum_{mn}\pi C_{mn}^2 W_{1,mn}(\mathbf{R}_1) \\ &\times W_{1,mn}(\mathbf{R}_2)\Bigg\{\Delta_{mn}(\frac{n}{bc})^2 e^{-\sqrt{\alpha_{mn}^2-(\frac{\omega_2}{c})^2}|R_{z_{12}}|}+(\frac{m}{a\omega_2})^2\Big[\alpha_{mn}^2 e^{-\alpha_{mn}|R_{z_{12}}|} \\ &-(\alpha_{mn}^2-(\frac{\omega_2}{c})^2)e^{-\sqrt{\alpha_{mn}^2-(\frac{\omega_2}{c})^2}|R_{z_{12}}|}\Big]\Bigg\} \qquad (3\text{-}54)\end{aligned}$$

where the $R_{z_{12}} \equiv R_{1z} - R_{2z}$ denotes the distance between the two particles. The dominant contribution is coming from the TE_{01} mode which proportional to the term Δ_{01}, which is negative sign. Therefore one can see the force between two dipoles is attractive as shown in Figure 3.12.

In Figure 3.12 we show the dominant component TE_{01} mode in Eq. (3-54) as a function of the distance between two dipoles, i.e $R_{z_{12}}$. The force is in the unit of $\mu_1 c^2/b$ and we choose the same parameters as the Figure 3.11.

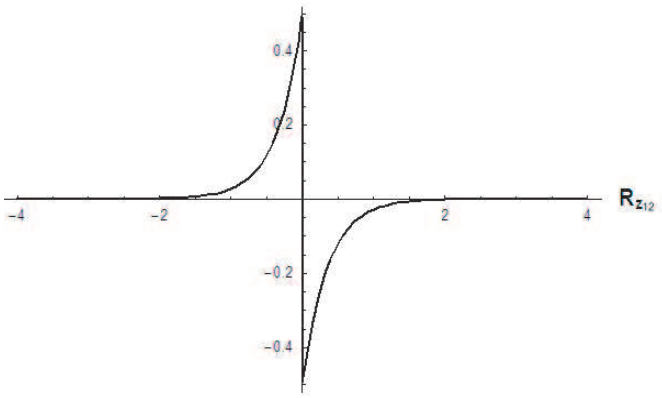

Figure 3.12: Classical van der Waals force. We plot the TE_{01} component of $\mathbf{F}_{1,od}|_z$ as function of the distance of two dipoles.

3.6 Discussion

We have shown that the absence of the resonance in the classical matter-field interaction leads to the existence of a quantum-like ground state in the classical system such as the existence of classical dressed ground state with the non-stopping accelerated motion, the classical Casimir-Polder force due to the overlapped dressing cloud with the walls of waveguide, and the classical van der Waals force due to the overlapped dressing cloud of two dipole molecules.

In fact there is another approach of calculating the forces acting on the center of mass in addition to the approach presented in Section 3.5.2. It is obtained through the derivative of the diagonalized Hamiltonian in Eq. (3-44) with respect to $\mathbf{R}_1$. As shown in Appendix D, the shifted frequencies $\tilde{\omega}_1$, $\tilde{\omega}_2$ and the perturbed actions $Q_1^* Q_1$, $Q_2^* Q_2$, and $Q_{\sigma,\mathbf{k}}^* Q_{\sigma,\mathbf{k}}$ all depend on $\mathbf{R}_1$. Therefore we can identify the force coming from shifted frequencies (denoted as $\mathbf{F}_{1,\delta\tilde{\omega}}$), and perturbed actions (denoted as $\mathbf{F}_{1,\delta\tilde{J}}$) separately in this approach. We have verified this approach is identical to the one in previous section.

Here we shall analyze the classical van der Waals force obtained in Eq. (3-53) and Eq. (3-54) from offered this approach. In fact one can verify the van der Waals force (which has $\mathbf{R}_{z_{12}}$ dependence) from frequency shift $\mathbf{F}^{od}_{1,\delta\tilde{\omega}}$ is $O(\lambda_1^2\lambda_2^2)$, while from perturbed actions $\mathbf{F}^{od}_{1,\delta\tilde{J}}$ is $O(\lambda_1\lambda_2)^2$. As a result, the dominant term of classical van der Waals force is coming from $\mathbf{F}^{od}_{1,\delta\tilde{J}} \sim O(\lambda^2)$ with the higher order correction from $\mathbf{F}^{od}_{1,\delta\tilde{\omega}} \sim O(\lambda^4)$.

On the other hand, in quantum ground state the action is independent of $\mathbf{R}_{z_{12}}$ as it is given by $\hbar/2$. As a result the quantum van der Waals force is purely

[2]This result is not valid for the case where $\omega_1 = \omega_2$. In that case, due to the degeneracy of the both frequencies, the $\mathbf{F}^{od}_{1,\delta\tilde{\omega}}$ becomes $O(\lambda_1\lambda_2)$ which is the same order as $\mathbf{F}^{od}_{1,\delta\tilde{J}}$.

due to frequency shift, which is the same as $\mathbf{F}^{od}_{1,\delta\tilde{\omega}} \sim O(\lambda^4)$. Comparing with the dominate term in classical van der Waals force $\mathbf{F}^{od}_{1,\delta\tilde{J}}$, we see we see our classical van der Waal force is order of magnitude greater than the quantum van der Waals force of the dressed ground state.

We also comment about the stability of the non-stopping motion for the very long time scale. In our Hamiltonian in Eq. (2-17), we had neglected the field-field component coming from the term proportional to $\mathbf{A}^2$ in Eq. (2-6). This term may destabilize the steady motion which we have obtained through the Bogoliubov transformation. However as we shall discussed in next chapter , the time scale of decay rate is proportional to the inverse of square of the interaction term. As a result our steady solution is a good approximation of the actual motion up to the time scale of $\omega_1 t \sim \lambda^{-4}$. After this long very long time, our steady motion will gradually stop. In other words, the approximation of exact Hamiltonian by Friedrichs model is only valid within that time scale. Nonetheless, the Friedrichs model is powerful as well as simple enough to study the effect of resonances.

Finally we numerate a possible extension of our approach to several interesting situations that have not been studied in this dissertation. These include the field as a heat bath in thermal equilibrium, or the scattering of the field as a wavepacket by dressed steady dipole.

It is also interesting to study the case where the discrete spectrum is slightly embedded in the continuum, for instance $\omega_1 - \omega_c \sim \lambda^2$. In that case the perturbation analysis fails due to the small denominator $1/(\omega_{\mathbf{k}} - \omega_1)$. However as shown in Eq. (3-11) that we may have the situation that the discrete spectrum is shifted outside the continuum, i.e., $\tilde{\omega}_1 < \omega_c < \omega_1$. Hence the Friedrichs solution of Q_1, $Q_{\sigma,\mathbf{k}}$ presented in Section 3.1 is still valid even in this case.

We have chosen a specific initial condition so that the rotation modes of the

dipole is absent in our Hamiltonian. For the general situation, the rotation mode will be excited, therefore the Hamiltonian is no longer in bi-linear form. In that case we lose the Bogoliubov diagonalization, and the system may become non-integrable. It is interesting to study how this non-linear effect from the rotation mode destroys the classical dressed ground state studied in our bi-linear Hamiltonian sytem.

In the next chapter we shall consider the unstable regime where $\omega_1 > \omega_c$.

Chapter 4

Classical radiation damping in waveguide

4.1 Diagonalization of the Hamiltonian

In this chapter we consider the unstable case that $\omega_1 > \omega_c$. For this case there appears resonance singularities at $\omega_{\mathbf{k}} = \omega_1$ in the perturbation expansion of Q_1 in Eq. (3-2a) As a result the invariant of motion $|Q_1|^2$ that would reduced to the unperturbed invariant $|q_1|^2$ in the limit $\lambda \to 0$ is destroyed. This implies that or classical Friedrichs model is non-integrable in the sense of Poincaré [3].

For this case, it is well known that the total Hamiltonian of the Friedrichs model is diagonalized only by the renormalized field mode $Q_{\sigma,\mathbf{k}}$ given in Eq. (3-2b) [5]. This gives,

$$H = \sum_{\sigma} \int' d\mathbf{k}\ \omega_{\mathbf{k}} Q^*_{\sigma,\mathbf{k}} Q_{\sigma,\mathbf{k}} \tag{4-1}$$

For this case, the inverse transformations are given by,

$$q_1 = -\lambda \sum_{\sigma',m',n'} \int dl \left[\frac{(\omega_{\mathbf{l}} + \omega_1) V_{\sigma',\mathbf{l}}(\mathbf{R})}{\xi_1^-(\omega_{\mathbf{l}})} Q_{\sigma',\mathbf{l}} + \frac{(\omega_{\mathbf{l}} - \omega_1) V^*_{\sigma',\mathbf{l}}(\mathbf{R})}{\xi_1^+(\omega_{\mathbf{l}})} Q^*_{\sigma',\mathbf{l}} \right] \tag{4-2}$$

$$q_{\sigma,\mathbf{k}} = Q_{\sigma,\mathbf{k}} + 2\lambda^2 \omega_1 V^*_{\sigma,\mathbf{k}}(\mathbf{R}) \sum_{\sigma',m',n'} \int dl \left[\frac{V_{\sigma',\mathbf{l}}(\mathbf{R}) Q_{\sigma,\mathbf{l}}}{\xi_1^-(\omega_{\mathbf{l}})(\omega_{\mathbf{l}} - \omega_{\mathbf{k}} - i\epsilon)} + \frac{V^*_{\sigma',l}(\mathbf{R}) Q^*_{\sigma',l}}{\xi_1^+(\omega_{\mathbf{l}})(\omega_{\mathbf{l}} + \omega_{\mathbf{k}})} \right] \tag{4-3}$$

Recall that the wavevector $\mathbf{k} \equiv (m\pi/a, n\pi/b, k)$.

4.2 Radiation damping of the dipole

In this section we focus our attention on the time evolution of the particle mode $q_1(t)$ in the unstable regime.

We start from the same initial condition in Eq. (3-19). Substituting the initial condition into Eq. (3-2b), we have the time evolution of the new normal modes,

$$Q_{\sigma,\mathbf{k}}(t) = -2\lambda\omega_1 q_1(0)\frac{V^*_{\sigma,\mathbf{k}}(\mathbf{R})}{\xi_1^+(\omega_\mathbf{k})}e^{-i\omega_\mathbf{k}t} \tag{4-4}$$

Applying the inverse transformation in Eq. (4-3) on $Q_{\sigma,\mathbf{k}}(t)$, we obtain

$$q_1(t) = 4\lambda^2\omega_1 q_1(0)\sum_{\sigma,m,n}\int_0^\infty dk\frac{|V_{\sigma,\mathbf{k}}(\mathbf{R})|^2}{|\xi_1^+(\omega_\mathbf{k})|^2}\left[(\omega_\mathbf{k}+\omega_1)e^{-i\omega_\mathbf{k}t}+(\omega_\mathbf{k}-\omega_1)e^{i\omega_\mathbf{k}t}\right] \tag{4-5}$$

where $\mathbf{k} \equiv (m\pi/a, n\pi/b, k)$. Here we specify the discrete spectrum is embedded in the continuous branches up to $(m,n) = (m_s, n_s)$ modes, i.e.

$$\omega_c < \omega_1 < \alpha_{m_s,n_s+1} \tag{4-6}$$

As a result we have resonance singularities for each (m,n) mode in Eq. (4-5) up to (m_s, n_s). These poles appear in the denominator $|\xi_1^+(\omega_\mathbf{k})|^2$, and the location of the poles on complex $\omega_\mathbf{k}$ plane is given by $\omega_\mathbf{k} = z_1,\ z_1^*$, which are the solution of

$$\xi_1^+(z_1) = 0 \qquad \xi_1^-(z_1^*) = 0 \tag{4-7}$$

It was shown [13] the solution z_1 is located at the lower complex plane,

$$z_1 = \tilde{\omega}_1 - i\gamma \tag{4-8}$$

with the shifted frequency $\tilde{\omega}_1$, and the decay rate γ. In terms of the function of k, the location of these poles of a given $(m,n) \leq (m_s, n_s)$ mode are given by

$$k_{mn,1+} = \sqrt{(z_1^*/c)^2 - \alpha_{mn}^2} \quad , \quad k_{mn,1-} = \sqrt{(z_1/c)^2 - \alpha_{mn}^2} \tag{4-9}$$

$$k_{mn,2+} = -\sqrt{(z_1/c)^2 - \alpha_{mn}^2} \quad , \quad k_{mn,2-} = -\sqrt{(z_1^*/c)^2 - \alpha_{mn}^2} \tag{4-10}$$

with $\pm$ denotes the pole at upper and lower complex k plane, respectively. As we shall see in Figure 4.1 that $k_{mn,2+}$, $k_{mn,2-}$ will never contribute due to the contour we choose. In additional to the poles, there is a pair of branch points located at imaginary axis $k = \pm i\alpha_{mn}$ for given mode, which comes from the dispersion relation in Eq. (2-15).

For $t > 0$, we deform the contour of integration over k in Eq. (4-5) to separate the pole contribution and the background-integral contribution. This gives

$$q_1(t) = q_{1p}(t) + q_{1b}(t) \tag{4-11}$$

As shown in Figure 4.1, for the term with $\exp(-i\omega_{\mathbf{k}}t)$ in Eq. (4-5), we choose the

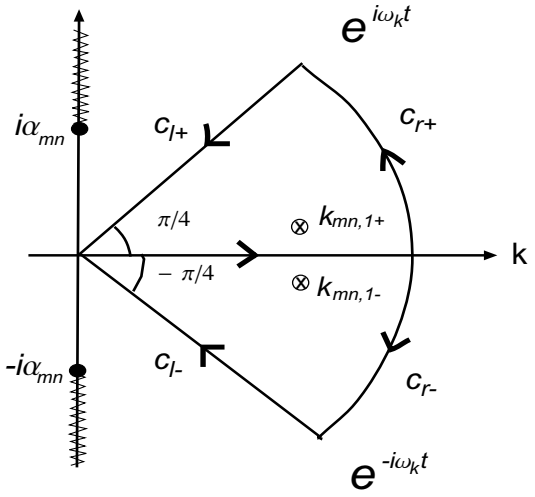

Figure 4.1: Contour deformation of the integration in $q_1(t)$. For illustration purpose, we show only the deformation for a given (m, n) mode. The pole for the case $(m, n) \leq (m_s, n_s)$ is denoted as $\otimes$. For the case $(m, n) > (m_s, n_s)$ there is no pole contribution. There are two branch points located at $k = \pm i\alpha_{mn}$, and the the zig-zag lines are the corresponding branch cuts. The C_{r+}, and C_{r-} correspond to the arc shaped paths, while the C_{l+}, and C_{l-} correspond to the straight line paths at ± 45 degree respectively.

contour going to lower complex plane, while we choose the contour going to upper half plane for the term with $\exp(i\omega_{\mathbf{k}}t)$.

Since our integrand vanishes for large k, the arc shaped paths C_{r+}, and C_{r-} does not contribute. As a result the $\int_0^\infty dk$ can be written as pole contribution and the background-integral corresponding to the paths C_{l+}, and C_{l-} inclined in ± 45 degree, respectively.

For the pole contribution, the term with $\exp(-i\omega_{\mathbf{k}}t)$ encircles the pole at $k_{mn,1-}$ while the term with $\exp(i\omega_{\mathbf{k}}t)$ encircles the pole at $k_{mn,1+}$. With the explicit potential given in Eq. (2-19a), and Eq. (2-19b), we evaluate the residues. This gives the pole contribution up to $O(\lambda^2)$

$$\begin{aligned} q_{1p}(t) \approx\ & 16\lambda^2 q_1(0)\frac{\pi\omega_1}{c}\sum_{m,n}^{m_s,n_s}\left\{\mathrm{Im}\left[\frac{z_1^2|V_{\sigma,\mathbf{k}}(\mathbf{R})|^2_{k=k_{mn,-}}e^{-iz_1t}}{\xi_1^-(z_1)\xi_1^{+'}(z_1)k_{mn,-}}\right]\right. \\ & \left. -i\mathrm{Re}\left[\frac{z_1\omega_1|V_{\sigma,\mathbf{k}}(\mathbf{R})|^2_{k=k_{mn,-}}e^{-iz_1t}}{\xi_1^-(z_1)\xi_1^{+'}(z_1)k_{mn,-}}\right]\right\} \end{aligned} \tag{4-12}$$

with the derivative of $\xi_1^+(\omega)$ defined by

$$\xi_1^{+'}(z_1) \equiv \left.\frac{d\xi_1^+(\omega)}{d\omega}\right|_{\omega=z_1} \tag{4-13}$$

It decays in strictly exponential in time. The decay rate γ can obtained by solving Eq. (4-7) perturbatively, which gives

$$\gamma = 2\pi\lambda^2\sum_\sigma\sum_{m,n}^{m_s,n_s}\frac{|V_{\sigma,\mathbf{k}}(\mathbf{R})|^2_{\omega_{\mathbf{k}}=\omega_1}}{c\chi_{mn}} + O(\lambda^4) \tag{4-14}$$

where the dimensionless χ_{mn} is defined as

$$\chi_{mn} \equiv \sqrt{|1-(\frac{c\alpha_{mn}}{\omega_1})^2|} < 1 \tag{4-15}$$

which measures the relative distance between ω_1 and the cut-off frequencies $c\alpha_{mn}$. Under the pole approximation up to $O(\lambda^2)$, we have

$$\xi_1^+(z) \approx (z-z_1)(z+z_1^*) \tag{4-16}$$

This gives the denominator in front of Eq. (4-12) $\xi_1^-(z_1) \approx -4i\gamma\omega_1 \sim \lambda^2$. As a result, the λ^2 in the numerator is compensated by the factor λ^2 in $\xi_1^-(z_1)$. Hence the leading term of Eq. (4-12) is of the order of λ^0, and we obtain

$$q_{1p}(t) = q_1(0)e^{-i\tilde{\omega}_1 t-\gamma t} \tag{4-17}$$

For the background-integral, we have

$$\begin{aligned} q_{1b}(t) &= -4\lambda^2\omega_1 q_1(0)\sum_{\sigma,m,n}\left[\int_{C_{l-}} dk\frac{|V_{\sigma,\mathbf{k}}(\mathbf{R})|^2}{|\xi_1^+(\omega_{\mathbf{k}})|^2}(\omega_{\mathbf{k}}+\omega_1)e^{-i\omega_{\mathbf{k}}t}\right. \\ &\quad \left. +\int_{C_{l+}} dk\frac{|V_{\sigma,\mathbf{k}}(\mathbf{R})|^2}{|\xi_1^+(\omega_{\mathbf{k}})|^2}(\omega_{\mathbf{k}}-\omega_1)e^{i\omega_{\mathbf{k}}t}\right] \end{aligned} \tag{4-18}$$

By explicitly evaluating these contours, we have

$$\begin{aligned} q_{1b}(t) &= 8\lambda^2 q_1^2(0)\sum_{m,n} C_{mn}^2 W_{1,mn}^2(\mathbf{R}) \\ &\times \left\{ Re\left[\int_0^\infty dk\frac{\left(\frac{n^2\Delta_{mn}}{b^2}-i\frac{m^2k^2c^2}{a^2(\alpha_{mn}^2-ik^2)}\right)e^{-ict\sqrt{\alpha_{mn}^2-ik^2}-i\frac{\pi}{4}}}{c^4[\alpha_{mn}^2-ik^2-(\frac{\omega_1}{c})^2]}\right]\right. \\ &+ \left. i\mathrm{Im}\left[\int_0^\infty dk\frac{\omega_1\left(\frac{n^2\Delta_{mn}}{b^2}-i\frac{m^2k^2c^2}{a^2(\alpha_{mn}^2-ik^2)}\right)e^{-ict\sqrt{\alpha_{mn}^2-ik^2}-i\frac{\pi}{4}}}{c^5\sqrt{\alpha_{mn}^2-ik^2}[\alpha_{mn}^2-ik^2-(\frac{\omega_1}{c})^2]}\right]\right\} \end{aligned} \tag{4-19}$$

Since the $q_{1b}(t)$ has the same structure of the q_{1Z} given in Eq. (3-24), we evaluate this integration by stationary phase approximation. For asymptotic t, we show the leading term is the same as q_{1Z} in Eq. (3-27). Hence for $\omega_1 t \gg 1$, the background-integral decay in power law,

$$q_{1b}(t) \sim \lambda^2(\sqrt{\frac{1}{\omega_1 t}}) \tag{4-20}$$

which is $O(\lambda^2)$ smaller than $q_{1p}(t)$. This background integral gives the non-Markov effect which is non-negligible in a very short time scale $t \sim 1/\omega_1$ and very long time scale $t \gg /\gamma$. The deviation from the exponential decay in short time scale

corresponds to the well-known "Zeno" period in quantum unstable system [14]. Our result shows that for classical radiation damping we have the Zeno period. After the Zeno period, the Markovian effect coming form pole will dominate. In this period ($t \sim 1/\gamma \gg 1/\omega_1$), the particle decays exponentially. For the decay rate given in Eq. (4-14), one may have already realized that by choosing very small χ_{mn} (i.e., $c\alpha_{mn} \approx \omega_1$), one can increase enormously the decay rate of the classical radiation damping inside the waveguide. For order estimation, let us consider the case that ω_1 is embedded only in the lowest continuous mode, i.e. $(m_s, n_s) = (0, 1)$, then the decay rate given in Eq. (4-14) becomes,

$$\gamma = 2\pi\lambda^2\omega_1(\frac{c}{a\omega_1})(\frac{c}{b\omega_1})/\chi_{01} \tag{4-21}$$

It is well known that the decay rate of classical radiation damping in the free space is given by[1] $2\lambda^2\omega_1/3$, which is extremely small due to the small coupling $\lambda \sim 10^{-6}$ in the classical regime. Therefore the relaxation time for a classical HCl dipole in free space is order of 10^{-2}s, which is much slower than that of quantum case, where the electron in hydrogen atom decay in 10^{-9}s.

However, as mentioned before that in the waveguide we have extra parameters to control the decay rate. In order to enhance it, we consider the case of a narrow waveguide where $b = 10a$. Then we calculate the decay rate of HCl dipole in the case[2], $\omega_1 = \omega_c + \lambda$ (i.e., $b \sim b_c + \lambda \sim 10\mu$m) which gives $\chi_{01} \sim \sqrt{\lambda} \sim 10^{-4}$. As a result, we found the relaxation time of the classical HCl dipole becomes 10^{-7}s which is 10^5 times faster than in the case of free space! As a result, by controlling the size of the waveguide, not only we can suppress the classical radiation damping,

[1] One can obtained it through Lorentz-Abraham equation, or considering the Friedrichs model in the case of free space.

[2] This is the closest distance we can obtain in unstable regime, since the spectrum will be "kicked" out to stable regime by interaction if we go further close.

but also enhance it tremendously, so that the relaxation time scale is much closer to the quantum regime. Also we shall in the discussion of this chapter that the group velocity of emitted field become $10^{-4}c$ under the same consideration. Therefore it turns out that the size of the emitted field for classical HCl dipole inside the waveguide is order of 10cm, which is shorter than the wavelength in the hydrogen atom which is 30cm!

After $t \gg 1/\gamma$, we shall again see the non-Markovian effect from q_{1p} plays an important role. This corresponds to the long time tail known in quantum unstable system. The traditional approach of radiation damping did not address the existence of the classical Zeno period and the long time tail [25], [26].

In Figure 4.2–Figure 4.5 we show some plots of our theoretical results. We have chosen the same unit system as pervious chapter, that the unit of length is b, the unit of time is b/c, and the unit of mass is μ_1. In all the figures in this chapter, we fixed $b = 2a = 1$, which gives the two lowest cut-off frequencies $c\alpha_{01} = \pi$, $c\alpha_{10} = 2\pi$ correspond to TE_{01} and TE_{10} modes, respectively. We choose the discrete spectrum $\pi < \omega_1 = 3.8 < 2\pi$ to ensure that it is well separated from TE_{10} mode. For this case, the contribution from the TE_{10} mode may be neglected. Hence we shall consider only the contribution only from TE_{01} mode, which is proportional to Δ_{01}.

By choosing $\lambda = 0.1$, we have the relaxation time $t_r = 1/2\gamma \approx 8.8$ where γ can be estimated by Eq. (4-14).

In Figure 4.2 we show the trajectory $(x_1(t), p_1(t))$ of the unstable particle in phase space for $0 \leq t \leq 7t_r$, We obtain $(x_1(t), p_1(t))$ by substituting Eq. (4-11) into the canonical transformation in Eq. (2-7). The integration in Eq. (4-19) of $q_{1b}(t)$ was evaluated numerically. At $t = 0$ we have $x_1(0) = 0.73$ and $p_1(0) = 0$. As time goes on, we see that the motion of the particle eventually stops.

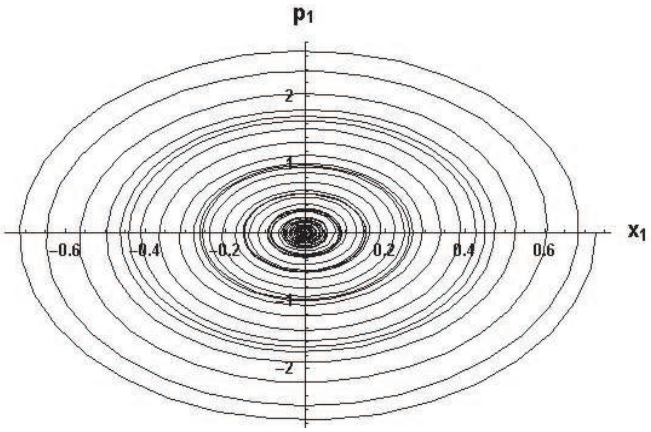

Figure 4.2: Time evolution of unstable particle in phase space.

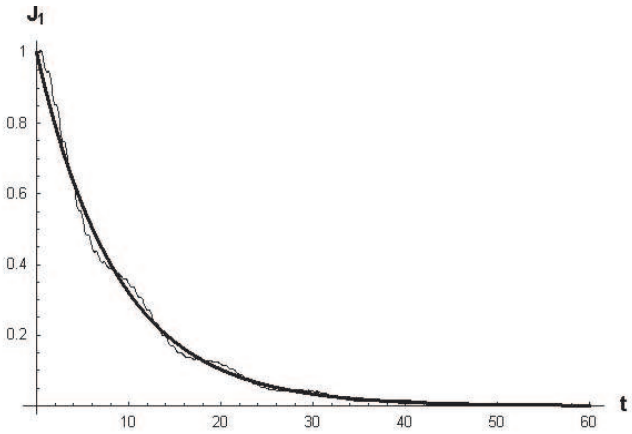

Figure 4.3: Exponential decay of action variable $J_1(t)$ in unstable regime. The thin line includes $q_{1b}(t)$ while the thick line is simply pole contribution $q_{1p}(t)$.

In Figure 4.3 we show the time evolution of the action variable $J_1(t) \equiv |q_1(t)|^2$ of the unstable particle under with the same setting as in the phase space plot. The thick line is the pole contribution given in Eq. (4-17) while the thin line with oscillations includes both the pole and background-integral contribution. The

integration in the $q_{1b}(t)$ in Eq. (4-19) is performed numerically. We see the deviation of the exponential decay is negligible during the time scale of $t \sim t_r = 8.5$.

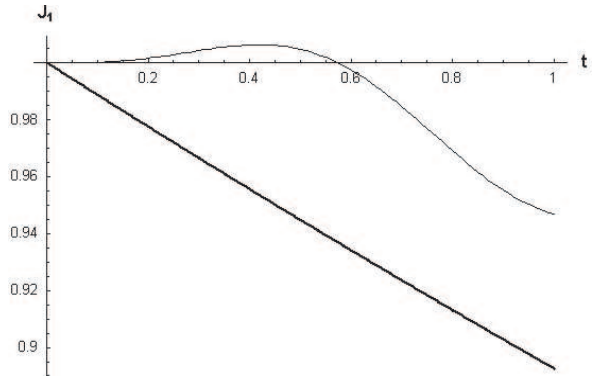

Figure 4.4: Classical Zeno effect in $J_1(t)$. This is the magnification of early time of Figure 4.3. The thick line corresponds to $|q_{1p}(t)|^2$ while the thin line includes the correction from $q_{1b}(t)$.

In Figure 4.4 we magnify a portion of the short time scale $t \sim 1/\omega_1 \sim 0.26$ of Figure 4.3. The thick line is again only the pole contribution while the thin line is the summation of the pole contribution and the background-integral. It shows the non-Markovian effect from background-integral is indeed non-negligible in this short time scale of the classical Zeno period.

In Figure 4.5 we magnify a portion of the very long time scale $t \sim 5/\gamma$ of Figure 4.3. The thick line is again only the pole contribution while the thin line is the summation of the pole contribution and the background-integral. It shows the non-Markovian effect coming from background-integral term is non-negligible in this long-time-tail period.

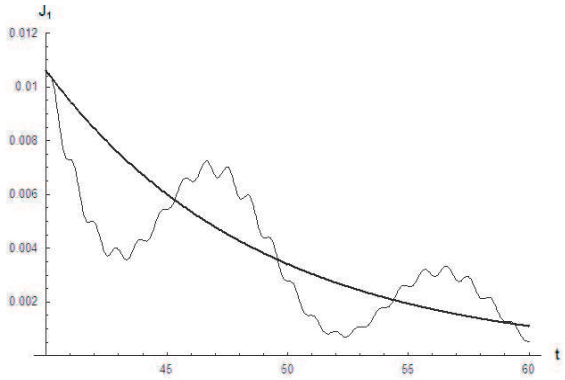

Figure 4.5: Long time tail in $J_1(t)$. This is the magnification of $t \sim 40 - 60$ of Figure 4.3. The thick line corresponds to $|q_{1p}(t)|^2$ while the thin line includes the correction from $q_{1b}(t)$.

4.3 Propagation of the radiated field

In this section we shall calculate the vector potential $\mathbf{A}_{TE}$ of the field radiated by the unstable particle for the same situation considered in the previous Section 4.2. In this situation , $\mathbf{A}_{TM}$ modes gives only a small correction.

We start with the same initial condition discussed in Section 4.2. Substituting $Q_{\sigma,\mathbf{k}}(t)$ in Eq. (4-4) into Eq. (4-3), we have

$$\begin{aligned} q_{\sigma,\mathbf{k}}(t) &= -2\lambda\omega_1 q_1(0)\frac{V^*_{\sigma,\mathbf{k}}(\mathbf{R})}{\xi_1^+(\omega_\mathbf{k})}e^{-i\omega_\mathbf{k}t} - 4\lambda^3\omega_1^2 V^*_{\sigma,\mathbf{k}}(\mathbf{R}) \\ &\quad \times \sum_{\sigma'}\int' d\mathbf{l}\frac{|V_{\sigma,\mathbf{l}}|^2}{|\xi_1^+(\omega_\mathbf{l})|^2}\left[\frac{e^{-i\omega_\mathbf{l}t}}{(\omega_\mathbf{l}-\omega_\mathbf{k}-i\epsilon)} + \frac{e^{i\omega_\mathbf{l}t}}{(\omega_\mathbf{l}+\omega_\mathbf{k})}\right] \end{aligned} \tag{4-22}$$

where we have used the pole approximation $\xi_1^+(\omega_\mathbf{k})$ in Eq. (4-16). Comparing the integration term with $q_1(t)$ in Eq. (4-5), they have similar structure that they both have poles located at $\omega_\mathbf{k} = z_1, z_1^*$ in the denominator $1/|\xi_1^+(\omega_\mathbf{k})|^2$. As we have seen in the previous section, that the residue of $1/|\xi_1^+(\omega_\mathbf{k})|^2$ at $\omega_\mathbf{k} = z_1$, z_1^* is proportional to $\lambda^{-2} \gg 1$. Hence the integration in Eq. (4-22) can be approximated by the pole contribution associated with $1/|\xi_1^+(\omega_\mathbf{k})|^2$. Notice there is another singularity

($\omega_{\mathbf{l}} = \omega_{\mathbf{k}} + i\epsilon$) in the denominator of Eq. (4-22). Since we choose the same contour as discussed in Section 4.2, this pole will not contribute for $t > 0$.

Under the pole approximation, we then obtain for $\lambda \ll 1$,

$$q_{\sigma,\mathbf{k}}(t) \approx -\lambda q_1(0) V^*_{\sigma,\mathbf{k}}(\mathbf{R}) \left[\frac{e^{-iz_1 t}}{z_1 - \omega_{\mathbf{k}}} + \frac{e^{iz_1^* t}}{z_1^* + \omega_{\mathbf{k}}} \right] - 2\lambda \frac{\omega_1 q_1(0) V^*_{\sigma,\mathbf{k}}(\mathbf{R}) e^{-i\omega_{\mathbf{k}} t}}{(\omega_{\mathbf{k}} + z_1^*)(\omega_{\mathbf{k}} - z_1)} \quad (4\text{-}23)$$

Comparing this with the corresponding stable case of $q_{\sigma,\mathbf{k}}(t)$ in Eq. (3-28), it shows the $\tilde{\omega}_1$ in the stable case is replaced by z_1 and z_1^* in the unstable case. For time $t \gg 1/\gamma$, we have the line shape

$$|q_{\sigma,\mathbf{k}}|^2 \propto \frac{\gamma}{(\omega_{\mathbf{k}} - \tilde{\omega}_1)^2 + \gamma^2} \quad (4\text{-}24)$$

which is Lorentzian with a peak at $\omega_{\mathbf{k}} = \omega_1$, and the width 2γ. Substituting $q_{\sigma,\mathbf{k}}(t)$ in Eq. (4-23) into Eq. (2-10) we calculate the vector potential of TE wave radiated by the unstable particle mode. Since $q_{\sigma,\mathbf{k}}$ contains pole located at $k = k_{mn,1-}$, $k_{mn,2+}$ as defined in Eq. (4-9), Eq. (4-10), we again separate the pole contribution and background-integral by choosing appropriate contours. This gives

$$\mathbf{A}_{TE}(\mathbf{r}, t) = \mathbf{A}^C_{TE}(\mathbf{r}, t) + \mathbf{A}^Z_{TE}(\mathbf{r}, t) + \mathbf{A}^R_{TE}(\mathbf{r}, t) \quad (4\text{-}25)$$

For the case $|z| < ct$ (inside the lightcone), the leading team of these components are given by

$$\mathbf{A}^C_{TE} \propto \lambda^3 q_1(0) e^{-i\omega_1 - \gamma t} \quad (4\text{-}26)$$

$$\begin{aligned} \mathbf{A}^Z_{TE} &\approx 2\lambda q_1(0) \sum_{mn} \frac{n}{b} \sqrt{\frac{2\Delta^2_{mn}}{\pi^2 c}} C^2_{mn} W_{1,mn}(\mathbf{R}) \Big[-\frac{n\pi}{b} W_{1,mn}(\mathbf{r}) \hat{e}_x + \frac{m\pi}{a} W_{2,mn}(\mathbf{r}) \hat{e}_y \Big] \\ &\quad \times \left(i\omega_1 \int_{C_{l-}} dk \frac{(e^{ikz} + e^{-ikz}) e^{-i\omega_{\mathbf{k}} t}}{\omega_{\mathbf{k}} (\omega_{\mathbf{k}} + z_1^*)(\omega_{\mathbf{k}} - z_1)} + c.c \right) \end{aligned} \quad (4\text{-}27)$$

$$\begin{aligned} \mathbf{A}^R_{TE} &\approx -4\sqrt{2}\lambda q_1(0) \sum_{mn}^{m_s, n_s} (\frac{n\Delta_{mn}}{b}) C^2_{mn} W_{1,mn}(\mathbf{R}) \frac{\omega_1 e^{-iz_1 t + iz k_{mn,1-}}}{c^2 \sqrt{c} \tilde{\omega}_1 k_{mn,1-}} \\ &\quad \times \Big[-\frac{n\pi}{b} W_{1,mn}(\mathbf{r}) \hat{e}_x + \frac{m\pi}{a} W_{2,mn}(\mathbf{r}) \hat{e}_y \Big] + c.c \end{aligned} \quad (4\text{-}28)$$

with the contour $C_{l,\pm}$ are defined as the straight line inclined at $\pm$ 45 degree in Figure 4.1.

The first two components in Eq. (4-25) are the background-integrals and the last component is pole contribution. We see $\mathbf{A}^C_{TE}$ is the decaying dressing cloud associated with the unstable particle. Due to the virtual processes, the dressing of unstable particle becomes $O(\lambda^3)$, which is negligible if compare with the other two components. $\mathbf{A}^Z_{TE}(\mathbf{r},t)$ is a travelling waves which corresponds to the "Zeno field" associated with the quantum Zeno effect mentioned before. $\mathbf{A}^R_{TE}(\mathbf{r},t)$ is a resonance field which only exist in the unstable case.

For $|z| > ct$ (outside lightcone), the contour of the term with $\exp(ikz - i\omega_{\mathbf{k}}t)$ in $\mathbf{A}^Z_{TE}$ should be replaced by C_{l+} while the term with $\exp(-ikz - i\omega_{\mathbf{k}}t)$ remain C_{l-}. Under this consideration, we verify the resonance field $\mathbf{A}^R_{TE}$ vanishes outside the lightcone. Moreover, as shown in Figure 4.6 that we verify the total $\mathbf{A}_{TE}$ is zero outside the lightcone with the integration in Eq. (4-26) and Eq. (4-27) performed numerically.

In Figure 4.6 we show the x component of the $\mathbf{A}_{TE_{01}}(a/2, b/2, z, t)$ mode at time $t = 20$ as a function of z (length is measured in b). We choose the same parameters as in the previous section that the ω_1 is embedded inside TE_{01} mode and it is well separated from other modes. The thin line, dashed line, and thick line correspond to Zeno field, resonance field, and the total vector potential $\mathbf{A}_{TE_{01}}$, respectively. The integration in the $\mathbf{A}^C_{TE_{01}}$ and $\mathbf{A}^Z_{TE_{01}}$ are performed numerically. We see the total radiated field obeys causality as it vanishes outside the lightcone ($z = 20$). Inside the lightcone, there is a region where the resonance field and Zeno field are out of phase, hence they cancel each other. As a result, the peak of the total radiated field is far from the edge. Due to the effective mass, the peak shall travel with a group velocity slower than the speed of light, while the edge keeps

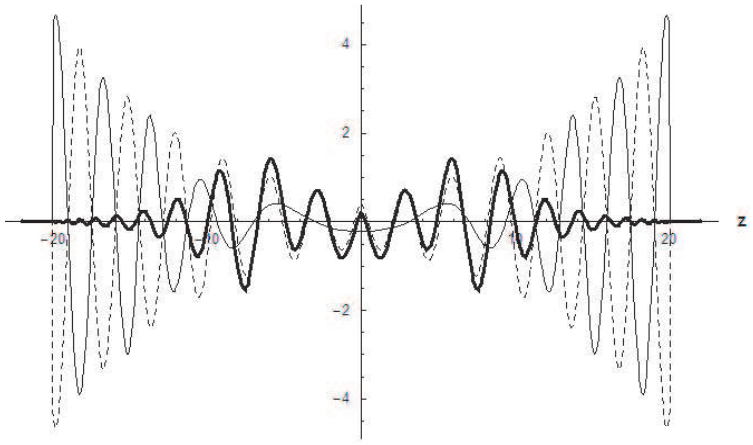

Figure 4.6: Decomposition of radiated field. We show the x component of $\mathbf{A}^Z_{TE_{01}}(a/2, b/2, z)$ (thin line) and $\mathbf{A}^Z_{TE_{01}}(a/2, b/2, z)$ (dashed line) at time $t = 20$ as a function z. The thick line is the summation of all components.

the speed of light. As a result, the radiated field will spread in space as time goes on. At t much greater than the relaxation time, the resonance field is well separated from the origin, and the field at origin is dominated by the Zeno field which is power decay as shown in Eq. (4-32).

4.4 Discussion

Let us discuss the time evolution of the resonance field and Zeno field in detail. The dressing cloud is negligible as it is $O(\lambda^3)$ and $\lambda \sim 10^{-6}$ for the classical case. Let us first focus our attention on the resonance field $\mathbf{A}^R_{TE}$. Under the condition[3] $(\omega_1^2 - c^2\alpha_{mn}^2) \gg \gamma\omega_1$, we can approximate

$$k_{mn,1-} \approx \frac{\omega_1 \chi_{mn}^2}{c} - i\frac{\gamma}{c\chi_{mn}} \tag{4-29}$$

[3]This condition is satisfied even in the extreme case that $\omega_1 = \omega_c + \lambda$.

where χ_{mn} is defined in Eq. (4-15). With this approximation, we have the resonance field in Eq. (4-28) written as

$$\begin{aligned}\mathbf{A}^R_{TE}(\mathbf{r},t) &\approx -4\sqrt{2}\lambda q_1(0)\sum_{mn}^{m_s,n_s}(\frac{n\Delta_{mn}}{b})C^2_{mn}W_{1,mn}(\mathbf{R})e^{-\gamma(t-\frac{z}{c\chi_{mn}})} \\ &\times\frac{\cos(\tilde{\omega}_1(t-\frac{\chi_{mn}z}{c}))}{c\sqrt{c}\omega_1\chi_{mn}}\left[-\frac{n\pi}{b}W_{1,mn}(\mathbf{r})\hat{e}_x+\frac{m\pi}{a}W_{2,mn}(\mathbf{r})\hat{e}_y\right] \quad (4\text{-}30)\end{aligned}$$

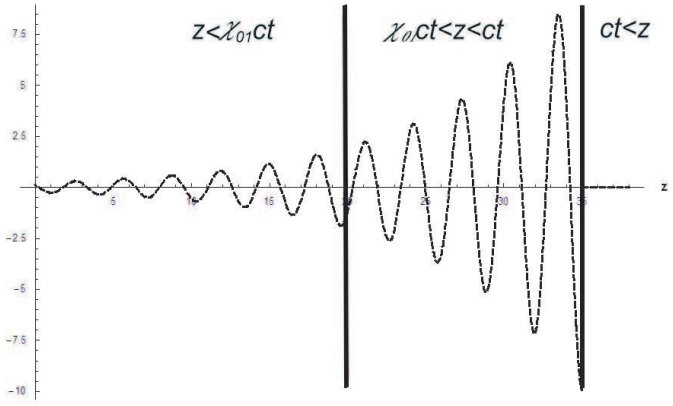

Figure 4.7: Distribution of Resonance field. We plot the x component of $\mathbf{A}^R_{TE_{01}}(a/2,b/2,z,t=35)$ as function of z.

In Figure 4.7, we plot the distribution of the resonance field $\mathbf{A}^R_{TE_{01}}(a/2,b/2,z,t)$ in space (with z measured in b) at time $t=35$ according to Eq. (4-28). We have chosen the same setting as before, that $c\alpha_{01}<\omega_1<c\alpha_{10}$. Therefore the resonance field in this case contains only TE_{01} mode. In general, for larger ω_1, the resonance field is superposition of each mode up to $(m,n)=(m_s,n_s)$ as shown in Eq. (4-30).

One can see the resonance field of a given mode (it is TE_{01} in Figure 4.7) consists of an oscillating function $\cos(\tilde{\omega}_1\chi_{mn}(z-ct/\chi_{mn})/c)$ modulated by an exponential profile $\exp[-\gamma(c\chi_{mn}t-z)/c\chi_{mn}]$. The "group velocity" for this profile

is given by $c\chi_{mn} < c$, which shows the resonance field inside the waveguide travel slower than the speed of light. Moreover, we can slow down the speed by choosing appropriate size of waveguide so that $\chi_{mn} \ll 1$. Recall if we consider for the case $\omega_1 = c\alpha_{mn} + \lambda$, then $\chi_{mn} \sim \sqrt{\lambda} \sim 10^{-4}$. This show the group velocity of the resonance field can be slower down to $10^{-4}c$! Combining with the fast decay rate we obtained for HCl in Section 4.2 (i.e.,10^{-7}s), the size of the exponential profile is about 10cm for a classical HCl dipole. This is relatively large compared with the quantum case where the wavepacket of emitted by the electron in hydrogen atom is about 1m.

For the oscillating factor, the number of peaks distributed inside the exponential profile increases in time. Since the wavelength of the oscillations is given by $2\pi c/\tilde{\omega}_1\chi_{mn}$, therefore the total number of peaks inside the exponential shape can be estimated by $(c\chi_{mn}/\gamma)/(2\pi c/\tilde{\omega}_1\chi_{mn}) \approx \omega_1\chi_{mn}^2/2\pi\gamma$. The phase velocity of these oscillations is given by $c/\chi_{mn} > c$ which is greater than speed of light, especially it can be reached to 10^4c for the case $\chi_{mn} \sim \sqrt{\lambda}$.

In Figure 4.7, we divide the field distribution into three regions. Outside the lightcone, as we have mentioned in previous section, that there is no resonance field. Inside the lightcone, for $c\chi_{01} < z < ct$, one can see the exponential factor in Eq. (4-30) become positive. This means the region will grow exponentially in time. However as shown in Figure 4.8, that this part will be cancelled out by the Zeno field which has an opposite phase (see Figure 4.8). As a result, the remaining part ($z < c\chi_{01}t$) will travel will the group velocity $c\chi_{01} < c$.

For the Zeno field inside the lightcone, it was given in Eq. (4-28) (outside the light cone, the contour will be different. Also, it can be shown numerically up to $O(\lambda^2)$ that the Zeno field vanishes outside the lightcone). By explicitly evaluating

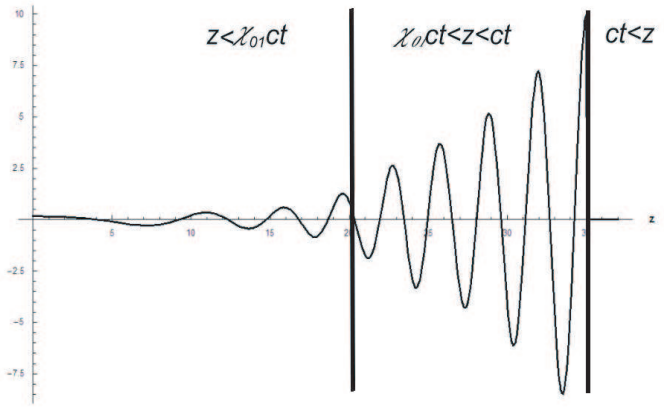

Figure 4.8: Distribution of Zeno field. We plot the x component of $\mathbf{A}^Z_{TE_{01}}(a/2, b/2, z, t)$ at time $t = 35$ as a function of z.

these contours, we rewrite $\mathbf{A}^Z_{TE}(\mathbf{r}, t)$

$$\begin{aligned}\mathbf{A}^Z_{TE} &\approx 2\sqrt{2}\lambda\omega_1 q_1(0)\sum_{mn}\frac{n\Delta_{mn}}{\pi b\sqrt{c}}C^2_{mn}W_{1,mn}(\mathbf{R})\left[\frac{n\pi}{b}W_{1,mn}(\mathbf{r})\hat{e}_x - \frac{m\pi}{a}W_{2,mn}(\mathbf{r})\hat{e}_y\right] \\ &\times \left\{\int_0^\infty dk \frac{ie^{\frac{i\pi}{4}}(e^{(\frac{1+i}{\sqrt{2}})kz} + e^{-(\frac{1+i}{\sqrt{2}})kz})e^{-ict\sqrt{\alpha^2_{mn}-ik^2}}}{c^3\sqrt{\alpha^2_{mn}-ik^2}(\sqrt{\alpha^2_{mn}-ik^2}+z_1^*)(\sqrt{\alpha^2_{mn}-ik^2}-z_1)} + c.c\right\} \quad (4\text{-}31)\end{aligned}$$

for $|z| < ct$.

In Figure 4.8 we plot the distribution of the Zeno field $\mathbf{A}^Z_{TE_{01}}(a/2, b/2, z, t)$ in space at time $t = 35$ according to Eq. (4-31), whose integration is performed numerically. Here we see in the intermediate region where $c\chi_{01}t < z < ct$, the Zeno field has an opposite phase with the resonance field shown in Figure 4.7. Therefore they cancel each other. As time goes on, we see this out-of-phase region which proportional $ct(1 - \chi_{01})$ will grow linearly in time. This indicates that it is highly possible to detect this region in experiment , which is a sign of the existence of Zeno field, thus Zeno effect.

Near the origin, we again apply the stationary phase approximation. For

the case $|z|/ct \ll 1$, the leading term of $\mathbf{A}^Z_{TE}$ is given by

$$\mathbf{A}^Z_{TE}(\mathbf{r},t) \approx 4\sqrt{2}\lambda q_1(0)\frac{\omega_1}{bc^4\sqrt{\pi t}}\sum_{m,n}\frac{n\Delta_{mn}C^2_{mn}W_{1,mn}(\mathbf{R})}{\sqrt{\alpha_{mn}}(\alpha^2_{mn}-(\frac{\omega_1}{c})^2)}\left[\frac{n\pi}{b}W_{1,mn}(\mathbf{r})\hat{e}_x - \frac{m\pi}{a}W_{2,mn}(\mathbf{r})\hat{e}_y\right]\sin\left(\alpha_{mn}ct(1-\frac{z^2}{2c^2t^2})+\frac{5\pi}{4}\right) \quad (4\text{-}32)$$

which is the same as $\mathbf{A}_{TE,Z}$ in Eq. (3-37). As a result the amplitude of $\mathbf{A}^Z_{TE}$ at origin decays in $1/\sqrt{\omega_1 t}$. It is much slower than the exponential decay of the dressing cloud $\mathbf{A}^C_{TE}$, and the resonance field $\mathbf{A}^R_{TE}$. Therefore as $t \gg 1/\gamma$ the field around the origin is dominated by the Zeno field.

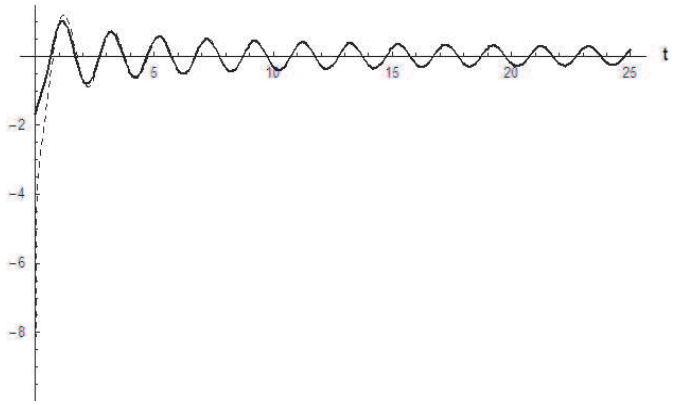

Figure 4.9: Stationary phase approximation of $\mathbf{A}^Z_{TE}(\mathbf{r},t)$. We show the x component of the $\mathbf{A}^Z_{TE_{01}}(a/2,b/2,0,t)$ as a function of time at the center of mass of the dipole. The solid line corresponds to Eq. (4-31) with the integration performed numerically, and the dashed line corresponds to the stationary phase approximation given in Eq. (4-32).

In Figure 4.9 we compare the Zeno field obtained from stationary phase approximation with the Zeno field obtained from Eq. (3-31) with the integration performed numerically. We plot the x component vector potential $\mathbf{A}^Z_{TE_{01}}(a/2,b/2,0,t)$ as a function of time at the center of mass of the dipole molecule. The time is The solid line is given by numerical integration of the form in Eq. (4-31)while the

dashed line is the stationary phase approximation given by Eq. (4-32). We see the stationary phase approximation again gives good approximation at the larger time scale $\omega_1 t \gg 1$. The oscillation period is given by $2\pi/c\alpha_{01}$.

As a summary, we have shown that not only our result in classical radiation damping does not show any unphysical effect, but also thank to the Friedrichs solution, we are able to analyze the time evolution in detail. Also due to the cut-off frequency of the waveguide, we can increase the decay rate for a classical dipole inside the waveguide 10^5 times faster than that in the free space, at the same time reducing the group velocity of the emitted resonance field 10^4 times slower than the speed of light.

Part II

Signature of Quantum Decoherence in the Field Bath

Chapter 5

Quantum decoherence in the field

5.1 Motivation

In previous chapters we have discussed a system in which the time evolution can be mapped into Friedrichs model. We now turn our interests to the quantum mechanics.

In this chapter we shall discuss a Hamiltonian which is very similar to the classical Friedrichs model. By replacing the normal modes q_α by annihilation operators a_α (and creation operators a_α^+ for the q_α^*) and dropping the virtual processes corresponding to $q_{\sigma,k}q_1$, $q_{\sigma,k}^*q_1^*$ term in the classical Friedrichs model in Eq. (2-17), we come to the Hamiltonian in Eq. (5-1) of our $1D$ quantum system.

Here we especially focus our attention on the problem of quantum decoherence as it is also an important concept of irreversibility. Recent development on the complex spectral representation of the Liouville-von Neumann equation in non-equilibrium statistical dynamics reveals the fact that irreversibility is a rigorous dynamical process coming from the resonance singularity.

To deal with the irreversible processes in non-equilibrium statistical physics there are two essential elements; the "extensivity" of the systems and the "non-integrability." In both equilibrium and nonequilibrium statistical mechanics, one deals with infinitely large systems which are characterized by extensive quantities that are proportional to the size of the system, such as the total number of particles or the total energy of the system. For this case, one can define the thermodynamic

limit through the introduction of non-vanishing "intensive quantities," such as number density per volume. As we shall see later, an important consequence of the existence of the thermodynamic limit is that density matrices in quantum mechanics (or distribution functions in classical mechanics) do not belong to a Hilbert space. For this case, the Liouville-von Neumann operator (the Liouvillian in short) may have complex eigenvalues that break time-symmetry without adding any dissipative terms to the Hamiltonian or the Liouvillian.

However, the extensivity itself alone is not sufficient to have irreversibility as it is well-known that the ideal gas is impossible to approach to equilibrium. This leads to the second ingredient of the irreversible processes, which is the non-integrability of the system. The interactions lead to the "small denominator" singularity (or resonance singularity) which prevents us from diagonalizing the Hamiltonian through a canonical (or unitary) transformation that is analytic with respect to a coupling constant (non-integrability in the sense of Poincaré) [4] . As a consequence, invariants of motion other than the total Hamiltonian are destroyed. Combining with the thermodynamic limit, the resonance singularities thus lead to contributions that break time-symmetry. In this situation, it had been shown that one can obtain the irreversible dynamics through the complex spectral representation of the Liouvillian [32, 33].

In section 5.2, we introduce our bilinear system which is Friedrichs model in the non-integrable case. In order to deal with thermodynamic situation, we adopt the box normalization formalism for this model. Then we specify the meaning of the thermodynamic limit. Under this limit, we show that it is necessary to deal with a larger class of density matrices which are not in the Hilbert space. Moreover, we show the failure of Bogoliubov transformation due to the resonance and the thermodynamic limit. An important consequence of the failure of the Bogoli-

ubov transformation is that in the thermodynamic limit one cannot reduce the time evolution of the state to the level of wave function.

In section 5.3, we overview the Liouvillian formulation of quantum mechanics. In this formulation, the bra-ket notation in wave function space is generalized to the double bra-ket notation in density matrices of Liouville space. The operator acting on wave functions is generalized to the super-operator acting on density matrices. We introduce the projection operators associated with the correlation between the particle and the field.

In section 5.4 we solve the eigenvalue problem of the Liouvillian outside the Hilbert space, which gives us the complex spectral representation. We show the eigenvalue problem of the Liouvillian is reduced to the eigenvalue problem of the collision operator that commonly appears in the kinetic theory in non-equilibrium statistical physics. We also introduce the concept of subdynamics which enable us to evaluate the non-Markovian effect (i.e. memory effect) in a systematic way.

In section 5.5, we apply the complex spectral representation to our system. Our result shows that already in a weak coupling limit, there exists a signature of decoherence in the field that appears through the secular effect coming from the resonances. This effect can only be observed if we start from a non-equilibrium thermodynamic field.

In section 5.6, We evaluate the non-Markovian effect that can be seen by going beyond the weak coupling limit (or the so-called $\lambda^2 t$ limit). By adding the non-Markovian effect, we have a complete description of the decoherence that incorporate both the short time non-Markov processes dominated quantum Zeno effect and the Markov processes of order $O(\lambda^{-2})$ which is dominated by the resonance effect.

In section 5.7, we compare our theoretical results with the numerical simulations.

5.2 The system

We consider a one-dimensional system which consists of a quantum harmonic oscillator linearly coupled to a bosonic massless scalar field. One can view it as a simplified version of a multi-level atom coupled with a surrounding field in the dipole approximation of the multipolar scheme [29]. By the rotating wave approximation [34], i.e., by neglecting the virtual processes associated with $a_1 a_k$ and $a_1^+ a_1^+$, the Hamiltonian of our system is given by the second quantization form[1],

$$\begin{aligned} H &= H_0 + \lambda V \\ &= \omega_1 a_1^+ a_1 + \sum_j \omega_{k_j} a_{k_j}^+ a_{k_j} + \lambda \sum_j V_{k_j} (a_1^+ a_{k_j} + a_1 a_{k_j}^+) \end{aligned} \tag{5-1}$$

with units $\hbar = c = 1$ where $\omega_1 > 0$ and λ is dimensionless positive coupling constant. We consider the weak coupling case that

$$\sum_k \frac{\lambda^2 |V_k|^2}{\omega_k} < \omega_1 \tag{5-2}$$

As a convention, we shall call the harmonic oscillator "particle" and the quanta of the field "photons." The spectrum of the field is given by the dispersion relation,

$$\omega_{k_j} = |k_j| > 0 \tag{5-3}$$

In order to deal with thermodynamic situation, we use the box normalization formalism. We impose the periodic boundary condition , as usual. Then the spectrum of the field is discrete,

$$k_j = \frac{j}{\Omega} \tag{5-4}$$

where $\Omega \equiv L/2\pi$ is a volume factor and j is arbitrary integer ranges from $-\infty$ to ∞. To simplify the notation, we hereafter ignore the index j in all of our notations,

[1] An extension of our argument to the case including virtual process is straightforward [35].

and replace the summation $\sum_j$ as $\sum_k$. The volume dependence of the potential V_k is given by

$$V_k = \frac{v_k}{\sqrt{\Omega}} \tag{5-5}$$

We assume that v_k is independent of Ω in the limit $\Omega \to \infty$, and satisfies

$$\frac{1}{\Omega}\sum_k |v_k|^2 < \infty \tag{5-6}$$

Given a form factor, one can obtain v_k explicitly. In the continuous limit $\Omega \to \infty$, we have a continuous spectrum with

$$\frac{1}{\Omega}\sum_k \to \int dk, \quad \Omega\delta_{k,0} \to \delta(k) \tag{5-7}$$

where $\delta_{k,0}$, $\delta(k)$ are the Kronecker delta, and Dirac delta function, respectively.

In the Hamiltonian in Eq. (5-1), the creation and annihilation operators for the particle a_1^+, a_1 and the field a_k^+, a_k obey the canonical commutation relations

$$[a_1, a_1^+] = 1, \quad [a_1, a_k^+] = 0, \quad [a_k, a_{k'}^+] = \delta_{k,k'} \tag{5-8}$$

Due to the rotating wave approximation, the total number of the unperturbed quanta are conserved, i.e

$$[H, a_1^+ a_1 + \sum_k a_k^+ a_k] = 0 \tag{5-9}$$

Due to the bilinear form of our Hamiltonian Eq. (5-1), it could be completely diagonalized by the Bogoliubov transformation, which gives

$$H = \sum_k \omega_k A_k^+ A_k \tag{5-10}$$

with the renormalized field A_k

$$A_k = a_k + \lambda \frac{V_k}{\eta^+(\omega_k)}(a_1 + \lambda {\sum_l}' \frac{V_l}{\omega_k - \omega_l + i\epsilon} a_l) \tag{5-11}$$

where the frequencies ω_k are unchanged as we assume the continuous limit $\Omega \to \infty$. Here $\sum_l{}'$ indicates $\sum_{l\neq k}$, but it will be replaced by $\Omega \int dl$ after we take the continuous limit. The $\eta(z)$ is defined by

$$\eta(z) \equiv z - \omega_1 + \sum_{k'} \frac{\lambda^2 |V_{k'}|^2}{\omega_{k'} - z} \tag{5-12}$$

where $\eta^{\pm}(\omega_k) \equiv \eta(\omega_k \pm i\epsilon)$ with a positive infinitesimal $\epsilon \to 0+$

We note that there is no renormalized particle such as A_1 in the new Hamiltonian Eq. (5-10), which is a characteristic property of the unstable system [36]. This is the same situation as in the case $\omega_1 > \omega_c$ for the waveguide. If one follows the usual perturbation theory approach to diagonalize the Hamiltonian Eq. (5-1) in the Hilbert space, there appears $1/(\omega_k - \omega_1)$ resonance singularity in the denominator which destroys the renormalized particle A_1, similar to the classical case discussed in the previous chapter. These renormalized fields themselves form a complete orthonormal basis,

$$[A_k, A_{k'}^+] = \delta_{k,k'} \tag{5-13}$$

$$\sum_k A_k^+ A_k = \mathbf{1} \tag{5-14}$$

It is obvious the renormalized fields in Eq. (5-11) approach to unperturbed field under the limit $\lambda \to 0$. We therefore lose the invariant $a_1^+ a_1$ due to the resonance between the particle and the fields, then our system is non-integrable in the sense of "Poincare". Moreoever, we shall see this resonance singularity also leads to a non-factorizable dynamical description of the system under the thermodynamic limit.

Let us first specify the meaning of the thermodynamic limit. To this end, we focus our attention on a complete orthonormal basis of the unperturbed Hamiltonian H_0 given by

$$H_0 |n_1, \{n_F\}\rangle = (\omega_1 n_1 + \sum_k \omega_k n_k) |n_1, \{n_F\}\rangle \tag{5-15}$$

where $\{n_F\} \equiv \{n_{k_1}, n_{k_2}, ...n_k\}$, and n_α is the occupation number for the state of particle ($\alpha = 1$) and field ($\alpha = k$), respectively. This basis spans a Hilbert space (Fock space) with the usual Hilbert norm $\||n_1, \{n_F\}\rangle\|^2 = 1$, where

$$\|\Psi\|^2 \equiv \langle\Psi|\Psi\rangle \tag{5-16}$$

Let us then consider an expectation value of the total Hamiltonian $\langle H\rangle$, where $\langle A\rangle \equiv Tr(A\rho)$ with a given density matrix ρ. For example, if the density matrix is diagonal in the number representation, we have in the limit $\Omega \to \infty$

$$\langle H\rangle = \omega_1\langle n_1\rangle + \Omega\int dk\omega_k\langle n_k\rangle \tag{5-17}$$

where we assume that $\int dk\omega_k\langle n_k\rangle < \infty$. We consider two different situations,

$$\langle n_k\rangle \sim O(\Omega^{-1}) \tag{5-18a}$$

$$\langle n_k\rangle \sim O(\Omega^0) \tag{5-18b}$$

In the first case in Eq. (5-18a) with the condition $\langle H\rangle < \infty$, we have a situation which is considered in a problem of a stimulated or spontaneous emission of photon from the excited particle.

For the second case in Eq. (5-18b), the total energy is an extensive quantity (as it is proportional to the volume) that characterizes the thermodynamic situations. We call that the limit $\Omega \to \infty$ with the condition Eq. (5-18b) as the "thermodynamic limit." We note that in order to satisfy the condition of the thermodynamic limit it is not necessary for the density matrix ρ to be a mixed state. Indeed, as we shall see later that one can construct a pure state that satisfies the condition of the thermodynamic limit by a superposition of coherent states of the field.

An important consequence of the thermodynamic limit is that the time evolution of states cannot be described in terms of the states in the Hilbert space.

Indeed, one can easily verify that the Hilbert norm of a state $|\Phi\rangle \equiv H|n_1, \{n_F\}\rangle$ diverges as $O(\Omega)$in the thermodynamic limit $\Omega \to \infty$. Hence we have to solve the time evolution of the state in an extended space that lies outside the Hilbert space.

As we have mentioned before, another important consequence of the thermodynamic limit, is whenever combined together the resonance singularity, one cannot reduce the time evolution of the state to the level of wave functions.

Due to the Bogoliubov transformation, we then have an infinite set of invariants of motion $\langle A_k^+ A_k \rangle$. However, this diagonalization of the Hamiltonian loses its meaning in the thermodynamic limit. Indeed, in the continuous spectrum limit the invariant $\langle \tilde{A}_k^+ \tilde{A}_k \rangle = \Omega \langle A_k^+ A_k \rangle$ involves a singular product of the distribution $|\omega_k - \omega_{k'} + i\epsilon|^{-2}$. In the non-thermodynamic case Eq. (5-18a), this product is negligible in the limit $\Omega \to \infty$ because of an extra volume factor Ω^{-1} in Eq. (5-18a). However, in the thermodynamic limit Eq. (5-18b) this singular product leads to a divergence as

$$\langle \tilde{A}_k^+ \tilde{A}_k \rangle \propto \int dk' \frac{\lambda^2 |v_{k'}|^2 \langle n_{k'} \rangle}{|\omega_{k'} - \omega_k + i\epsilon|^2} \propto \frac{1}{\epsilon} \longrightarrow \infty \tag{5-19}$$

The divergence comes from the contribution at the resonance $\omega_k = \omega_{k'}$, which destroys the invariant of motion. we also show

We also show in Appendix E that Bogoliubov transformation gives inconsistent result to the conservation law of the total number of the unperturbed particle and photons in the thermodynamic limit. As a result one cannot follow the time evolution of the field through the diagonalization of the Hamiltonian as Eq. (5-10) in the thermodynamic limit.

Since the Hamiltonian in Eq. (5-1) is bilinear in the annihilation and creation operators, the nonexistence of a diagonal form of the total Hamiltonian through a linear transformation in the thermodynamic limit is a nontrivial result. As a consequence of the failure of the diagonalization, one cannot reduce the time evolution

of a given density matrix to an evolution of a product of the renormalized normal modes, or a product of wave functions. One has to deal with a non-factorizable evolution of the density matrix, even though one starts with a pure state as an initial condition.

5.3 Liouville equation

Since one cannot follow the time evolution of the system in terms of the wave functions in the thermodynamic limit, one has to directly deal with the evolution of the density matrices in Liouville space. This space is spanned by the basis formed by dyadic operators generated from the basis in wave function space. The density matrices obey the Liouville-von Neumann equation

$$i\frac{\partial}{\partial t}\rho(t) = L_H\rho(t) \tag{5-20}$$

where $L_H\rho \equiv H\rho - \rho H$. Corresponding to the decomposition of the Hamiltonian in Eq. (5-1), we have the Liouvillian decomposed into an unperturbed part L_0 and an interaction part L_V,

$$L_H = L_0 + \lambda L_V \tag{5-21}$$

whereL_0 and L_V are given by

$$L_0 = H_0 \times 1 - 1 \times H_0 \tag{5-22}$$

$$L_V = V \times 1 - 1 \times V \tag{5-23}$$

Here a factorizable *superoperator* $A \times B$ operating on the density matrix is defined as

$$(A \times B)\rho = A\rho B \tag{5-24}$$

where A and B are linear operators acting in wave functions space. The Liouville space is spanned by the linear operators A,B,... of the wave function space. We

define the inner product in the Liouville space as

$$\langle\langle A|B\rangle\rangle = \mathrm{Tr}(A^+B) \tag{5-25}$$

where A^+ is the hermitian conjugate of the linear operator A in the wave function space. Thus we introduce the Hilbert norm of a state in the Liouville space as

$$\|\rho\| \equiv \sqrt{\langle\langle\rho|\rho\rangle\rangle} \tag{5-26}$$

To distinguish a state in Liouville space from a state in the wave function space, we have adopted the double-ket notation $|A\rangle\rangle$ for the former, and the single-ket notation $|k\rangle$ for the latter. We denote S^+ as the adjoint of the superoperator S with the definition

$$\langle\langle\rho'|S^+|\rho\rangle\rangle = \langle\langle\rho|S|\rho'\rangle\rangle^* \tag{5-27}$$

where the superscript $*$ is the complex conjugate. Let us denote the complete orthogonal set of the eigenstates of the unperturbed Hamiltonian by $\{|\alpha\rangle\}$, i.e.,

$$H_0|\alpha\rangle = \omega_\alpha|\alpha\rangle \tag{5-28}$$

where $|\alpha\rangle = |n_1, \{n_F\}\rangle$ in Eq. (5-15) for our system. They form a complete orthonormal basis in wave function space. For the case of Liouville space, we have the dyads $|\alpha;\beta\rangle\rangle \equiv |\alpha\rangle\langle\beta| = [\langle\langle\alpha;\beta|]^+$ as a complete orthonormal basis, i.e.,

$$\sum_{\alpha,\beta} |\alpha;\beta\rangle\rangle\langle\langle\alpha;\beta| = 1, \quad \langle\langle\alpha;\beta|\alpha';\beta'\rangle\rangle = \delta_{\alpha,\alpha'}\delta_{\beta',\beta} \tag{5-29}$$

with

$$L_0|\alpha;\beta\rangle\rangle = w^{(\alpha,\beta)}|\alpha;\beta\rangle\rangle \tag{5-30}$$

where $w^{(\alpha,\beta)} \equiv \omega_\alpha - \omega_\beta$. The matrix element of the usual operator A in the wave function space is given by

$$\langle\langle\alpha;\beta|A\rangle\rangle = \langle\alpha|A|\beta\rangle \tag{5-31}$$

while the matrix element of a superoperator S is given by

$$S_{\alpha'\beta':\alpha\beta} = \langle\langle \alpha'; \beta' | S | \alpha; \beta \rangle\rangle \tag{5-32}$$

For a factorizable superoperator we have

$$(A \times B)_{\alpha'\beta':\alpha\beta} = A_{\alpha'\alpha} B_{\beta'\beta} \tag{5-33}$$

We note that the eigenstates of the unperturbed Liouvillian are infinitely degenerate as $L_0|\nu\rangle\rangle = w^{(\nu)}|\nu\rangle\rangle$ where $|\nu\rangle\rangle \equiv \sum_\alpha |\nu_\alpha\rangle\rangle$ and α is a degeneracy index. For example, all diagonal dyads $|\alpha;\alpha\rangle\rangle$ belong to zero eigenstate of L_0, i.e., we have $|0\rangle\rangle \equiv \sum_\alpha |\alpha;\alpha\rangle\rangle$. These degeneracies lead to a quite rich structure of the eigenvalue problem of the total Liouvillian L_H, as we shall see in the next section.

The eigenstates of L_0 define a complete orthogormal set of eigen-projection operators of L_0 as

$$P^{(\nu)} \equiv |\nu\rangle\rangle\langle\langle\nu| \tag{5-34}$$

that satisfies

$$\sum_\nu P^{(\nu)} = 1, \qquad P^{(\nu)} P^{(\mu)} = \delta_{\nu,\mu} P^{(\nu)} \tag{5-35}$$

Its complementary operator $Q^{(\nu)} \equiv 1 - P^{(\nu)}$ satisfies

$$(Q^{(\nu)})^2 = Q^{(\nu)}, \qquad Q^{(\nu)} P^{(\nu)} = P^{(\nu)} Q^{(\nu)} = 0 \tag{5-36}$$

We recall that each projection operator $P^{(\nu)}$ defines the ν-th "correlation subspace" of the density matrix [33]. Of special interest is the "vacuum-of-correlation" subspace $P^{(0)}$ that extracts uncorrelated components of the density matrix among the particle and the field. Other components extract particle-field correlation components, field-field correlation components, and so on. With the interaction potential λV these $P^{(\nu)}$ are no longer eigen-projection operators of the Liouvillian. We shall formulate the new set of eigen-projection operators $\Pi^{(\nu)}$ of the Liouvillian in the following section.

5.4 Complex spectral representation of the Liouvillian

In [33], Petrosky and Prigogine have extended the eigenvalue problem of the Liouvillian L_H to a class of density matrices that do not belong to the Hilbert space, and have shown that the Liouvillian may have complex eigenvalues that break time symmetry. The complex spectral representation of the Liouvillian then leads to the "dynamics of correlations [37]." In the correlation dynamics the non-Markovian evolution is described in terms of a set of infinite number of Markovian equations. This set includes the Pauli master equation. The detailed derivation of the solution of the eigenvalue problem of the Liouvillian as well as the derivation of the correlation dynamics has been given in [33]. Here we briefly summarize the complex spectral representation, the reader should consult the original article [33] for detail.

Let us now consider the eigenvalue problem of the Liouvillian[2]. Let us denote $|F_\alpha^{(\nu)}\rangle\!\rangle$, and $\langle\!\langle \tilde{F}_\alpha^{(\nu)}|$ as the right and left eigenstates of the total Liouvillian L_H respectively, [33],

$$L_H|F_\alpha^{(\nu)}\rangle\!\rangle = z_\alpha^{(\nu)}|F_\alpha^{(\nu)}\rangle\!\rangle, \qquad \langle\!\langle \tilde{F}_\alpha^{(\nu)}|L_H = \langle\!\langle \tilde{F}_\alpha^{(\nu)}|z_\alpha^{(\nu)} \tag{5-37}$$

where we assume that they satisfy bi-orthogonality and bi-completeness relations,

$$\langle\!\langle \tilde{F}_\alpha^{(\nu)}|F_\beta^{(\mu)}\rangle\!\rangle = \delta_{\nu,\mu}\delta_{\alpha,\beta}, \qquad \sum_\nu \sum_\alpha |F_\alpha^{(\nu)}\rangle\!\rangle\langle\!\langle \tilde{F}_\alpha^{(\nu)}| = 1 \tag{5-38}$$

The index α together with ν is a parameter characterizing the eigenfunctions, and we assume there is no degeneracy with respect to different indices of α and ν . As mentioned before, since we consider the eigenvalue problem of the Liouvillian L_H

[2]We formulate the eigenvalue problem of L_H in the thermodynamic limit. In this limit, special care is necessary for a general Hamiltonian, as the perturbed Liouvillian L_V usually gives rise to divergence due to disconnected processes (see connected and disconnected diagrams in Refs.[33, 37]). However, in the case of our Hamiltonian we do not encounter this divergence as all processes are connected to the tagged mode ω_1 through the specific form of interaction involving a_1 or a_1^+.

outside Hilbert space, the left-eigenstate is generally different from the hermitian conjugate of the right-eigenstate. Moreover the eigenvalues $z_\alpha^{(\nu)}$ are complex, and the time evolution of the system splits into two semigroups. For the semigroup corresponding to $t > 0$, the eigenstates are associated with the eigenvalues with $\mathrm{Im} z_\alpha^{(\nu)} \leq 0$ and equilibrium is reached in our future for $t \to +\infty$, while for the other the eigenvalues are the complex conjugate of $z_\alpha^{(\nu)}$ and equilibrium is reached in our past. Experience shows that all irreversible processes have the same time orientation.

To be self-consistent, we have to choose the semigroup oriented towards our future. We consider the case where the eigenstates are analytic with respect to the coupling constant λ, i.e.,

$$\lim_{\lambda\to 0} |F_\alpha^{(\nu)}\rangle\!\rangle = \lim_{\lambda\to 0} P^{(\nu)}|F_\alpha^{(\nu)}\rangle\!\rangle, \qquad \lim_{\lambda\to 0} \langle\!\langle \tilde{F}_\alpha^{(\nu)}| = \lim_{\lambda\to 0} \langle\!\langle \tilde{F}_\alpha^{(\nu)}|P^{(\nu)} \tag{5-39}$$

and

$$\lim_{\lambda\to 0} z_\alpha^{(\nu)} = w^{(\nu)} \tag{5-40}$$

Using $P^{(\nu)} + Q^{(\nu)} = \mathbf{1}$ in Eq. (5-37) one can find the $Q^{(\nu)}$ component of the eigenstates as

$$Q^{(\nu)}|F_\alpha^{(\nu)}\rangle\!\rangle = \mathcal{C}^{(\nu)}(z_\alpha^{(\nu)})P^{(\nu)}|F_\alpha^{(\nu)}\rangle\!\rangle \tag{5-41}$$

where the "creation-of-correlation operator" (creation operator in short) is defined as

$$\begin{aligned} \mathcal{C}^{(\nu)}(z) &\equiv \frac{-1}{Q^{(\nu)}L_H Q^{(\nu)} - z} Q^{(\nu)}\lambda L_V P^{(\nu)} \\ &= Q^{(\nu)}\frac{-1}{L_0 - z}\sum_{n=0}^{\infty}\left(Q^{(\nu)}\lambda L_V Q^{(\nu)}\frac{-1}{L_0 - z}\right)^n Q^{(\nu)}\lambda L_V P^{(\nu)} \end{aligned} \tag{5-42}$$

This operator is an off-diagonal operator as it describes an "off-diagonal transition" between the different subspace $Q^{(\nu)}$ and $P^{(\nu)}$. Care has to be taken in the analytic

continuation of z to have the time evolution approaching equilibrium in our future $t > 0$.

Substituting Eq. (5-41) into the eigenvalue equation in Eq. (5-37), we obtain

$$\psi^{(\nu)}(z_\alpha^{(\nu)})|u_\alpha^{(\nu)}\rangle\!\rangle = z_\alpha^{(\nu)}|u_\alpha^{(\nu)}\rangle\!\rangle \tag{5-43}$$

where

$$|u_\alpha^{(\nu)}\rangle\!\rangle \equiv [N_\alpha^{(\nu)}]^{-1/2} P^{(\nu)}|F_\alpha^{(\nu)}\rangle\!\rangle \tag{5-44}$$

Here $N_\alpha^{(\nu)}$ is a normalization constant, and $\psi^{(\nu)}(z)$ are the *collision operators* defined by

$$\psi^{(\nu)}(z) \equiv P^{(\nu)} L_0 P^{(\nu)} + P^{(\nu)} \lambda L_V \mathcal{C}^{(\nu)}(z) P^{(\nu)} \tag{5-45}$$

This operator is extension of the collision operator that appears in the kinetic theory in non-equilibrium statistical physics. The collision operator is a "diagonal operator" since it describes a "diagonal transition" within the same subspace $P^{(\nu)}$. As indicated in Eq. (5-43), the eigenvalue problem of the Liouville operator is then reduced to the eigenvalue problem of the collision operator which has the same eigenvalues $z^{(\nu)}$ as L_H. The eigenvalue equation Eq. (5-43) is "non-linear" as the eigenvalue appears in the collision operator.

Using Eq. (5-41), we obtain the right-eigenstates of L_H from the corresponding right-eigenstates of $\psi^{(\nu)}(z_\alpha^{(\nu)})$ as

$$|F_\alpha^{(\nu)}\rangle\!\rangle = [N_\alpha^{(\nu)}]^{1/2}(P^{(\nu)} + \mathcal{C}^{(\nu)}(z_\alpha^{(\nu)}))|u_\alpha^{(\nu)}\rangle\!\rangle \tag{5-46}$$

A construction parallel to the above, leads to the left-eigenstates of L_H with the same eigenvalues $z_\alpha^{(\nu)}$,

$$\langle\!\langle \tilde{F}_\alpha^{(\nu)}| = \langle\!\langle \tilde{v}_\alpha^{(\nu)}|(P^{(\nu)} + \mathcal{D}^{(\nu)}(z_\alpha^{(\nu)}))[N_\alpha^{(\nu)}]^{1/2} \tag{5-47}$$

where the "destruction operator" is defined by

$$\begin{aligned}\mathcal{D}^{(\nu)}(z) &\equiv P^{(\nu)}\lambda L_V Q^{(\nu)}\frac{1}{z - Q^{(\nu)}L_H Q^{(\nu)}} \\ &= P^{(\nu)}\lambda L_V Q^{(\nu)}\frac{1}{z-L_0}\sum_{n=0}^{\infty}\left(Q^{(\nu)}\lambda L_V Q^{(\nu)}\frac{1}{z-L_0}\right)^n \end{aligned} \tag{5-48}$$

and $\langle\!\langle\tilde{v}_\alpha^{(\nu)}| \equiv \langle\!\langle\tilde{F}_\alpha^{(\nu)}|P^{(\nu)}{N_\alpha^{(\nu)}}^{-1/2}$ are the left-eigenstates of the collision operator,

$$\langle\!\langle\tilde{v}_\alpha^{(\nu)}|\psi^{(\nu)}(z_\alpha^{(\nu)}) = \langle\!\langle\tilde{v}_\alpha^{(\nu)}|z_\alpha^{(\nu)} \tag{5-49}$$

Since the collision operator depends on the eigenvalue $z_\alpha^{(\nu)}$, the state $\langle\!\langle\tilde{v}_\alpha^{(\nu)}|$ is generally not bi-orthogonal to $|u_\alpha^{(\nu)}\rangle\!\rangle$. Assuming, however, bi-completeness of these states in each $P^{(\nu)}$ subspace, we may always construct sets of states $\{\langle\!\langle\tilde{u}_\alpha^{(\nu)}|\}$ and $\{|v_\alpha^{(\nu)}\rangle\!\rangle\}$ bi-orthogonal to $\{|u_\alpha^{(\nu)}\rangle\!\rangle\}$ and $\{\langle\!\langle\tilde{v}_\alpha^{(\nu)}|\}$, respectively,

$$\langle\!\langle\tilde{u}_\alpha^{(\nu)}|u_\beta^{(\mu)}\rangle\!\rangle = \delta_{\nu,\mu}\delta_{\alpha,\beta} \qquad \sum_\alpha |u_\alpha^{(\nu)}\rangle\!\rangle\langle\!\langle\tilde{u}_\alpha^{(\nu)}| = P^{(\nu)} \tag{5-50}$$

and similarly for $|v_\alpha^{(\nu)}\rangle\!\rangle$ and $\langle\!\langle\tilde{v}_\alpha^{(\nu)}|$.

In order to connect the kinetic theory to the eigenvalue problem of L_H, we introduce the "global" creation and destruction operators,

$$\mathbf{C}^{(\nu)} \equiv \sum_\alpha \mathcal{C}^{(\nu)}(z_\alpha^{(\nu)})|u_\alpha^{(\nu)}\rangle\!\rangle\langle\!\langle\tilde{u}_\alpha^{(\nu)}| \tag{5-51}$$

$$\mathbf{D}^{(\nu)} \equiv \sum_\alpha |v_\alpha^{(\nu)}\rangle\!\rangle\langle\!\langle\tilde{v}_\alpha^{(\nu)}|\mathcal{D}^{(\nu)}(z_\alpha^{(\nu)}) \tag{5-52}$$

Then, we can write the eigenstates as

$$|F_\alpha^{(\nu)}\rangle\!\rangle = [N_\alpha^{(\nu)}]^{1/2}(P^{(\nu)} + \mathbf{C}^{(\nu)})|u_\alpha^{(\nu)}\rangle\!\rangle \tag{5-53}$$

$$\langle\!\langle\tilde{F}_\alpha^{(\nu)}| = \langle\!\langle\tilde{v}_\alpha^{(\nu)}|(P^{(\nu)} + \mathbf{D}^{(\nu)})[N_\alpha^{(\nu)}]^{1/2} \tag{5-54}$$

The normalization constant can be found from the bi-orthonormality condition in Eq. (5-38) of the eigenstates,

$$[N_\alpha^{(\nu)}]^{-1} = \langle\langle \tilde{v}_\alpha^{(\nu)} | [(P^{(\nu)} + \mathbf{D}^{(\nu)}\mathbf{C}^{(\nu)})] | u_\alpha^{(\nu)} \rangle\rangle \tag{5-55}$$

The global collision operator associated with the creation operator $\mathbf{C}^{(\nu)}$ are given by[3]

$$\theta^{(\nu)} \equiv \sum_\alpha \psi^{(\nu)}(z_\alpha^{(\nu)}) | u_\alpha^{(\nu)} \rangle\rangle \langle\langle \tilde{u}_\alpha^{(\nu)} | \tag{5-56}$$

Then we have

$$\theta^{(\nu)} | u_\alpha^{(\nu)} \rangle\rangle = z_\alpha^{(\nu)} | u_\alpha^{(\nu)} \rangle\rangle \tag{5-57}$$

Substituting Eq. (5-45) into Eq. (5-48), we have

$$\theta^{(\nu)} = P^{(\nu)} L_0 P^{(\nu)} + P^{(\nu)} \lambda L_V \mathbf{C}^{(\nu)} P^{(\nu)} \tag{5-58}$$

Now we define the dressed projection operators in each subspace in terms of eigenstates Eq. (5-53) and Eq. (5-54),

$$\Pi^{(\nu)} \equiv \sum_\alpha | F_\alpha^{(\nu)} \rangle\rangle \langle\langle \tilde{F}_\alpha^{(\nu)} | \tag{5-59}$$

This leads to the relation

$$\begin{aligned} e^{-iL_H t} \Pi^{(\nu)} &= \Pi^{(\nu)} e^{-iL_H t} \\ &= (P^{(\nu)} + \mathbf{C}^{(\nu)}) e^{-i\theta^{(\nu)} t} A^{(\nu)} (P^{(\nu)} + \mathbf{D}^{(\nu)}) \end{aligned} \tag{5-60}$$

with

$$A^{(\nu)} \equiv (P^{(\nu)} + \mathbf{D}^{(\nu)}\mathbf{C}^{(\nu)})^{-1} \tag{5-61}$$

$$= \sum_\alpha N_\alpha^{(\nu)} | u_\alpha^{(\nu)} \rangle\rangle \langle\langle \tilde{v}_\alpha^{(\nu)} | \tag{5-62}$$

[3] One could also define another global collision operator associated with the destruction operator $\mathbf{D}^{(\nu)}$, see Ref.[33]

where Eq. (5-62) is not a spectral representation of super-operator $A^{(\nu)}$ as the state $|u_\alpha^{(\nu)}\rangle\rangle$ generally different from $|v_\alpha^{(\nu)}\rangle\rangle$. From Eq. (5-37) and Eq. (5-38) we have

$$L_H\Pi^{(\nu)} = \Pi^{(\nu)}L_H, \qquad \sum_\nu \Pi^{(\nu)} = 1, \qquad \Pi^{(\nu)}\Pi^{(\mu)} = \Pi^{(\nu)}\delta_{\nu,\mu} \tag{5-63}$$

Hence, $\Pi^{(\nu)}$ is a generalization of $P^{(\nu)}$ for the total Liouvillian L_H, and each of the correlation subspace evolves independently in time under L_H. For this reason $\Pi^{(\nu)}$ is associated with *subdynamics*. However Eq. (5-59) shows that $\Pi^{(\nu)}$ is not a hermitian super-operator. We call the component $P^{(\nu)}\rho^{(\nu)}$ as the "privileged" component of $\rho^{(\nu)} \equiv \Pi^{(\nu)}\rho$, which obeys the Markovian kinetic equation,

$$i\frac{\partial P^{(\nu)}\rho^{(\nu)}(t)}{\partial t} = \theta^{(\nu)}P^{(\nu)}\rho^{(\nu)}(t) \tag{5-64}$$

There is an infinite set of Markovian processes associated with each $\Pi^{(\nu)}$ subspace. Recall that we are interested in the weak coupling case. In that case, we apply series expansion in terms of λ up to $O(\lambda^2)$ which gives us

$$\theta^{(\nu)} = P^{(\nu)}L_0P^{(\nu)} + \lambda^2 P^{(\nu)}L_V\frac{-1}{L_0 - (w^{(\nu)} + i\epsilon)}Q^{(\nu)}L_VP^{(\nu)} + O(\lambda^4) \tag{5-65}$$

where we have analytically continued $z_\alpha^{(\nu)}$ from the upper-half plane to ensure that the time evolution is oriented to our future $t > 0$. Similarly, we have the global creation and global destruction operators expanded up to $O(\lambda^2)$

$$\mathbf{C}^{(\nu)} = \lambda\mathcal{C}_1^{(\nu)}(w^{(\nu)}) + \lambda^2\mathcal{C}_2^{(\nu)}(w^{(\nu)}) + O(\lambda^3) \tag{5-66}$$

$$\mathbf{D}^{(\nu)} = \lambda\mathcal{D}_1^{(\nu)}(w^{(\nu)}) + \lambda^2\mathcal{D}_2^{(\nu)}(w^{(\nu)}) + O(\lambda^3) \tag{5-67}$$

with a suitable analytic continuation of $w^{(\nu)}$, where $\lambda^n\mathcal{C}_n^{(\nu)}$,$\lambda^n\mathcal{D}_n^{(\nu)}$ are the n-th order terms of the expansion of $C^{(\nu)}$, and $D^{(\nu)}$ in Eq. (5-42) and Eq. (5-48), respectively. By perform the same expansion of operator $\mathbf{A}^{(\nu)}$ in Eq. (5-62), we have

$$\mathbf{A}^{(\nu)} = P^{(\nu)} - \lambda^2\mathcal{D}_1^{(\nu)}(w^{(\nu)})\mathcal{C}_1^{(\nu)}(w^{(\nu)}) + O(\lambda^3) \tag{5-68}$$

5.5 Markovian kinetic equation

In this section, we shall apply our complex spectral analysis to the problem of quantum decoherence. We shall first demonstrate the decoherence appearing in the particle by obtaining a Markov approximation for the off-diagonal component of the reduced density function associated with the particle.

An important consequence of the complex spectral represention of the Liouvillian is that non-Markov processes can be written as a superposition of Markov process of each subspace. For example, let us consider a subspace $P^{(\nu_1)}$ with $\nu_1 \equiv (n_1, m_1)$ where the field components are diagonal so that it is associated to the eigenvalue of the unperturbed Liouvillian as

$$L_0 P^{(\nu_1)} = (n_1 - m_1)\omega_1 P^{(\nu_1)} \tag{5-69}$$

Then we have

$$\begin{aligned} & P^{(\nu_1)} e^{-iL_H t} |\rho(0)\rangle\rangle \\ & = e^{-i\theta^{(\nu_1)} t} P^{(\nu_1)} \Pi^{(\nu_1)} |\rho(0)\rangle\rangle \\ & + \sum_{\mu \neq \nu_1} P^{(\nu_1)} \mathbf{C}^{(\mu)} e^{-i\theta^{(\mu)} t} A^{(\mu)} (P^{(\mu)} + \mathbf{D}^{(\mu)}) |\rho(0)\rangle\rangle \end{aligned} \tag{5-70}$$

The so-called Markov approximation corresponds to neglecting the second line in the right-hand side of Eq. (5-70). For the case where the expansion parameter of the perturbation analysis is the coupling constant λ, this approximation is valid only for the weakly coupling limit called as the "$\lambda^2 t$ limit [37]." In this Markov approximation the first line in Eq. (5-70) obeys Eq. (5-64), which leads to the following equation for the off-diagonal component of the reduced density function of

the particle,

$$\begin{aligned}
&\frac{\partial}{\partial t} f_{n_1,m_1}(t) - i\omega_1(m_1 - n_1) f_{n_1,m_1}(t) \\
&= \int dk \gamma_k [\sqrt{n_1 m_1}\langle n_k(t)\rangle f_{n_1-1,m_1-1}(t) \\
&-[(n_1 + m_1 + 1)\langle n_k(t)\rangle + \frac{1}{2}(n_1 + m_1)] f_{n_1,m_1}(t) \\
&+\sqrt{(n_1+1)(m_1+1)}(\langle n_k(t)\rangle + 1) f_{n_1+1,m_1+1}(t)]
\end{aligned} \tag{5-71}$$

Here the reduced density functions for the particle is defined as

$$f_{n_1,m_1}(t) = \langle n_1 | Tr_F[P^{(\nu_1)}\rho(t)] | m_1\rangle, \tag{5-72}$$

where Tr_F means that the partial trace is taken with respect to all field components, and $\langle n_k(t)\rangle$ is the average number of the field at time t.

In the lowest order approximation in λ, γ_k in ν_1 subspace is given by

$$\gamma_k \approx 2\pi\lambda^2 |v_k|^2 \delta(\omega_k - \omega_1) \tag{5-73}$$

If we incorporate higher order correction in this subspace, $\delta(\omega_k - \omega_1)$ should be replaced by a Lorentzian distribution that has a peak at the shifted frequency $\omega_k = \omega_1 + \delta\omega_1$ and the width $\Gamma \equiv \Omega^{-1}\sum_k \gamma_k$. A detailed derivation of Eq. (5-71) has been presented in [35].It was shown that the Eq. (5-71) in the Wigner representation indeed describes the decoherence as a result of the irreversible diffusion processes that come from the resonance effect between the particle and the field.

In the kinetic theory, to go beyond the $\lambda^2 t$ limit including memory effects (non-Markovian effects) has been a long standing extremely difficult problem. Our complex spectral representation gives a consistent description of the non-Markovian effects by systematically evaluating the second line in Eq. (5-70). For example, applying the expression Eq. (5-70) to our system, we have shown that the memory

effect dies out in the time scale of the order $1/\omega_1 \ll \lambda^{-2}$ [35], [38]. Therefore, $1/\omega_1$ gives a time scale of transition of the evolution from the non-Markovian regime to the Markovian regime. This transition time scale is just quantum Zeno time mentioned in previous chapter, only after the Zeno time does the first term in Eq. (5-70) dominate. Hence, the Zeno time serves as a lower bound for the decoherence time [35], [38].

In the following, we shall focus ourselves on the time evolution of the field, which was commonly neglected in the literature [15–19]. We derive a closed set of equation for the reduced number density of the field, and the particle.

The reduced number densities of the particle and the field are belong to the vacuum of correlation subspace, i.e., $P^{(0)}$ component of the density matrix. By applying the completeness relation of $\Pi^{(\nu)}$ in Eq. (5-63), the reduced number densities are decomposed into

$$\begin{aligned} \langle n_\alpha(t)\rangle &\equiv \mathrm{Tr}(a_\alpha^+ a_\alpha P^{(0)}\rho(t)) \\ &= \langle n_\alpha(t)\rangle_{\Pi^{(0)}} + \sum_{\nu\neq 0}\langle n_\alpha(t)\rangle_{\Pi^{(\nu)}} \end{aligned} \tag{5-74}$$

for $\alpha = 1$, and k correspond to the reduced number density of the particle, and the field. Here we denote

$$\langle n_\alpha(t)\rangle_{\Pi^{(\nu)}} \equiv \mathrm{Tr}(a_\alpha^+ a_\alpha P^{(0)}\Pi^{(\nu)}\rho(t)) \quad , \quad \alpha = 1, k \tag{5-75}$$

The decomposition in Eq. (5-74) is parallel with Eq. (5-70) that the first term follows the Markov kinetic equation in Eq. (5-64), and the second term is the non-Markov effect. By taking the derivative of $\langle n_\alpha(t)\rangle$ with respect to time, one can show

$$\lim_{t\to 0}\frac{d\langle n_\alpha(t)\rangle}{dt} = 0 \qquad , \alpha = 1, k \tag{5-76}$$

which corresponds to the quantum Zeno effect [14]. This result is incompatible with the exponential decay obtained from the Markov approximation. Therefore we have

to analyze carefully the non-Markov effect coming from subspaces other than $\Pi^{(0)}$ in the Eq. (5-74).

We first obtain a Pauli type of master equation in the weak coupling limit ($\lambda^2 t$ approximation) for the first Markovian term in Eq. (5-74). In the next section, we shall calculate the correction from non-Markov effect which is non-negligible in the time scale of $O(1/\omega_1)$.

By multiplying $a_\alpha^+ a_\alpha$ at both sides of Eq. (5-64) with $\nu = 0$, we then have the following closed equation for the reduced number densities

$$i\frac{\partial \langle n_1(t)\rangle_{\Pi^{(0)}}}{\partial t} = \theta^{(0)}_{11:11}\langle n_1(t)\rangle_{\Pi^{(0)}} + \sum_l \theta^{(0)}_{11:ll}\langle n_l(t)\rangle_{\Pi^{(0)}} \tag{5-77}$$

$$i\frac{\partial \langle n_k(t)\rangle_{\Pi^{(0)}}}{\partial t} = \theta^{(0)}_{kk:11}\langle n_1(t)\rangle_{\Pi^{(0)}} + \sum_l \theta^{(0)}_{kk:ll}\langle n_l(t)\rangle_{\Pi^{(0)}} \tag{5-78}$$

where the matrix elements $\theta^{(0)}_{\alpha\beta:\alpha'\beta'} \equiv \langle\langle \alpha;\beta|\theta^{(0)}|\alpha';\beta'\rangle\rangle$, and we abbreviate $|1\rangle \equiv |1_1, \{0_F\}\rangle$, and $|k\rangle \equiv |0_1, ...0_{k_{j-1}}, 1_{k_j}, 0_{k_{j+1}}...\rangle$. To derive the above equations, we have used a formula for an arbitrary superoperator S of the function of L_H(including $\lambda = 0$ case),

$$\mathrm{Tr}(a_\alpha^+ a_\alpha S(L_H)\rho(t)) = \sum_{\beta\beta'}\langle\langle \alpha;\alpha|S(L_H)|\beta;\beta'\rangle\rangle \mathrm{Tr}(a^+_{\beta'}a_\beta \rho(t)) \tag{5-79}$$

which is valid for our Friedrichs model that dose not involve the virtual processes. For example, one can easily verify Eq. (5-79) for the case S is L_H itself, hence it valid for the any power of L_H. From the expansion of $\theta^{(0)}$ in Eq. (5-65) , we calculate the matrix elements of the collision operator up to $O(\lambda^2)$. The derivation is presented in Appendix F. Substituting Eqs. (F-3)–(F-5) into Eq. (5-77), and Eq. (5-78), we obtain the Markovian kinetic equation under the $\lambda^2 t$ approximation,

$$\frac{\partial}{\partial t}\langle n_1(t)\rangle_{\Pi^{(0)}} = \frac{1}{\Omega}\sum_k \gamma_k[\langle n_k(t)\rangle_{\Pi^{(0)}} - \langle n_1(t)\rangle_{\Pi^{(0)}}] \tag{5-80}$$

$$\frac{\partial}{\partial t}\langle n_k(t)\rangle_{\Pi^{(0)}} = \frac{1}{\Omega}\gamma_k[\langle n_1(t)\rangle_{\Pi^{(0)}} - \langle n_k(t)\rangle_{\Pi^{(0)}}] \tag{5-81}$$

Recall that $\Gamma \equiv \Omega^{-1} \sum_k \gamma_k$. These equations correspond to the well-known Uhling-Uhlenbeck equation for the average number of particles and the field for the case of nonlinear interaction. The solutions of these equations up to $\mathrm{O}(\Omega^{-1})$ are given by,

$$\langle n_1(t)\rangle_{\Pi^{(0)}} \approx e^{-\Gamma t}\langle n_1(0)\rangle_{\Pi^{(0)}} + \frac{1}{\Omega\Gamma}\sum_l \gamma_l \langle n_l(0)\rangle_{\Pi^{(0)}}(1-e^{-\Gamma t}) \tag{5-82}$$

$$\begin{aligned}\langle n_k(t)\rangle_{\Pi^{(0)}} \approx\ & \langle n_k(0)\rangle_{\Pi^{(0)}} + \frac{\gamma_k}{\Omega\Gamma}(1-e^{-\Gamma t})\langle n_1(0)\rangle_{\Pi^{(0)}} \\ & -\frac{\gamma_k}{\Omega\Gamma^2}\sum_l \gamma_l \langle n_l(0)\rangle_{\Pi^{(0)}}(1-e^{-\Gamma t}) \\ & +\frac{\gamma_k t}{\Omega}\left[\frac{1}{\Omega\Gamma}\sum_l \gamma_l \langle n_l(0)\rangle_{\Pi^{(0)}} - \langle n_k(0)\rangle_{\Pi^{(0)}}\right]\end{aligned} \tag{5-83}$$

Let us first focus our attention on the decoherence of the particle by assuming the initial background field is in a thermal equilibrium in a given temperature where the photon probability density is given by the Plank distribution. We assume the particle is initially in the ground state. This situation is often considered in the phenomenological approaches of decoherence problem.

In Figure 5.1, we compare the theoretical result of the time evolution of the number density of particle $\langle n_1(t)\rangle$ in Eq. (5-82) with the numerical simulation. The detail discussion of the numerical simulation will be given in Section 5.7. We choose the dimensionless coupling constant $\lambda = 0.1$, and the temperature of the background field $T = 1$ in the unit of ω_1/k_B where k_B is the Boltzmann constant. The dotted line is the numerical result while the solid line is the theoretical prediction from the solution of the Markovian kinetic equation. It shows that the Markovian approximation that leads to the exponentially decay of the particle gives very good approximation in the time scale $t \sim O(1/\Gamma)$.

In Figure 5.2, we show a magnification of the early stage $t \sim 1/\omega_1$ of figure Figure 5.1. In this short time period, we see the non-Markov contribution is non-negligible which leads to the deviation of exponential processes. It is associated with

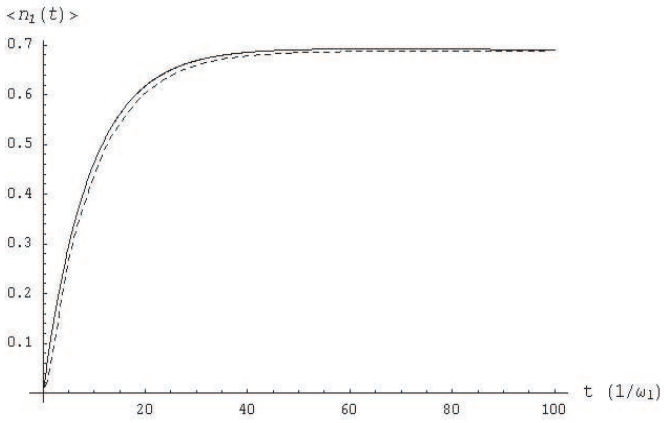

Figure 5.1: Decoherence of bare particle in thermal heat bath which obey Plank distribution. We plot the time evolution of the number density of the particle. The solid line is the theoretical prediction in Eq. (5-82) obtained through Markovian approximation, while the dotted line is the numerical simulation.

the well-known quantum Zeno effect. Petrosky and Barsegov [35] have shown that the memory effect follows a power law decay, then the time evolution undergoes a transition from non-Markovian regime to the Markovian regime. As a result the transition time $t \sim 1/\omega_1$ gives a lower bound for the decoherence time. Only after this time scale, the results obtained from the Markovian kinetic equation become valid.

Let us next consider the time evolution of the field. Under the thermodynamic limit Eq. (5-18b), the last term of our solution in Eq. (5-83) has a non-negligible t-linear contribution as compared with the first term. This is a secular effect that appears through the resonance effect that destroys the factorizability to the evolution of the density matrix into the product of the wave functions.

However if the initial condition of the field is in thermal equilibrium of the unperturbed system (which is a common setting of phenomenological environmental approach [15–19]), the secular effect vanishes due to the symmetric dependence of

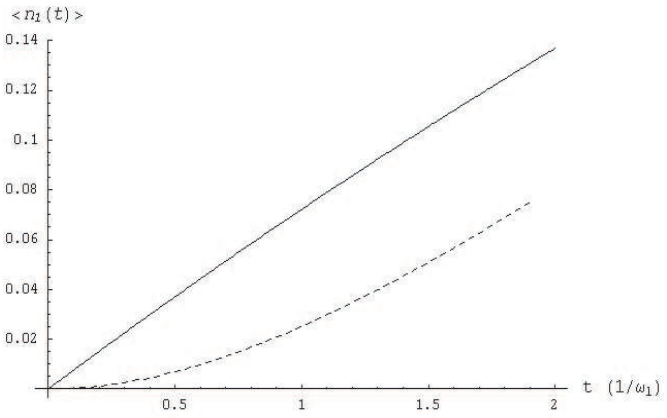

Figure 5.2: Magnification of a portion of the short time scale (the Zeno period) of $t \sim 1/\omega_1$.

$\langle n_k(0) \rangle$ with respect to an interchange of k to $-k$ in the equilibrium state. Hence, in order to see this effect, we have to choose a non-equilibrium initial condition. In the next section, we shall consider a far-from-equilibrium case where the initial field is a pure state, and show how it evolves to mixed state dynamically through the secular effect due to the resonance between the particle and the field.

5.5.1 Decoherence in a scattered field

In this section, we shall calculate explicitly the t-linear effect for the case where initial field is in a far-from-equilibrium situation. Let us assume the initial state is in a pure state given by

$$\rho(0) = |\Phi(0)\rangle\langle\Phi(0)| \tag{5-84}$$

To achieve the thermodynamic limit of the field in a pure state, we consider a case with a large rectangular shaped wavepacket of the field with a size $L_{21} \equiv L_2 - L_1 > 0$ in one dimensional coordinate space shown in Figure 5.3 that consists

of a superposition of the coherent states of the field, i.e.,

$$|\Phi(0)\rangle = \sum_k^{\infty} \Phi_k |\hat{\alpha}_k\rangle \tag{5-85}$$

with

$$\Phi_k \equiv \frac{i}{\sqrt{L_{21}L}} \left[\frac{e^{-iL_2(k-k_0)} - e^{-iL_1(k-k_0)}}{k - k_0 - i\epsilon} \right] \tag{5-86}$$

and

$$|\hat{\alpha}_k\rangle = e^{-|\alpha_k|^2/2} \sum_{n_k=0}^{\infty} \frac{(\alpha_k a_k^+)^{n_k}}{\sqrt{n_k!}} |0_1, \{0_F\}\rangle \tag{5-87}$$

where 0_1 and $\{0_F\}$ denote the vacuums of the particle and the field, respectively. We have

$$a_k|\Phi(0)\rangle = \alpha_k \Phi_k |\hat{\alpha}_k\rangle \tag{5-88}$$

$$\langle\hat{\alpha}_k|\hat{\alpha}_l\rangle = \delta_{kl} \tag{5-89}$$

We assume that $\alpha_k = \sqrt{nL_{21}}$ for all modes k, where n is a number density of the photon per unit length. Then the total number of the photon in the initial wavepacket is proportional to the size of the wavepacket as $\sum_k \langle\Phi(0)|a_k^+ a_k|\Phi(0)\rangle = nL_{21}$.

To observe the spatial structure, we introduce the x representation of creation operator a_k^+ by

$$a^+(x) \equiv \frac{1}{\sqrt{L}} \sum_k e^{-ikx} a_k^+ \tag{5-90}$$

The x representation of our wavepacket is then given by

$$\langle x|\Phi\rangle = \sqrt{n}\left[\theta_S(x - L_1) - \theta_S(x - L_2)\right] e^{ik_0 x} \tag{5-91}$$

where

$$|x\rangle \equiv \sum_{n_1} a^+(x)|n_1, \{0_F\}\rangle \tag{5-92}$$

and $\theta_S(x)$ is the step function

$$\theta_S(x) = \begin{cases} 0 & : \quad x < 0 \\ 1 & : \quad x \geq 1 \end{cases} \tag{5-93}$$

The Figure 5.3 is the case with $L_2 < L_1 < 0$. If the size of the wavepacket L_{21} is the

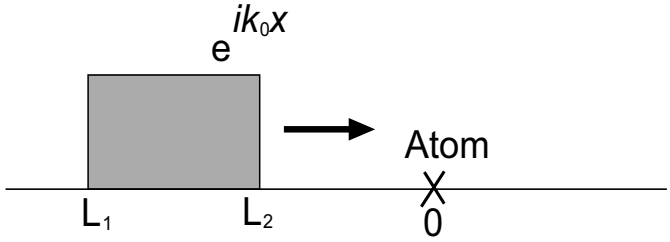

Figure 5.3: The diagram of the scattering of a rectangular wavepacket with a particle. The atom is located at the origin which the size of the wavepacket is $L_{21} \equiv L_2 - L_1$

same order of L, then the field satisfies the thermodynamic condition Eq. (5-18b). For the special case $L_1 = -L_2 = L/2$, Eq. (5-86) reduces to $\Phi_k = \delta_{k,k_0}$, i.e., the density matrix becomes $\rho(0) = \delta_{k,k_0}|\hat{\alpha}_{k_0}\rangle\langle\hat{\alpha}_{k_0}|$. This corresponds to a "plane wave." In Appendix F and Appendix H, we have calculated $\langle n_k(0)\rangle_{\Pi^{(0)}}$ for both the rectangular wavepacket and the plane wave. Both have the same dominate term in $O(\lambda^0)$, i.e.

$$\langle n_k(0)\rangle_{\Pi^{(0)}} \approx nL_{12}|\Phi_k|^2 \tag{5-94}$$

Since $\langle n_k(0)\rangle_{\Pi^{(0)}}$ is not symmetry under the changing from k to $-k$, we have the non-vanishing t-linear term as

$$\langle n_k(t)\rangle_{\Pi^{(0)},t-linear} \approx \frac{\gamma_k n L_{21}}{2\Omega} t(|\Phi_{-k}|^2 - |\Phi_k|^2) \tag{5-95}$$

However, cares have to be taken to analyze the evolution. From Eq. (5-95) the t-linear term contributed from $\Pi^{(0)}$ subspace itself does not obey the causality. The expression does not contain the information of when the rectangular wave starts to

hit the particle at the origins. To be consistence with the causality, we must include the contribution from other subspaces. In the $\lambda^2 t$ approximation the non-Markov effects coming from the subspaces other than $\Pi^{(0)}$ has been neglected. Only by going beyond the $\lambda^2 t$ approximation, one can consistently discuss the decoherence process in the field evolution. In next section we shall explicitly calculate the corrections from other subspaces.

5.6 Non-Markovian corrections

In this section we calculate the non-Markov contribution coming from subspaces other than $\Pi^{(0)}$. From Eq. (5-75), we have the reduced number density contributed from $P^{(\nu)}$ subspace as

$$\begin{aligned} \langle n_k(t)\rangle_{\Pi^{(\nu)}} &= \mathrm{Tr}(a_k^+ a_k P^{(0)}\Pi^{(\nu)}\rho(t)) \\ &= \sum_{\beta,\beta'} \langle\langle k;k|e^{iL_H t}\Pi^{(\nu)}|\beta;\beta'\rangle\rangle \mathrm{Tr}(a_{\beta'}^+ a_\beta \rho(0)) \end{aligned} \tag{5-96}$$

where we have again applied the formula from Eq. (5-79).

In the following, we shall calculate the reduced number density of the field corresponds to these subspaces. The calculation for the special case of a plane wave is presented separated in Appendix H.

Substituting the initial condition from Eq. (5-84), and $\Pi^{(\nu)}$ from Eq. (5-60) into Eq. (5-96), we have

$$\langle n_k(t)\rangle_{\Pi^{(\nu)}} = nL_{21}\sum_{l,l'}\Phi_l\Phi_{l'}^*\langle\langle\alpha;\alpha|(P^{(\nu)}+\mathbf{C}^{(\nu)})e^{-i\theta^{(\nu)}t}A^{(\nu)}(P^{(\nu)}+\mathbf{D}^{(\nu)})|l;l'\rangle\rangle \tag{5-97}$$

Let us first consider the case $\nu = (1k)$. From the expansion of $\mathbf{A}^{(\nu)}$, $\mathbf{C}^{(\nu)}$, and $\mathbf{D}^{(\nu)}$

in Eqs. (5-66)–(5-68), we have up to $O(\lambda^2)$

$$\begin{aligned}
\langle n_k(t)\rangle_{\Pi^{(1k)}} &\approx nL_{21}\sum_{l,l'}\Phi_l\Phi_{l'}^*\langle\langle k;k|\lambda\mathcal{C}_1^{(1k)}e^{-i\theta^{(1k)}t}\lambda\mathcal{D}_1^{(1k)}|l;l'\rangle\rangle \\
&= nL_{21}\Phi_k^*\sum_l\Phi_l\langle\langle k;k|\frac{-1}{L_0-w^{(1k)}+i\epsilon}\lambda L_V|1;k\rangle\rangle \\
&\quad\times e^{i\theta_{1k:1k}^{(1k)}t}\langle\langle 1;k|\lambda L_V\frac{1}{w^{(1k)}+i\epsilon-L_0}|l;k\rangle\rangle \\
&= -nL_{21}\frac{V_k\Phi_k^*e^{-i\theta_{1k:1k}^{(1k)}t}}{\omega_k-\omega_1+i\epsilon}\sum_l\frac{V_l\Phi_l}{\omega_1-\omega_l+i\epsilon} \qquad (5\text{-}98)
\end{aligned}$$

By using the expansion from Eq. (5-65), we have

$$\begin{aligned}
\theta_{1k:1k}^{(1k)} &\approx \langle\langle 1;k|P^{(1k)}L_0P^{(1k)}|1;k\rangle\rangle \\
&\quad+\lambda^2\langle\langle 1;k|P^{(1k)}L_V\frac{-1}{L_0-w^{(1k)}-i\epsilon}Q^{(1k)}L_VP^{(1k)}|1;k\rangle\rangle \\
&= w^{(1k)}+\lambda^2\sum_{\alpha,\beta}\langle\langle 1;k|L_V|\alpha;\beta\rangle\rangle\frac{-1}{w^{(\alpha\beta)}-w^{(1k)}-i\epsilon}\langle\langle\alpha;\beta|L_V|1;k\rangle\rangle \\
&= w^{(1k)}+\lambda^2\sum_l\frac{-V_l^2}{w^{(lk)}-w^{(1k)}-i\epsilon} \qquad (5\text{-}99) \\
&= \tilde{\omega}_1-i\gamma-\omega_k \qquad (5\text{-}100)
\end{aligned}$$

where we have taken the continuous limit in the last step. The $\tilde{\omega}_1$, and γ are defined by

$$\begin{aligned}
\tilde{\omega}_1 &= \omega_1-\lambda^2\mathrm{Pr}\left[\int_{-\infty}^{\infty}dl\frac{|v_l|^2}{\omega_l-\omega_1}\right] \qquad (5\text{-}101) \\
\gamma &= 2\pi\lambda^2v_{\omega_1}^2 \qquad (5\text{-}102)
\end{aligned}$$

where Pr[...] denotes the principal part of the integration. Compare with Eq. (5-73), we have $\gamma=\sum_k\gamma_k/s\Omega=\Gamma/2$. Substituting $\theta_{1k:1k}^{(1k)}$ to Eq. (5-98) we have

$$\langle n_k(t)\rangle_{\Pi^{(1k)}}=\lambda^2\frac{nL_{21}}{\Omega}\frac{v_k\Phi_k^*e^{i(\omega_k-\tilde{\omega}_1)t-\gamma t}}{(\omega_k-\omega_1+i\epsilon)}\sum_l\frac{v_l\Phi_l}{(\omega_l-\omega_1-i\epsilon)} \qquad (5\text{-}103)$$

For the $\Pi^{(k1)}$ subspace, one can verify that $\langle n_k(t)\rangle_{\Pi^{(k1)}}$ is the complex conjugate of Eq. (5-103). The same relationship applies to the $\Pi^{(kl)}$ and $\Pi^{(lk)}$ cases. We apply the same procedure for $\Pi^{(lk)}$ subspace[4]. Then we obtain

$$\begin{aligned}
\sum_{l\neq k}\langle n_k(t)\rangle_{\Pi^{(lk)}} &\approx nL_{21}\Phi_k^*\sum_{l\neq k}\Phi_l\langle\langle k;k|\lambda^2 C_2^{(lk)}e^{-i\theta^{(lk)}t}|l;k\rangle\rangle \\
&= nL_{21}\Phi_k^*\sum_{l\neq k}\Phi_l\langle\langle k;k|\frac{-1}{L_0-w^{(lk)}+i\epsilon}\lambda L_V|1;k\rangle\rangle \\
&\quad\times\langle\langle 1;k|\frac{-1}{L_0-w^{(lk)}+i\epsilon}\lambda L_V|l;k\rangle\rangle e^{-i\theta^{(lk)}_{lk;lk}t} \\
&\approx -\lambda^2\frac{nL_{21}}{\Omega}v_k\Phi_k^*e^{i\omega_k t}\sum_l\frac{v_l\Phi_l e^{-i\omega_l t}}{(\omega_k-\omega_l+i\epsilon)(\omega_l-\omega_1-i\epsilon)} \qquad (5\text{-}104)
\end{aligned}$$

where we have replaced $\sum_{l\neq k}$ by $\sum_l$ as the one point contribution is negligible under the continuous limit where the summation is replaced by integration. This formula does not satisfy the causality for the evolution of $\langle n_k(t)\rangle$. Indeed if we use this approximated forms in Eq. (5-103) and Eq. (5-104), $\langle n_k(t)\rangle$ has already the interaction before the wavepacket reaches to the particle. Therefore we have to incorporate the higher order contribution and renormalize the denominator incorporating the effect of interaction in such a way ω_1 is replaced by $\tilde{\omega}_1 - i\gamma$. Then we obtain

$$\langle n_k(0)\rangle_{\Pi^{(0)}} \approx |\Phi_k|^2 - \left\{\lambda^2\frac{nL_{21}}{\Omega}\frac{v_k\Phi_k^*}{(\omega_k-\tilde{\omega}_1+i\gamma)}\sum_l\frac{v_l\Phi_l}{(\omega_l-\omega_k-i\epsilon)}+c.c\right\} \qquad (5\text{-}105)$$

$$\langle n_k(t)\rangle_{\Pi^{(1k)}+\Pi^{(k1)}} = \lambda^2 nL_{21}\frac{v_k\Phi_k^*e^{i(\omega_k-\tilde{\omega}_1)t-\gamma t}}{\Omega(\omega_k-\tilde{\omega}_1+i\epsilon)}\sum_l\frac{v_l\Phi_l}{(\omega_l-\tilde{\omega}_1+i\gamma)^+}+c.c \qquad (5\text{-}106)$$

$$\langle n_k(t)\rangle_{\Pi^{(lk)}+\Pi^{(kl)}} = -\lambda^2 nL_{21}\frac{v_k\Phi_k^*e^{i\omega_k t}}{\Omega}\sum_l\frac{v_l\Phi_l e^{-i\omega_l t}}{(\omega_k-\omega_l+i\epsilon)(\omega_l-\omega_1+i\gamma)^+}+c.c \qquad (5\text{-}107)$$

Here we have chosen the analytic continuation of the denominator in the integral over l as $1/(\omega_l-\omega_1+i\gamma)^+$ where superscript "+" means that the analytic continuation

[4]For the case of plane wave, $\langle n_k(t)\rangle_{\Pi^{(lk)}} \sim \lambda^6$ which was neglected in Appendix H

is taken from the upper-half plane of z to the lower half plane. As we shall see later that this analytic continuation guarantees the causality of $\langle n_k(t)\rangle$. In the following section, we shall compare our theoretical results with the numerical simulation.

5.7 Numerical simulation

To verify our theoretical predictions, we have performed the numerical simulation which is presented in Appendix I. In the simulation, we consider the system of a finite box with size L. For this case our system is exactly diagonalizable through the linear transformation. In order to compare our numerical result with the case with continuous spectrum, we restrict our observation time to $t \ll L/c$. We have used the form factor v_k for the interaction as $v_k = \sqrt{\omega_k}\left[1 + (\omega_k/\omega_M)^2\right]^{-2}$ [39]. The cut-off frequency ω_M is introduced to avoid the ultraviolet divergence. We have used a unit system where the length is measured by the unit c/ω_1, while the time is measure by the unit $1/\omega_1$. We have used a fixed size of box $L = 209$, the coupling constant $\lambda = 0.1$ and the cut-off frequency $\omega_M = 10$ in all cases. The relaxation time scale is given by $1/\Gamma = 9.3$ (see Eq. (5-73)) in all these figures.

In Figure 5.4 we plot the numerical result of the time evolution of the number density $\langle n(x,t)\rangle \equiv \mathrm{Tr}(a^+(x)a(x)\rho(t))$ of the photon from $t = 0$ to $t = 5/\Gamma$, starting at $t = 0$ with $\langle n_1\rangle = 0$ and $\langle n_k\rangle \equiv 1/(\exp(\beta\omega_k) - 1)$ is the Plank distribution with the temperature $\beta_1 \equiv 1/k_B T_1 = 1/\omega_1$. The particle is located at $x = 0$. At $t = 0$ we have a constant density $\langle n(x,0)\rangle = 1.52$. About $t = 1/\Gamma$ a non-negligible steady cloud of field surrounding the particle with a size of c/ω_1 has been established. Generally the size of this cloud is much larger than the size of the molecule, and it causes the long-range van der Waals forces or Casimir-Polder forces [29]. One can see the propagation of the fronts of the field, obeying causality. The shape of the fronts generally depends on the initial condition of $\langle n_1\rangle$. Due to the dispersion

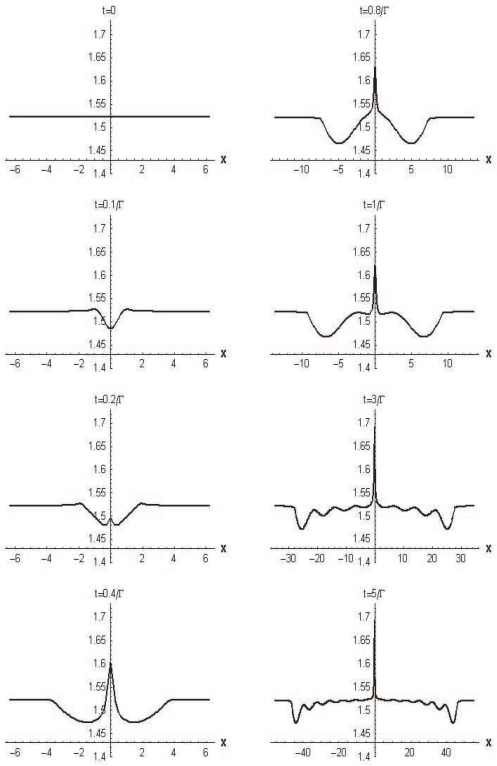

Figure 5.4: Scenario of time evolution of $\langle n(x,t)\rangle$. The particle located at ground state is surrounded initially by a thermodynamics field initially.

relation $\omega_k = |k|$, the fronts do not change their shape for the one-dimensional case. The field has a non-negligible time evolution , which is commonly neglected in the decoherence problem [15–19],

From Figure 5.5 – Figure 5.8, we show several results in the case of the scattering of a rectangular wavepacket by the particle, whose initial condition is given by Eq. (5-86).

In Figure 5.5, we plot $\langle n_{k=k_0}(t)\rangle$ with the mode $k_0 = 5$ as a function of time t. We have chosen $\langle n_1(0)\rangle = 0$ and $\langle n_k(0)\rangle$ is the plane wave. The dashed line is the

numerical result. The theoretical result due to the Markov approximation Eq. (5-83) with intial condition given in Appendix H is plotted by the thick line, while the theoretical result including a dominant correction due to the non-Markovian effects coming from Eq. (H-6) is plotted by the thin line. In the Markovian approximation, we have taken account of the higher order effect of λ in such a way that the delta function $\delta(\omega_{k_0} - \omega_1)$ in Eq. (5-73) is replaced by the Lorentzian with the width of Γ. Since the $k_0 \gg \omega_1 = 1$ in our case ,we are far from the peak of the Lorentzian shape. After a time scale of a few oscillations of the particle, one can clearly see the t-linear secular effect.

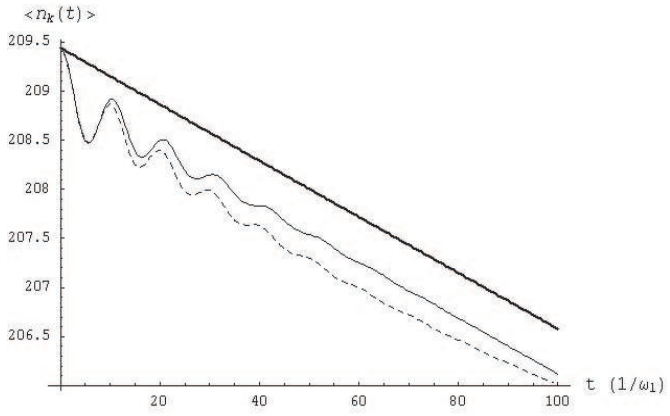

Figure 5.5: Time evolution of the number density of $\langle n_k(t) ket$. The theoretical result due to the Markovian approximation Eq. (5-83) is plotted by the thick line, while the theoretical result including corrections from non-Markov effects is plotted by the thin line. The dashed line is the numerical simulation.

In Figure 5.6, we magnify the Zeno period $t \sim 1/\omega_1$ in the early stage of the time evolution in Figure 5.5. We show the numerical result (the dotted line) and the theoretical result (the solid line) with non-Markov effects. These results shows that the time derivative of $\langle n_k(t) \rangle$ vanishes at $t = 0$, which consistent with the Zeno effect shown in Eq. (5-76). Our theoretical result consistently recovers this

well-known non-Markov effect by going beyond $\lambda^2 t$ approximation.

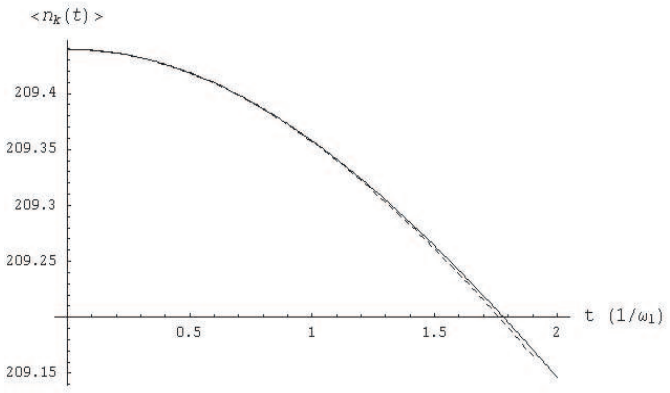

Figure 5.6: Magnification of the early time scale $t \sim 1/\omega_1$ of Figure 5.5. It shows our theoretical result with non-Markovian terms (solid line) included is in good agreement with numerical result (dashed line).

In Figure 5.7 we plot the numerical result of the line shape $\langle n_k(t) \rangle$ for several times $t = 10$, 20, 30, and 40. Here we choose the wave packet of size $L_{21} = 35$, and $k_0 = \omega_1 = 1$. It evolves from the thinnest line to the thickest line. During the moment the wave packet overlaps with the particle, the height of the line shape grows linearly in time in the negative direction as predicted by our theory in Eq. (5-95), then the height is saturated after the moment the wave packet is dissociated from the particle.

In Figure 5.8 we plot the numerical simulation of the time evolution of the number density of particle. The parameters of incident wavepacket are given $L_1 = -52$, $L_2 = 0$, and $k_0 = \omega_1$. During the moment $(0 < t < 52)$ when the wavepacket interacts with the particle, we see the particle is excited from the ground state whose time evolution is proportional to $(1 - \exp(-\Gamma t))$ given in Eq. (5-82). After the wavepacket passes through $(t > 52)$, it decays exponential in time. The

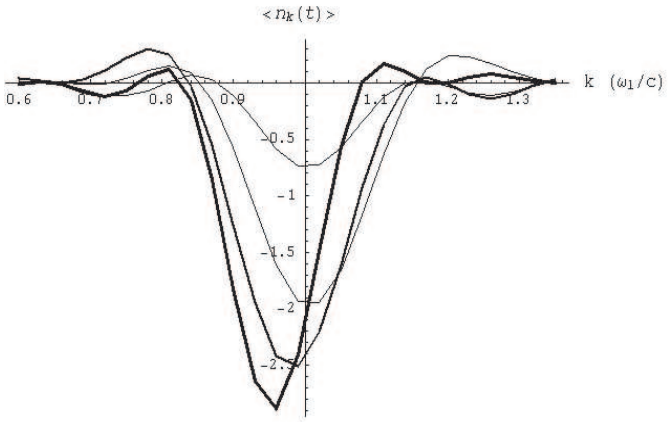

Figure 5.7: Line shape of the scattered field at several times t = 10, 20, 30, and 40. It evolves from the thinnest line to the thickest line

numerical result shows the saturation of the particle and then decay exponentially after the passage of the wave packet.

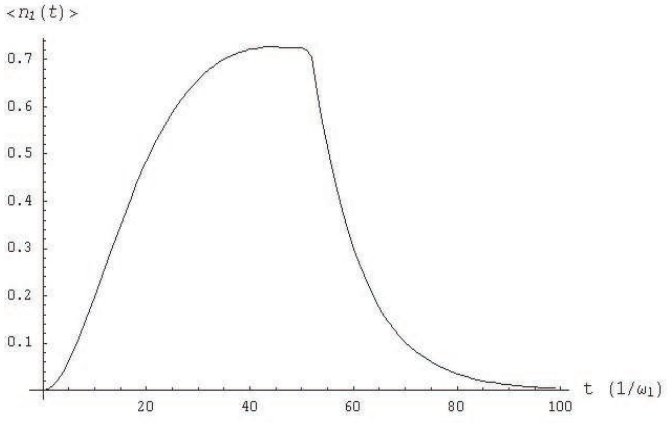

Figure 5.8: Time evolution of $\langle n_1(t) \rangle$ in the scattering of wavepacket

In summary we have obtained that there is non-negligible t-linear time evolution of $\langle n_k(t) \rangle$ in the field. This contribution comes from the secular effect of

resonance that breaks the purity of the state in decoherence process. We have indeed shown that this secular effect does not disappear even by adding non-Markovian contributions from subspaces other than $\Pi^{(0)}$.

Appendices

Appendix A

Electromagnetic field in rectangular waveguide

In this appendix, we shall show the field inside the waveguide can be expanded into TE wave and TM wave [11] with the form given in Eq. (2-10) and Eq. (2-11).

From the sourceless Maxwell equations[1],

$$\vec{\nabla} \times \mathbf{E} = -\frac{1}{c}\frac{\partial \mathbf{B}}{\partial t} \tag{A-1}$$

$$\vec{\nabla} \times \mathbf{B} = \frac{1}{c}\frac{\partial \mathbf{E}}{\partial t} \tag{A-2}$$

$$\vec{\nabla} \cdot \mathbf{E} = 0 \tag{A-3}$$

$$\vec{\nabla} \cdot \mathbf{B} = 0 \tag{A-4}$$

Since the waveguide is open in z direction, we expanded the z dependence part in terms of plane wave with wave vector k and oscillation frequency $\omega_{\mathbf{k}}$,

$$\mathbf{E}(x, y, z, t) = \vec{E}(x, y)e^{ikz - i\omega_{\mathbf{k}}t} \tag{A-5}$$

$$\mathbf{B}(x, y, z, t) = \vec{B}(x, y)e^{ikz - i\omega_{\mathbf{k}}t} \tag{A-6}$$

where the dispersion relation will be derived later. Substituting them into Eq. (A-4), we obtain

$$\vec{\nabla}_t^2 + (\frac{\omega_{\mathbf{k}}^2}{c^2} - k^2)\begin{pmatrix}\vec{E}(x, y)\\ \vec{B}(x, y)\end{pmatrix} = 0 \tag{A-7}$$

[1]Unless otherwise specified, we use gaussian unit as default unit in the waveguide problem

By decomposing the fields into z components $\vec{E}_z$, $\vec{B}_z$, and transverse components $\vec{E}_t$, $\vec{B}_t$, we rewrite Eq. (A-4) as

$$\frac{\partial \vec{E}_t}{\partial z} + i\frac{\omega_{\mathbf{k}}}{c}\hat{e}_z \times \vec{B}_t = \vec{\bigtriangledown}_t E_z \tag{A-8}$$

$$\frac{\partial \vec{B}_t}{\partial z} - i\frac{\omega_{\mathbf{k}}}{c}\hat{e}_z \times \vec{E}_t = \vec{\bigtriangledown}_t B_z \tag{A-9}$$

$$\hat{e}_z \cdot (\vec{\bigtriangledown}_t \times \vec{E}_t) = i\frac{\omega_{\mathbf{k}}}{c} B_z \tag{A-10}$$

$$\hat{e}_z \cdot (\vec{\bigtriangledown}_t \times \vec{B}_t) = -i\frac{\omega_{\mathbf{k}}}{c} E_z \tag{A-11}$$

$$(\vec{\bigtriangledown}_t \cdot \vec{E}_t) = -\frac{\partial E_z}{\partial z} \tag{A-12}$$

$$(\vec{\bigtriangledown}_t \cdot \vec{B}_t) = -\frac{\partial B_z}{\partial z} \tag{A-13}$$

which shows the relationship of transverse components and z components. Assuming the waveguide is made of perfect conductor, we then have the boundary conditions

$$E_z = 0 \qquad \text{on surface} \tag{A-14}$$

$$\hat{e}_n \cdot \vec{\bigtriangledown}_t B_z = 0 \qquad \text{on surface} \tag{A-15}$$

with $\hat{e}_n$ defined as the unit vector perpendicular to the surface. According to these two independent boundary conditions, the solutions are divided into two independent groups of wave, i.e. Transverse Electric(TE) wave, and Transverse Magnetic(TM) wave, which are subjected to the following conditions,

$$\text{TE wave} \begin{cases} E_z = 0 & \text{everywhere} \\ \hat{e}_n \cdot \vec{\bigtriangledown}_t B_z = 0 & \text{on boundary} \end{cases} \tag{A-16}$$

$$\text{TM wave} \begin{cases} B_z = 0 & \text{everywhere} \\ E_z = 0 & \text{on boundary} \end{cases} \tag{A-17}$$

Substituting the conditions Eq. (A-16) and Eq. (A-17) into Eq. (A-13), the equations for TE and TM waves are separated

$$\begin{cases} \vec{E}_t = \frac{ck}{\omega_{\mathbf{k}}}\hat{e}_z \times \vec{B}_t \\ \vec{B}_t = i\frac{k}{(\frac{\omega_{\mathbf{k}}^2}{c^2} - k^2)}\vec{\bigtriangledown}_t B_z \qquad \text{TE wave} \\ (\vec{\bigtriangledown}_t^{\,2} + \frac{\omega_{\mathbf{k}}^2}{c^2} - k^2)B_z = 0 \end{cases} \tag{A-18}$$

$$\begin{cases} \vec{B}_t = \frac{\omega_{\mathbf{k}}}{ck}\hat{e}_z \times \vec{E}_t \\ \vec{E}_t = i\frac{k}{(\frac{\omega_{\mathbf{k}}^2}{c^2}-k^2)}\vec{\bigtriangledown}_t E_z \qquad \text{TM wave} \\ (\vec{\bigtriangledown}_t^{\,2} + \frac{\omega_{\mathbf{k}}^2}{c^2} - k^2)E_z = 0 \end{cases} \tag{A-19}$$

For TE modes we solve the wave equation for B_z with the boundary condition in Eq. (A-16), which gives

$$B_z = B_{mn}(k)\cos(\frac{m\pi x}{a})\cos(\frac{n\pi y}{b}) \qquad m,n \in \{0,1,2..\} \tag{A-20}$$

with $B_{mn}(k)$ is the coefficient associated to each mode. The number m, n can be any combination of integers from 0 to ∞ besides $(m,n) = \{0,0\}$. The dispersion relation is given by

$$\omega_{\mathbf{k}} = c\sqrt{\alpha_{mn}^2 + k^2} \tag{A-21}$$

with the smallest wave vector of given (m,n) mode is defined as

$$\alpha_{mn} = \sqrt{(\frac{m\pi}{a})^2 + (\frac{n\pi}{b})^2} \tag{A-22}$$

From the formulae we obtained in Eq. (A-18) with the $\vec{B}_z$ in Eq. (A-20), we have the electric field $\vec{\mathbf{E}}_{TE}$ associated with the TE modes,

$$\begin{aligned} \vec{\mathbf{E}}_{TE}(x,y,z,t) &= \int' d\mathbf{k}\frac{i\omega_{\mathbf{k}}B_{mn}(k)}{c\alpha_{mn}^2}\Big[-\frac{n\pi}{b}\cos(\frac{m\pi x}{a})\sin(\frac{n\pi y}{b})\hat{e}_x \\ &\quad +\frac{m\pi}{a}\sin(\frac{m\pi x}{a})\cos(\frac{n\pi y}{b})\hat{e}_y\Big]e^{i(kz-\omega_{\mathbf{k}}t)} \end{aligned} \tag{A-23}$$

To avoid heavy notations, we have abbreviated,

$$\int' d\mathbf{k} \equiv \sum_{m,n}\int_{-\infty}^{\infty} dk \tag{A-24}$$

where the summation goes from 0 to ∞ besides $(m,n) = \{0,0\}$. Finally, we derive the vector potential $\vec{\mathbf{A}}_{TE}$ of the TE modes

$$\begin{aligned} \vec{\mathbf{A}}_{TE}(x,y,z,t) &= -\int dt'\vec{\mathbf{E}}_{TE}(x,y,z,t') \\ &= \int' d\mathbf{k}\sqrt{\frac{4c^2\Delta_{mn}}{ab\alpha_{mn}^2}}\frac{1}{\sqrt{\omega_{\mathbf{k}}}}\Big[-\frac{n\pi}{b}\cos(\frac{m\pi x}{a})sin(\frac{n\pi y}{b})\hat{e}_x \\ &\quad +\frac{m\pi}{a}sin(\frac{m\pi x}{a})\cos(\frac{n\pi y}{b})\hat{e}_y\Big]q_{E,\mathbf{k}}(t)e^{ikz} + c.c \end{aligned} \tag{A-25}$$

The constant factor Δ_{mn} is defined by

$$\Delta_{mn} \equiv \begin{cases} 1 & m,n \neq 0 \\ \frac{1}{2} & \min(m,n) = 0 \end{cases} \tag{A-26}$$

with $\min(m,n)$ returns the smaller one of m,n. Notice in Eq. (A-25) we have introduced the "normal modes" of the fields, which are defined by

$$q_{E,\mathbf{k}}(t) \equiv \sqrt{\frac{ab\omega_{\mathbf{k}}}{16c^2\Delta_{mn}\alpha_{mn}^2}} B_{mn}(k) e^{-i\omega_{\mathbf{k}}t} \tag{A-27}$$

For the case where there exists interaction between the fields and the particle, the time evolution of these normal modes are given by Hamiltonian equations. We therefore turn our problem of solving Maxwell equations into solving Hamiltonian equations of these normal modes.

The field energy associated of the TE wave is given by

$$\begin{aligned} U_{TE} &= \frac{1}{8\pi}\int d^3\mathbf{x}(|\mathbf{E}_{TE}|^2 + |\mathbf{B}_{TE}|^2) \\ &= \int' d\mathbf{k}\omega_{\mathbf{k}} q_{E,\mathbf{k}}^* q_{E,\mathbf{k}} \end{aligned} \tag{A-28}$$

which shares the same form of the energy of harmonic oscillator in quantum theory. However in the second quantization of quantum theory there is an additional term related to quantum vacuum energy which is absence in our classical regime. For TM wave we apply the same procedure, which gives

$$\begin{aligned} \vec{\mathbf{A}}_{TM}(x,y,z,t) &= \int' d\mathbf{k}\sqrt{\frac{4c^2}{ab\alpha_{mn}^2}}\frac{c}{\sqrt{\omega_{\mathbf{k}}^3}}\Big[i\frac{km\pi}{a}\cos(\frac{m\pi x}{a})\sin(\frac{n\pi y}{b})\hat{e}_x \\ &\quad + i\frac{kn\pi}{b}\sin(\frac{m\pi x}{a})\cos(\frac{n\pi y}{b})\hat{e}_y \\ &\quad + \alpha_{mn}^2 sin(\frac{m\pi x}{a})sin(\frac{n\pi y}{b})\hat{e}_z\Big] q_{M,\mathbf{k}}(t)e^{ikz} + c.c \end{aligned} \tag{A-29}$$

with the field energy associated with TM wave

$$U_{TM} = \int' d\mathbf{k}\omega_{\mathbf{k}} q_{M,\mathbf{k}}^* q_{M,\mathbf{k}} \tag{A-30}$$

Summing up Eq. (A-28) and Eq. (A-30) we have total field energy of the fields as

$$U = \sum_{\sigma=E,M} \int' d\mathbf{k} \omega_{\mathbf{k}} q^*_{\sigma,\mathbf{k}} q_{\sigma,\mathbf{k}} \tag{A-31}$$

One can show from the canonical relationship of $(\mathbf{A}(\mathbf{r}), \partial\mathbf{A}(\mathbf{r})/\partial t)$, these normal modes obey

$$\{q_{\sigma,\mathbf{k}}, q^*_{\sigma,\mathbf{k}'}\}_{PB} = -i\delta_{\sigma\sigma'}\delta(\mathbf{k}-\mathbf{k}') \tag{A-32}$$

with the poisson bracket is given by

$$\{A, B\}_{PB} \equiv -i \sum_{\sigma} \int' dk \left(\frac{\partial A}{\partial q_{\sigma,\mathbf{k}}} \frac{\partial B}{\partial q^*_{\sigma,\mathbf{k}}} - \frac{\partial B}{\partial q_{\sigma,\mathbf{k}}} \frac{\partial A}{\partial q^*_{\sigma,\mathbf{k}}} \right) \tag{A-33}$$

where A, B is functions of these canonical variables $(q_{\sigma,\mathbf{k}}, q^*_{\sigma,\mathbf{k}})$.

Appendix B

Calculation of N_1 and $\tilde{\omega}_1$

In this appendix we calculate the perturbed frequency $\tilde{\omega}_1$ and normalization constant N_1 for the stable regime $\omega_1 < \omega_c$.

From transcendental equation in Eq. (3-7) we have

$$\tilde{\omega}_1^2 = \omega_1^2 - 4\lambda^2\omega_1 \sum_\sigma \int' d\mathbf{k} \frac{\omega_\mathbf{k} |V_{\sigma,\mathbf{k}}(\mathbf{R})|^2}{(\omega_\mathbf{k}^2 - \tilde{\omega}_1^2)} \tag{B-1}$$

By restricting $\tilde{\omega}_1$ is analytic in coupling constant λ,

$$\lim_{\lambda \to 0} \tilde{\omega}_1 = \omega_1 \tag{B-2}$$

All the negative solutions in Eq. (B-1) are exlucded. Then we solve $\tilde{\omega}_1$ perturbatively. For the $O(\lambda^0)$ we have $\tilde{\omega}_1 \approx \omega_1$. Substituting this lowest order approximation into the L.H.S of Eq. (B-1), it gives

$$\tilde{\omega}_1 = \omega_1 - 2\lambda^2 \sum_\sigma \int' d\mathbf{k} \omega_\mathbf{k} \frac{|V_{\sigma,\mathbf{k}}(\mathbf{R})|^2}{(\omega_\mathbf{k}^2 - \omega_1^2)} + O(\lambda^4) \tag{B-3}$$

With the potential given in Eq. (2-19a), and Eq. (2-19b), we perform the integration over k, which gives the frequency shift up to $O(\lambda^2)$,

$$\begin{aligned} \delta\tilde{\omega}_1 &\equiv \tilde{\omega}_1 - \omega_1 \\ &\approx -2\lambda^2\pi \sum_{m,n} C_{mn}^2 W_{1,mn}^2(\mathbf{R}) \left[(\frac{n}{bc})^2 \frac{\Delta_{mn}}{\sqrt{\alpha_{mn}^2 - (\frac{\omega_1}{c})^2}} \right. \\ &\quad \left. + (\frac{m}{a\omega_1})^2 \left(\alpha_{mn} - \sqrt{\alpha_{mn}^2 - \left(\frac{\omega_1}{c}\right)^2} \right) \right] \end{aligned} \tag{B-4}$$

with the first line and second line in the parenthesis associated to TE wave and TM wave respectively. If there is no cut-off for the $\sum_{m,n}$, then $\tilde{\omega}_1$ diverges, which is so-called ultra-violet divergence. We shall discuss this in Appendix C.

In the following, we calculate the normalization factor N_1 up to $O(\lambda^2)$. From the definition of N_1 in Eq. (3-6) we have

$$\begin{aligned} N_1 &= \sqrt{\frac{\omega_1}{\tilde{\omega}_1}}\left[1+4\lambda^2\omega_1\sum_\sigma\int' d\mathbf{k}\frac{\omega_\mathbf{k}|V_{\sigma,\mathbf{k}}(\mathbf{R})|^2}{(\omega_\mathbf{k}^2-\tilde{\omega}_1^2)^2}\right]^{\frac{-1}{2}} \\ &\approx 1+\lambda^2\sum_\sigma\int' d\mathbf{k}\frac{\omega_\mathbf{k}(\omega_\mathbf{k}^2-3\omega_1^2)}{\omega_1(\omega_\mathbf{k}^2-\omega_1^2)^2}|V_{\sigma,\mathbf{k}}(\mathbf{R})|^2 \end{aligned} \tag{B-5}$$

where we have applied the expansion of $\tilde{\omega}_1$ in Eq. (B-3). Again we substitute the interaction potentials of both TE and TM waves and carry out the integration of k explicitly, then we have

$$\begin{aligned} N_1 = 1+\lambda^2\frac{\pi}{\omega_1 c^2}\sum_{mn}C_{mn}^2W_{1,mn}^2(\mathbf{R})\Bigg\{&\frac{n^2\Delta_{mn}}{b^2}\frac{\alpha_{mn}^2-2(\frac{\omega_1}{c})^2}{(\alpha_{mn}^2-(\frac{\omega_1}{c})^2)^{\frac{3}{2}}} \\ &+(\frac{m}{a})^2\frac{3(\frac{\omega_1}{c})^4-3\alpha_{mn}^2(\frac{\omega_1}{c})^2-\alpha_{mn}^4-6\alpha_{mn}(\frac{\omega_1}{c})\sqrt{\alpha_{mn}^2-(\frac{\omega_1}{c})^2}}{(\frac{\omega_1}{c})^2\sqrt{\alpha_{mn}^2-(\frac{\omega_1}{c})^2}}\Bigg\} \end{aligned} \tag{B-6}$$

Appendix C

Frequency shift in classical regime

In this appendix, we propose an alternative way to overcome this divergence without introducing a cut-off factor [1]proportional to $mc/\hbar$.

As shown in Appendix B, the frequency shift up to $O(\lambda^2)$ is given as

$$\begin{aligned} \delta\omega_1 &\equiv \tilde{\omega}_1 - \omega_1 \\ &= -2\lambda \sum_{\sigma} \int d\mathbf{k} \frac{\omega_{\mathbf{k}} |V_{\sigma,\mathbf{k}}(\mathbf{R})|^2}{\omega_1^2 - \omega_{\mathbf{k}}^2} \end{aligned} \tag{C-1}$$

From Eq. (2-19a) and Eq. (2-19b) one can verify the asymptotic form of potential at $\omega_{\mathbf{k}} \gg 1$ as

$$V_{\sigma,\mathbf{k}} \sim \frac{1}{\sqrt{\omega_{\mathbf{k}}}} \tag{C-2}$$

Substituting it into Eq. (C-1), we have $\delta\omega_1 \sim \lim_{x\to\infty} x \log x$ which diverges.

$$\delta\omega_1 \sim \sum_{m,n}^{\infty} \frac{1}{n} \to \infty \tag{C-3}$$

To remove this divergence, we follow a treatment similar to the quantum case proposed by Bethe [40], that he removed the divergence by subtractions. The divergence in $\delta\tilde{\omega}_1$ is contributed by large $\omega_{\mathbf{k}}$, which is in the order of

$$\delta\omega_{1,div} = -2\lambda \sum_{\sigma} \int d\mathbf{k} \frac{\omega_{\mathbf{k}} |V_{\sigma,\mathbf{k}}(\mathbf{R})|^2}{-\omega_{\mathbf{k}}^2} \tag{C-4}$$

[1]In general, the ultra-violet divergence occurs in other quantity such as the vector potential. We only focus on removing the divergence in frequency shift as it is one of the most direct observed quantities in experiment.

Subtracting it out from Eq. (C-1), we have finite $\delta\omega_{1,finite}$

$$\begin{aligned}\delta\omega_{1,finite} &= \delta\omega_1 - \delta\omega_{1,div} \\ &= -2\lambda\omega_1^2 \sum_\sigma \int d\mathbf{k} \frac{|V_{\sigma,\mathbf{k}}(\mathbf{R})|^2}{\omega_\mathbf{k}(\omega_1^2 - \omega_k^2)} \end{aligned} \tag{C-5}$$

With the $V_{\sigma,\mathbf{k}}(\mathbf{R})$ given in Eq. (2-19a), Eq. (2-19b) we have [30]

$$\delta\omega_{1,finite} \approx -4\lambda^2 \frac{\pi^3\omega_1^2}{abc} \sum_{\substack{m=even \\ n=odd}}^{\infty} \frac{1}{\alpha_{mn}^5} \left(\frac{n^2\Delta_{mn}}{b^2} + \frac{m^2}{4a^2} \right) \tag{C-6}$$

where we assume $\omega_1 \ll \pi c/b$ and the center of mass of the dipole is located at the center of the waveguide. This summation does not diverge. Hence in the Friedrich model with virtual process, we obtained a finite $\delta\omega_{1,Obs}$ by applying removal by subtraction once[2]. By letting $a = 0.5b$, we sum the right hand side in Eq. (C-6) up to $m = n = 1000$ which gives

$$\frac{\delta\omega_{1,finite}}{\omega_1}| \approx -4.412\lambda^2 \frac{b\omega_1}{\pi^2 c} \tag{C-7}$$

with 4 effective digits. As a conclusion we have proposed a non-diverging frequency shift in classical mechanics. We shall comment this method also work for the $3D$ Friedrichs model in free space. However we have verified $\delta\tilde{\omega}_{1,Obs} \sim O(\lambda^4)$ in that situation.

[2]For the case of neglecting virtual process, the summation after the substraction still diverge in logarithmic. Hence the virtual processes play a subtle role here.

Appendix D

Bogoliubov transformation of two dipoles case

For the case of two dipole molecules inside the rectangular waveguide, the Hamiltonian is given by Eq. (3-42)

$$\begin{aligned} H &= \omega_1 q_1^* q_1 + \omega_2 q_2^* q_2 + \sum_{\sigma=E,M} \int' d\mathbf{k} \omega_{\mathbf{k}} q_{\sigma,\mathbf{k}}^* q_{\sigma,\mathbf{k}} \\ &\quad + \lambda_1 \int' d\mathbf{k} (V_{1\sigma,\mathbf{k}} q_{\sigma,\mathbf{k}} - V_{1\sigma,\mathbf{k}}^* q_{\sigma,\mathbf{k}}^*)(q_1 - q_1^*) \\ &\quad + \lambda_2 \int' d\mathbf{k} (V_{2\sigma,\mathbf{k}} q_{\sigma,\mathbf{k}} - V_{2\sigma,\mathbf{k}}^* q_{\sigma,\mathbf{k}}^*)(q_2 - q_2^*) \end{aligned} \tag{D-1}$$

which is an extension of Friedrichs model [5]. It can be diagonalized by Bogoliubov transformation. For the case $\omega_1 < \omega_2 < \omega_c$, we show the results of diagonalization, which gives

$$H = \tilde{\omega}_1 Q_1^* Q_1 + \tilde{\omega}_2 Q_2^* Q_2 + \sum_{\sigma} \int' dk \omega_{\mathbf{k}} Q_{\sigma,\mathbf{k}}^* Q_{\sigma,\mathbf{k}} \tag{D-2}$$

where the perturbed normal modes Q_1, Q_2, and Q_k are given by

$$\begin{aligned} Q_1 &= N_1 \left\{ \frac{\omega_1 + \tilde{\omega}_1}{2\omega_1} q_1 + \frac{\omega_1 - \tilde{\omega}_1}{2\omega_1} q_1^* \right. \\ &\quad + \lambda_1 \sum_{\sigma} \int' d\mathbf{k} \left[\frac{q_{\sigma,\mathbf{k}}}{\omega_{\mathbf{k}} - \tilde{\omega}_1} \left(V_{1\sigma,\mathbf{k}} - 2\lambda_1 \lambda_2 \frac{\omega_2 V_{2\sigma,\mathbf{k}} \zeta(\tilde{\omega}_1)}{\xi_2(\tilde{\omega}_1)} \right) \right. \\ &\quad \left. + \frac{q_{\sigma,\mathbf{k}}^*}{\omega_{\mathbf{k}} + \tilde{\omega}_1} \left(V_{1\sigma,\mathbf{k}}^* - 2\lambda_1 \lambda_2 \frac{\omega_2 V_{2\sigma,\mathbf{k}}^* \zeta(\tilde{\omega}_1)}{\xi_2(\tilde{\omega}_1)} \right) \right] \\ &\quad \left. - \lambda_1 \lambda_2 \frac{(\omega_2 + \tilde{\omega}_1)\zeta(\tilde{\omega}_1)}{\xi_2(\tilde{\omega}_1)} q_2 - \lambda_1 \lambda_2 \frac{(\omega_2 - \tilde{\omega}_1)\zeta(\tilde{\omega}_1)}{\xi_2(\tilde{\omega}_1)} q_2^* \right\} \end{aligned} \tag{D-3}$$

$$
\begin{aligned}
Q_2 &= N_2 \Bigg\{ \frac{\omega_2+\tilde{\omega}_2}{2\omega_2} q_2 + \frac{\omega_2-\tilde{\omega}_2}{2\omega_2} q_2^* \\
&\quad +\lambda_2 \sum_\sigma \int d\mathbf{k} \Bigg[\frac{q_{\sigma,\mathbf{k}}}{\omega_\mathbf{k}-\tilde{\omega}_2} \left(V_{2\sigma,\mathbf{k}} - 2\lambda_1\lambda_2 \frac{\omega_1 V_{1\sigma,k}\zeta^*(\tilde{\omega}_2)}{\xi_1(\tilde{\omega}_2)} \right) \\
&\quad + \frac{q^*_{\sigma,k}}{\omega_\mathbf{k}+\tilde{\omega}_2} \left(V^*_{2\sigma,\mathbf{k}} - 2\lambda_1\lambda_2 \frac{\omega_1 V^*_{1\sigma,k}\zeta^*(\tilde{\omega}_2)}{\xi_1(\tilde{\omega}_2)} \right) \Bigg] \\
&\quad -\lambda_1\lambda_2 \frac{(\omega_1+\tilde{\omega}_2)\zeta^*(\tilde{\omega}_2)}{\xi_1(\tilde{\omega}_2)} q_1 - \lambda_1\lambda_2 \frac{(\omega_1-\tilde{\omega}_2)\zeta^*(\tilde{\omega}_2)}{\xi_1(\tilde{\omega}_1)} q_1^* \Bigg\} \qquad \text{(D-4)}
\end{aligned}
$$

$$
\begin{aligned}
Q_{\sigma,\mathbf{k}} &= q_{\sigma,\mathbf{k}} - \left\{ \lambda_1 \gamma^*_{1\sigma,+}(\omega_\mathbf{k}) \left[(\omega_1+\omega_\mathbf{k}) q_1 + (\omega_1-\omega_\mathbf{k}) q_1^* \right] \right. \qquad \text{(D-5)} \\
&\quad \left. +\lambda_2 \gamma^*_{2\sigma,+}(\omega_\mathbf{k}) \left[(\omega_2+\omega_\mathbf{k}) q_1 + (\omega_2-\omega_\mathbf{k}) q_2^* \right] \right\} \\
&\quad -2 \sum_{\sigma'} \int' d\mathbf{l} \Bigg\{ \frac{q_{\sigma,l}}{\omega_\mathbf{l} - \omega_\mathbf{k} - i\epsilon} \left[\omega_1 \lambda_1^2 \gamma^*_{1\sigma,+}(\omega_\mathbf{k}) V_{1\sigma',\mathbf{l}} + \omega_2 \lambda_2^2 \gamma^*_{2\sigma,+}(\omega_\mathbf{k}) V_{2\sigma',\mathbf{l}} \right] \\
&\quad + \frac{q^*_{\sigma,\mathbf{l}}}{\omega_\mathbf{l}+\omega_\mathbf{k}} \left[\omega_1 \lambda_1^2 \gamma^*_{1\sigma,+}(\omega_\mathbf{k}) V^*_{1\sigma',\mathbf{l}} + \omega_2 \lambda_2^2 \gamma^*_{2\sigma,+}(\omega_\mathbf{k}) V^*_{2\sigma',\mathbf{l}} \right] \Bigg\} \qquad \text{(D-6)}
\end{aligned}
$$

with the normalization constants

$$
\begin{aligned}
N_1 &\equiv \sqrt{\frac{\omega_1}{\tilde{\omega}_1}} \Bigg[1 + \lambda_1^2 \frac{\omega_1}{\tilde{\omega}_1} \sum_\sigma \int' d\mathbf{l} \frac{\left| V_{1\sigma,\mathbf{l}} - 2\lambda_2^2 \frac{\omega_2 V_{2\sigma,\mathbf{l}} \zeta^*(\tilde{\omega}_1)}{\xi_2(\tilde{\omega}_1)} \right|^2}{\omega_\mathbf{l} - \tilde{\omega}_1} \\
&\quad - \frac{\left| V_{1\sigma,\mathbf{l}} - 2\lambda_2^2 \frac{\omega_2 V_{2\sigma,\mathbf{l}} \zeta(\tilde{\omega}_1)}{\xi_2(\tilde{\omega}_1)} \right|^2}{\omega_\mathbf{l} + \tilde{\omega}_1} + 4\lambda_1^2\lambda_2^2 \omega_1\omega_2 \frac{|\zeta(\tilde{\omega}_1)|^2}{\xi_2(\tilde{\omega}_1)^2} \Bigg]^{\frac{1}{2}} \qquad \text{(D-7)}
\end{aligned}
$$

$$
\begin{aligned}
N_2 &\equiv \sqrt{\frac{\omega_2}{\tilde{\omega}_2}} \Bigg[1 + \lambda_2^2 \frac{\omega_2}{\tilde{\omega}_2} \sum_\sigma \int' d\mathbf{l} \frac{\left| V_{2\sigma,\mathbf{l}} - 2\lambda_1^2 \frac{\omega_1 V_{1\sigma,\mathbf{l}} \zeta^*(\tilde{\omega}_2)}{\xi_1(\tilde{\omega}_2)} \right|^2}{\omega_\mathbf{l} - \tilde{\omega}_2} \\
&\quad - \frac{\left| V_{2\sigma,\mathbf{l}} - 2\lambda_1^2 \frac{\omega_1 V_{2\sigma,\mathbf{l}} \zeta(\tilde{\omega}_2)}{\xi_1(\tilde{\omega}_2)} \right|^2}{\omega_\mathbf{l} + \tilde{\omega}_2} + 4\lambda_1^2\lambda_2^2 \omega_2\omega_1 \frac{|\zeta(\tilde{\omega}_2)|^2}{\xi_1(\tilde{\omega}_2)^2} \Bigg]^{\frac{1}{2}} \qquad \text{(D-8)}
\end{aligned}
$$

The functions $\xi_1(\omega_\mathbf{k})$, $\xi_2(\omega_\mathbf{k})$,$\zeta(\omega_\mathbf{k})$, $\chi(\omega_\mathbf{k})$, $\gamma_{1\sigma,\pm}$, $\gamma_{2\sigma,\pm}$ are defined by

$$
\xi_1(\omega_\mathbf{k}) \equiv \omega_\mathbf{k}^2 - \omega_1^2 + 4\lambda_1^2\omega_1 \sum_\sigma \int' d\mathbf{l} \frac{\omega_\mathbf{l} |V_{1\sigma,\mathbf{l}}|^2}{\omega_l^2 - \omega_\mathbf{k}^2} \qquad \text{(D-9)}
$$

$$\xi_2(\omega_{\mathbf{k}}) \equiv \omega_{\mathbf{k}}^2 - \omega_2^2 + 4\lambda_2^2\omega_2 \sum_\sigma \int' d\mathbf{l} \frac{\omega_{\mathbf{l}}|V_{2\sigma,\mathbf{l}}|^2}{\omega_2^2 - \omega_{\mathbf{k}}^2} \tag{D-10}$$

$$\zeta(\omega_{\mathbf{k}}) \equiv \sum_\sigma \int' d\mathbf{l} \left[\frac{V_{1\sigma,\mathbf{l}} V_{2\sigma,l}^*}{\omega_{\mathbf{l}} + \omega_{\mathbf{k}}} + \frac{V_{1\sigma,l}^* V_{2\sigma,l}}{\omega_{\mathbf{l}} - \omega_{\mathbf{k}}} \right] \tag{D-11}$$

$$\chi(\omega_{\mathbf{k}}) \equiv \xi_1(\omega_{\mathbf{k}})\xi_2(\omega_{\mathbf{k}}) - 4\lambda_1^2\lambda_2^2\omega_1\omega_2\zeta(\omega_{\mathbf{k}})\zeta^*(\omega_{\mathbf{k}}) \tag{D-12}$$

$$\gamma_{1\sigma,\pm}(\omega_{\mathbf{k}}) \equiv \frac{\xi_{2,\pm}(\omega_{\mathbf{k}})V_{1\sigma,\mathbf{k}} - 2\lambda_2^2\omega_2\zeta_\pm^*(\omega_{\mathbf{k}})V_{2\sigma,\mathbf{k}}}{\chi_\pm(\omega_{\mathbf{k}})} \tag{D-13}$$

$$\gamma_{2\sigma,\pm}(\omega_{\mathbf{k}}) \equiv \frac{\xi_{1,\pm}(\omega_{\mathbf{k}})V_{2\sigma,\mathbf{k}} - 2\lambda_1^2\omega_1\zeta_\pm^*(\omega_{\mathbf{k}})V_{1\sigma,\mathbf{k}}}{\chi_\pm(\omega_{\mathbf{k}})} \tag{D-14}$$

with

$$\zeta_\pm^*(\omega_{\mathbf{k}}) \equiv \zeta^*(\omega_{\mathbf{k}} \pm i\epsilon) \tag{D-15}$$

$$\chi_\pm(\omega_{\mathbf{k}}) \equiv \xi_{1,\pm}(\omega_{\mathbf{k}})\xi_{2,\pm}(\omega_{\mathbf{k}}) - 4\lambda^4\omega_1\omega_2\zeta_\pm^*(\omega_{\mathbf{k}})\zeta_\pm(\omega_{\mathbf{k}}) \tag{D-16}$$

Notice the complex conjugate is taken before the analytic continuation. Hence we have $\zeta_-^*(\omega_{\mathbf{k}}) \neq \zeta_+(\omega_{\mathbf{k}})$. The perturbed frequencies are given by the solution of

$$\xi(\tilde{\omega}_1) = \xi(\tilde{\omega}_2) = 0 \tag{D-17}$$

The inverse transformations are given by,

$$\begin{aligned} q_1 &= N_1 \left[\frac{\tilde{\omega}_1 + \omega_1}{2\omega_1} Q_1 + \frac{\tilde{\omega}_1 - \omega_1}{2\omega_1} Q_1^* \right] \\ &\quad -\lambda_1 \sum_\sigma \int' d\mathbf{l} \left[(\omega_{\mathbf{l}} + \omega_1)\gamma_{1\sigma,-}(\omega_{\mathbf{l}})Q_{\sigma,\mathbf{l}} + (\omega_{\mathbf{l}} - \omega_1)\gamma_{1\sigma,+}^*(\omega_{\mathbf{l}})Q_{\sigma,\mathbf{l}}^* \right] \\ &\quad -\lambda_1\lambda_2 N_2 \left[\frac{\zeta^*(\tilde{\omega}_2)(\tilde{\omega}_2 + \omega_1)}{\xi_1(\tilde{\omega}_2)} Q_2 + \frac{\zeta(\tilde{\omega}_2)(\tilde{\omega}_2 - \omega_1)}{\xi_1(\tilde{\omega}_2)} Q_2^* \right] \end{aligned} \tag{D-18}$$

$$\begin{aligned} q_2 &= N_2 \left[\frac{\tilde{\omega}_2 + \omega_2}{2\omega_2} Q_2 + \frac{\tilde{\omega}_2 - \omega_2}{2\omega_2} Q_2^* \right] \\ &\quad -\lambda_2 \sum_\sigma \int' d\mathbf{l} \left[(\omega_{\mathbf{l}} + \omega_2)\gamma_{2\sigma,-}(\omega_{\mathbf{l}})Q_{\sigma,\mathbf{l}} + (\omega_{\mathbf{l}} - \omega_2)\gamma_{2\sigma,+}^*(\omega_{\mathbf{l}})Q_{\sigma,\mathbf{l}}^* \right] \\ &\quad -\lambda_1\lambda_2 N_1 \left[\frac{\zeta^*(\tilde{\omega}_1)(\tilde{\omega}_1 + \omega_2)}{\xi_2(\tilde{\omega}_1)} Q_1 + \frac{\zeta(\tilde{\omega}_1)(\tilde{\omega}_1 - \omega_2)}{\xi_2(\tilde{\omega}_1)} Q_1^* \right] \end{aligned} \tag{D-19}$$

$$
\begin{aligned}
q_{\sigma,\mathbf{k}} &= Q_{\sigma,\mathbf{k}} - \lambda_1 N_1 \left[\frac{V_{1\sigma,\mathbf{k}}\xi_2(\tilde{\omega}_2) - 2\lambda_1\lambda_2\omega_2 V_{2\sigma,\mathbf{k}}\zeta(\tilde{\omega}_1)}{\xi_2(\tilde{\omega}_1)(\tilde{\omega}_1 - \omega_{\mathbf{k}})} Q_1 \right. \\
&\quad \left. + \frac{V^*_{1\sigma,\mathbf{k}}\xi_2(\tilde{\omega}_2) - 2\lambda_1\lambda_2\omega_2 V^*_{2\sigma,\mathbf{k}}\zeta^*(\tilde{\omega}_1)}{\xi_2(\tilde{\omega}_1)(\tilde{\omega}_1 + \omega_{\mathbf{k}})} Q^*_1 \right] \\
&- \lambda_2 N_2 \left[\frac{V^*_{2\sigma,\mathbf{k}}\xi_1(\tilde{\omega}_1) - 2\lambda_1\lambda_2\omega_1 V^*_{1\sigma,\mathbf{k}}\zeta(\tilde{\omega}_2)}{\xi_1(\tilde{\omega}_2)(\tilde{\omega}_2 - \omega_{\mathbf{k}})} Q_2 \right. \\
&\quad \left. + \frac{V^*_{2\sigma,\mathbf{k}}\xi_1(\tilde{\omega}_1) - 2\lambda_1\lambda_2\omega_1 V^*_{2\sigma,\mathbf{k}}\zeta(\tilde{\omega}_2)}{\xi_1(\tilde{\omega}_2)(\tilde{\omega}_2 + \omega_{\mathbf{k}})} Q^*_2 \right] \\
&- 2\sum_{\sigma'} \int' d\mathbf{l} \left\{ \frac{Q_{\sigma',\mathbf{l}}}{\omega_{\mathbf{k}} - \omega_{\mathbf{l}} + i\epsilon} \left[\omega_1 \lambda_1^2 \gamma_{1\sigma',-}(\omega_{\mathbf{l}}) V^*_{1\sigma',\mathbf{k}} + \omega_2 \lambda_2^2 \gamma_{2\sigma',-}(\omega_{\mathbf{l}}) V^*_{2\sigma',\mathbf{k}} \right] \right. \\
&+ \left. \frac{Q^*_{\sigma',\mathbf{l}}}{\omega_{\mathbf{k}} + \omega_{\mathbf{l}}} \left[\omega_1 \lambda_1^2 \gamma^*_{1\sigma',-}(\omega_{\mathbf{l}}) V^*_{1\sigma',\mathbf{k}} + \omega_2 \lambda_2^2 \gamma^*_{2\sigma',-}(\omega_{\mathbf{l}}) V^*_{2\sigma',\mathbf{k}} \right] \right\} \qquad \text{(D-20)}
\end{aligned}
$$

Due to the symmetry between particle 1 and 2, we have these formulae invariant under permuting label 1 and 2. One can also verify these formulae reduce to the one dipole case by taking the limit $\lambda_2 \to 0$, together with $\omega_2 \to 0$.

Appendix E

Failure of Bogoliubov transformation

In this appendix, we show under the thermodynamic condition as Eq. (5-18b) , the Bogoliubov transformation shown in Eq. (5-11) leads to the divergence of the total photon number density, i.e., $\langle n_k(t)\rangle$.

The inverse Bogoliubov transformation corresponds to Eq. (5-11) is given by

$$a_1 = \lambda \sum_l \frac{V_l}{\eta^-(\omega_k)} A_k \tag{E-1}$$

$$a_k = A_k - \lambda^2 {\sum_l}' \frac{V_k V_l}{\eta^-(\omega_l)(\omega_k - \omega_l + i\epsilon)} A_l \tag{E-2}$$

where the time evolution of renormalized field is given by

$$A_k(t) = e^{-i\omega_k t} A_k(0) \tag{E-3}$$

In the following, let us calculate the time evolution of $\langle n_k(t)\rangle$, which is defined by

$$\langle n_k(t)\rangle = \langle a_k^+(t) a_k(t)\rangle \tag{E-4}$$

with the initial condition

$$\begin{aligned} \langle a_1^+(0) a_1(0)\rangle &= 0 \\ \langle a_k^+(0) a_l(0)\rangle &= \delta_{kl}\langle n_k(0)\rangle \end{aligned} \tag{E-5}$$

Substituting Eq. (E-2) into Eq. (E-4), we have

$$\begin{aligned}\langle n_k(t)\rangle &= \langle A_k^+(t)A_k(t)\rangle + \lambda^2 {\sum_l}' \left(\frac{V_k V_l \langle A_k^+(t)A_l(t)\rangle}{\eta^-(\omega_l)(\omega_l-\omega_k-i\epsilon)} + c.c\right) \\ &+ \lambda^4 {\sum_{l_1}}' {\sum_{l_2}}' \frac{V_k^2 V_{l_1} V_{l_2} \langle A_{l_1}^+(t)A_{l_2}(t)\rangle}{\eta^+(\omega_{l_1})\eta^-(\omega_{l_2})(\omega_{l_1}-\omega_k+i\epsilon)(\omega_{l_2}-\omega_k-i\epsilon)} \\ &= \langle n_k(t)\rangle_I + \langle n_k(t)\rangle_{II} + \langle n_k(t)\rangle_{III} \end{aligned} \tag{E-6}$$

where $\langle n_k(t)\rangle_I$, $\langle n_k(t)\rangle_{II}$, and $\langle n_k(t)\rangle_{III}$ correspond with the terms $\langle A_k^+(t)A_k(t)\rangle$, $\langle A_k^+(t)A_l(t)\rangle$, and $\langle A_{l_1}^+(t)A_{l_2}(t)\rangle$ respectively. Here we present the detail calculation of the first term. Substituting the Bogoliubov transformation and the initial condition Eq. (E-5), Eq. (E-5) into $\langle n_k(t)\rangle_I$,

$$\langle n_k(t)\rangle_I \equiv \langle A_k^+(t)A_k(t)\rangle \tag{E-7}$$

$$\begin{aligned} &= \langle n_k(0)\rangle + \lambda^4 \frac{V_k^2}{|\eta^+(\omega_k)|^2} {\sum_l}' \frac{V_l^2}{|\omega_l-\omega_k-i\epsilon|^2}\langle n_l(0)\rangle \\ &= \langle n_k(0)\rangle + i\lambda^4 \frac{V_k^2}{2\epsilon|\eta^+(\omega_k)|^2} {\sum_l}' V_l^2 \left(\frac{1}{\omega_l-\omega_k+i\epsilon} - \frac{1}{\omega_l-\omega_k-i\epsilon}\right) \end{aligned} \tag{E-8}$$

where we have used the partial fraction formula

$$\frac{1}{|\omega_l-\omega_k-i\epsilon|^2} = \frac{1}{2\epsilon}\left(\frac{1}{\omega_l-\omega_k+i\epsilon} - \frac{1}{\omega_l-\omega_k-i\epsilon}\right) \tag{E-9}$$

Notice the second term in Eq. (E-8) proportional to $O(1/\Omega\epsilon)$, which causes $1/\epsilon$ divergence in total photon number. By taking the continuous limit, we replace the $V_k = v_k/\sqrt{\Omega}$ by the volume independent potential v_k, and the summation ${\sum_l}'/\Omega$ by integration $\int dl$[1], then

$$\begin{aligned}\langle n_k(t)\rangle_{I,\epsilon} &= i\lambda^4 \frac{1}{2\Omega\epsilon}\frac{v_k^4}{|\eta^+(\omega_k)|^2}\int_{-\infty}^{\infty} dl\ v_l^2 \left(\frac{1}{\omega_l-\omega_k+i\epsilon} - \frac{1}{\omega_l-\omega_k-i\epsilon}\right)\langle n_l(0)\rangle \\ &= i\lambda^4 \frac{1}{2\Omega\epsilon}\frac{v_k^2}{|\eta^+(\omega_k)|^2}\int_0^{\infty} dl\ v_l^2[-2\pi i\delta(l-k)]\left(\langle n_l(0)\rangle + \langle n_{-l}(0)\rangle\right) \\ &= \lambda^4 \frac{1}{\Omega\epsilon}\frac{\pi v_k^4}{|\eta^+(\omega_k)|^2}(\langle n_k(0)\rangle + \langle n_{-k}(0)\rangle) \end{aligned} \tag{E-10}$$

[1]We omit the hole $l = k$ as it is $O(1/\Omega)$ smaller as compare to the dominant summation.

where the subscript ϵ denotes the $1/\epsilon$ divergence related terms in $\langle n_k(t)\rangle_I$. Similarly, we obtain the $1/\epsilon$ divergence related terms for $\langle n_k(t)\rangle_{II}$, and $\langle n_k(t)\rangle_{III}$, which gives up to (λ^4)

$$\langle n_k(t)\rangle_{II,\epsilon} \approx \lambda^4 \frac{\pi v_k^4}{\Omega\epsilon}\left[\frac{4}{|\eta^+(\omega_k)|^2}\langle n_k(0)\rangle\left(\frac{1}{\eta^+(\omega_k)^2}+c.c\right)(\langle n_k(0)\rangle+\langle n_{-k}(0)\rangle)\right] \tag{E-11}$$

$$\langle n_k(t)\rangle_{III,\epsilon} \approx \lambda^4 \frac{1}{\Omega\epsilon}\frac{\pi v_k^4}{|\eta^+(\omega_k)|^2}(\langle n_k(0)\rangle+\langle n_{-k}(0)\rangle) \tag{E-12}$$

Summing them up for all possible k, we have

$$\begin{aligned}\sum_k \langle n_k(t)\rangle_\epsilon &\approx \lambda^4\int_{-\infty}^{\infty} dk \frac{\pi v_k^4}{\epsilon}\left[\frac{1}{|\eta^+(\omega_k)|^2}(6\langle n_k(0)\rangle+2\langle n_{-k}(0)\rangle)\right. \\ &\quad \left.+\left(\frac{1}{\eta^+(\omega_k)^2}+c.c\right)(\langle n_k(0)\rangle+\langle n_{-k}(0)\rangle)\right] \qquad \text{(E-13)} \\ &\approx \lambda^2\frac{v_{\omega_1}^2}{\epsilon}(3\langle n_k(0)\rangle+\langle n_{-k}(0)\rangle) \\ &\propto \frac{1}{\epsilon}\to\infty \qquad \text{(E-14)}\end{aligned}$$

where we have taken the pole approximation of the integration, with the pole of $1/\eta^+(\omega_k)$ located at $\omega_k=\omega_1-i\gamma$, and $\gamma\approx 2\pi\lambda^2 v_{\omega_1}^2$. Hence we show the Bogoliubov transformation leads to the divergence in the time evolution of total photon number.

Appendix F

Calculations of $\theta^{(0)}_{\alpha\beta:\alpha'\beta'}$ and $\langle n_\alpha(0)\rangle_{\Pi^{(0)}}$

F.1 Calculation of $\theta^{(0)}_{\alpha\beta:\alpha'\beta'}$

In this appendix we calculate of matrix elements of the collision operator $\theta^{(\nu)}$ appeared in the kinetic equations Eqs. (5-77) and (5-78).

From Eq. (5-65) with $\nu = 0$, we have the collision operator up to $\mathrm{O}(\lambda^2)$

$$\theta^{(0)} = P^{(0)}\lambda L_V \frac{-1}{L_0 - w^{(0)} - i\epsilon} Q^{(0)}\lambda L_V P^{(0)} \tag{F-1}$$

where we have dropped $P^{(0)}L_0P^{(0)} = 0$. Due to the diagonal transition of collision operator, we have six non-vanishing matrix elements. $\theta^{(0)}$, i.e. $\theta^{(0)}_{kk:kk}$, $\theta^{(0)}_{11:11}$, $\theta^{(0)}_{kk:11}$,$\theta^{(0)}_{11:kk}$ and $\theta^{(0)}_{kk:ll}$, and $\theta^{(0)}_{ll:kk}$. The last two terms are $\mathrm{O}(\lambda^4)$ since it takes four interactions to convert two l-mode photons to two k-mode photons. Recall that $|1\rangle \equiv |1_1, \{0_F\}\rangle$, and $|k\rangle \equiv |0_1, ...0_{k_{j-1}}, 1_{k_j}, 0_{k_{j+1}}...\rangle$

We shall demonstrate the calculation of $\theta^{(0)}_{kk:11}$ as an example.

$$\begin{aligned}
\theta^{(0)}_{kk:11} &= \lambda^2 \langle\langle k;k|L_V \frac{-1}{L_0 - w^{(0)} - i\epsilon} Q^{(0)}\lambda L_V|1;1\rangle\rangle \\
&= \lambda^2 \langle\langle k;k|L_V|1;k\rangle\rangle \frac{-1}{w^{(1k)} - i\epsilon} \langle\langle 1;k|L_V|1;1\rangle\rangle \\
&\quad + \lambda^2 \langle\langle k;k|L_V|k;1\rangle\rangle \frac{-1}{w^{(k1)} - i\epsilon} \langle\langle k;1|\lambda L_V|1;1\rangle\rangle \\
&= \frac{\lambda^2 V_k^2}{\omega_1 - \omega_k - i\epsilon} - c.c
\end{aligned} \tag{F-2}$$

The calculation of all other matrix elements can be performed in the same way, here

we summarize the results up to $O(\lambda^2)$,

$$\theta^{(0)}_{kk:kk} = \frac{\lambda^2 V_k^2}{\omega_k - \omega_1 + i\epsilon} - c.c \tag{F-3}$$

$$\theta^{(0)}_{11:11} = \sum_l \frac{\lambda^2 V_l^2}{\omega_1 - \omega_l + i\epsilon} - c.c \tag{F-4}$$

$$\theta^{(0)}_{kk:11} = -\theta^{(0)}_{kk:11} = \frac{\lambda^2 V_k^2}{\omega_1 - \omega_k - i\epsilon} - c.c \tag{F-5}$$

$$\tag{F-6}$$

Substituting these matrix elements into Eq. (5-77) and Eq. (5-78), we obtain the Markovian kinetic equations Eq. (5-80), Eq. (5-81) under the limit $\epsilon \to 0$.

F.2 Calculation of $\langle n_\alpha(0)\rangle_{\Pi^{(0)}}$

In the following we calculate the initial condition $\langle n_\alpha(0)\rangle_{\Pi^{(0)}}$ for the case of the scattering of wavepacket discussed in Section 5.5.1. The initial density matrix is in a pure state given by Eq. (5-84). From Eq. (5-60), Eq. (5-42), Eq. (5-48) we have the $\langle n_\alpha(0)\rangle_{\Pi^{(0)}}$ up to $\mathrm{O}(\lambda^2)$

$$\begin{aligned}\langle n_\alpha(0)\rangle_{\Pi^{(0)}} &= Tr(a^+_\alpha a_\alpha \rho(0)) + \lambda^2 Tr(a^+_\alpha a_\alpha \mathcal{D}_2^{(0)} \rho(0)) \\ &\quad -\lambda^2 Tr(a^+_\alpha a_\alpha \mathcal{D}_1^{(0)} \mathcal{C}_1^{(0)} P^{(0)} \rho(0))\end{aligned} \tag{F-7}$$

with $\alpha = 1$, and k. The first term is the free motion, while the interaction terms start from $\mathrm{O}(\lambda^2)$. Since the last term is diagonal transition, it is $\mathrm{O}(1/\Omega)$ smaller than the off diagonal transition term $\mathcal{D}_2^{(0)}$ unless the $\mathcal{D}_2^{(0)}$ contribution vanishes. That corresponds to the special case of a plane wave which we shall discuss separately in Appendix H. Let us first consider the general case that L_1, $L_2 \neq \pm L/2$. In this case, the last term in Eq. (F-7) is neglected and from Eq. (5-67) we have the contribution

from $\mathcal{D}_2^{(0)}$ as

$$\begin{aligned}
&\lambda^2 \mathrm{Tr}(a_\alpha^+ a_\alpha \mathcal{D}_2^{(0)} \rho(0)) \\
&= \mathrm{Tr}(a_\alpha^+ a_\alpha P^{(0)} \lambda L_V Q^{(0)} \frac{1}{i\epsilon - L_0} Q^{(0)} \lambda L_V Q^{(0)} \frac{1}{i\epsilon - L_0} \rho(0)) \\
&= \sum_{l \neq l'} \langle\langle \alpha;\alpha | P^{(0)} \lambda L_V Q^{(0)} \frac{1}{i\epsilon - L_0} Q^{(0)} \lambda L_V Q^{(0)} \frac{1}{i\epsilon - L_0} | l;l' \rangle\rangle \mathrm{Tr}(a_{l'}^+ a_l \rho(0)) \qquad \text{(F-8)}
\end{aligned}$$

where we have applied the $i\epsilon$ rule [33] in order to obtain a consistent time ordering in the analytical continuation. By substituting the initial $\rho(0)$, and the complete basis in between two interactions λL_V, we have

$$\langle n_1(0) \rangle_{\Pi^{(0)}} = \lambda^2 \frac{n L_{21}}{\Omega} \sum_k \frac{v_k \Phi_k^*}{(\omega_k - \omega_1 + i\epsilon)} \sum_l \frac{v_l \Phi_l}{(\omega_l - \omega_k + i\epsilon)} + c.c \qquad \text{(F-9)}$$

$$\langle n_k(0) \rangle_{\Pi^{(0)}} = n L_2 1 |\Phi_k|^2 - \left\{ \lambda^2 \frac{n L_{21}}{\Omega} \frac{v_k \Phi_k^*}{(\omega_k - \omega_1 + i\epsilon)} \sum_l \frac{v_l \Phi_l}{(\omega_l - \omega_k - i\epsilon)} + c.c \right\} \qquad \text{(F-10)}$$

where we again replace $\sum_{l \neq k}$ by $\sum_l$ as the one point contribution is negligible under the continuous limit.

Appendix G

Pole approximation of $\langle n_k(t)\rangle$

In this appendix we present the $\langle n_k(t)\rangle$ based on the pole approximation of the integral in Eq. (5-105), Eq. (5-106), Eq. (5-107) after taking the continuous limit. We specify $L_1 < L_2 < 0$. From Eq. (5-83) and Eq. (5-105) we have $\langle n_k(t)\rangle_{\Pi^{(0)}}$ under pole approximation as

$$\langle n_k(t)\rangle_{\Pi^{(0)}} \approx nL_{21}|\Phi_k|^2 - 2\pi\lambda^2 nL_{21}v_k v_{\omega_k}\left[i\frac{\Phi_k^*\Phi_{\omega_k}}{\omega_k-\omega_1+i\epsilon}+c.c\right] \tag{G-1}$$

Similarly, we have $\langle n_k(t)\rangle_{\Pi^{(1k)}+\Pi^{(k1)}}$ approximated as Eq. (5-106) ,

$$\langle n_k(t)\rangle_{\Pi^{(1k)}+\Pi^{(k1)}} \approx 2\pi\lambda^2 nL_{21}v_k v_{\omega_1}\left[\frac{\Phi_k^*\Phi_{\omega_1-i\gamma}e^{i(\omega_k-\omega_1)t-\gamma t}}{(\omega_k-\omega_1+i\epsilon)}+c.c\right] \tag{G-2}$$

In the calculation of $\Pi^{(kl)}$, and $\Pi^{(lk)}$, the contour deformation depends on the time t as Eq. (5-107) involves $e^{-i\omega_l t}$. We have

$$\langle n_k(t)\rangle_{\Pi^{(lk)}+\Pi^{(kl)}} = \begin{cases} -2\pi\lambda^2 nL_{21}\frac{v_k e^{i\omega_k t}\Phi_k^*}{\omega_k-\omega_1+i\gamma} & \\ \Big[v_{\omega_1}\Phi_{\omega_1-i\gamma}e^{-i\omega_1 t-\gamma t} & (L_1+t)<(L_2+t)<0 \\ -v_{\omega_k}\Phi_{\omega_k}^* e^{-i\omega_k t}\Big]+c.c & \\ 2\pi\lambda^2 nv_k\Phi_k^*\sqrt{\frac{L_{21}}{L}}\Big[\frac{v_{\omega_k}e^{-iL_1(\omega_k-k_0)}}{(\omega_k-\omega 1)} & \\ -\frac{v_{\omega_1}e^{-iL_1(\omega_1-k_0-i\gamma)-i(\omega_1-\omega_k-i\gamma)t}}{(\omega_k-\omega_1+i\epsilon)(\omega_1-k_0)} & (L_1+t)<0<(L_2+t) \\ +\frac{v_{k_0}e^{i(\omega_k-k_0)t}}{(\omega_k-k_0)(\omega_1-k_0)}\Big]+c.c & \\ 0 & 0<(L_1+t)<(L_2+t) \end{cases}$$

By summing all the subspaces contributions from Eq. (G-1), Eq. (G-2) and Eq. (G-3), we have

$$\langle n_k(t)\rangle = \begin{cases} nL_{21}|\Phi_k|^2 & (L_1+t)<(L_2+t)<0 \\ nL_{21}|\Phi_k|^2 + 2\pi\lambda^2 n\frac{v_k}{L}\Big[\frac{v_{\omega_k}e^{-iL_2(\omega_k-k_0)}}{(\omega_k-k_0)(\omega_k-\omega_1+i\epsilon)} & \\ -\frac{v_{\omega_1}e^{-iL_2(\omega_1-k_0-i\gamma)-i(\omega_1-\omega_k-i\gamma)t}}{(\omega_k-\omega_1+i\epsilon)(\omega_1-k_0)} & (L_1+t)<0<(L_2+t) \\ +\frac{v_{k_0}e^{i(\omega_k-k_0)t}}{(\omega_k-k_0)(\omega_1-k_0)}+c.c\Big] & \\ nL_{21}|\Phi_k|^2 + 2\pi\lambda^2 nL_{21}v_k v_{\omega_k}\Big[i\frac{\Phi_k^*\Phi_{\omega_k}}{\omega_k-\omega_1+i\epsilon} & \\ +\frac{\Phi_k^*\Phi_{\omega_1-i\gamma}e^{i(\omega_k-\omega_1)t-\gamma t}}{(\omega_k-\omega_1+i\epsilon)}+c.c\Big] & 0<(L_1+t)<(L_2+t) \end{cases}$$

Since the number density does not evolve before the wavepacket hits the particle, this indicates our result obeys causality.

Appendix H

Calculation of $\langle n_k(t)\rangle_{\Pi^{(\nu)}}$ for plane wave

In this appendix we calculate $\langle n_k(t)\rangle_{\Pi^{(\nu)}}$ for the special case of Section 5.5.1 where the incident wave is a plane wave, i.e., $L_2 = -L_1 = L/2$. Recall that in this case we have the initial density matrix as

$$\rho(0) = \delta_{k,k_0}|\hat{\alpha}_{k_0}\rangle\langle\hat{\alpha}_{k_0}| \tag{H-1}$$

Let us first calculate the initial condition for $\Pi^{(0)}$ subspaces, i.e., $\langle n_\alpha(0)\rangle_{\Pi^{(0)}}$ with $\alpha = 1, k$. According to Eq. (F-7), we have

$$\langle n_\alpha(0)\rangle_{\Pi^{(0)}} = Tr(a_\alpha^+ a_\alpha \rho(0)) - \lambda^2 Tr(a_\alpha^+ a_\alpha \mathcal{D}_1^{(0)} \mathcal{C}_1^{(0)} P^{(0)} \rho(0)) \tag{H-2}$$

Compare with Eq. (F-7), the $\mathcal{D}_2^{(0)}$ term vanishes here due to the initial condition $\rho(0)$ given in Eq. (H-1) is in $P^{(0)}$. Substituting the expansions in λ from Eq. (5-42) and Eq. (5-48), we have

$$\begin{aligned}&\lambda^2 Tr(a_\alpha^+ a_\alpha \mathcal{D}_1^{(0)} \mathcal{C}_1^{(0)} P^{(0)} \rho(0)) \\ &= \mathrm{Tr}(a_\alpha^+ a_\alpha P^{(0)} \lambda L_V Q^{(0)} \frac{1}{i\epsilon - L_0} \frac{-1}{L_0 - i\epsilon} Q^{(0)} \lambda L_V Q^{(0)} \rho(0))\end{aligned} \tag{H-3}$$

where we again used the $i\epsilon$ rule[33]. Applying the same approach used in Appendix F.2, we have

$$\langle n_1(0)\rangle_{\Pi^{(0)}} = \lambda^2 \frac{nL}{\Omega} \frac{v_{k_0}^2}{(\omega_{k_0} - \omega_1 - i\epsilon)^2} + c.c \tag{H-4}$$

$$\langle n_{k_0}(0)\rangle_{\Pi^{(0)}} = nL - \lambda^2 \frac{nL}{\Omega} \frac{v_{k_0}^2}{(\omega_{k_0} - \omega_1 - i\epsilon)^2} + c.c \tag{H-5}$$

For the case $\langle n_{k\neq k_0}(0)\rangle_{\Pi^{(0)}}$, the contribution from the right hand side of Eq. (H-2) vanishes, as it is higher order effect proportional to λ^4. Substituting these initial conditions into Eq. (5-83), we obtain the Markovian contribution to $\langle n_{k_0}(t)\rangle$.

For the non-Markovian correction, it is dominated by contributions from $\Pi^{(1k)}$, and $\Pi^{(k1)}$ subspaces. In contrast to the general case discussed in Section 5.6, the contribution from $\Pi^{(lk)}$, and $\Pi^{(kl)}$ subspaces for the case of plane wave is order of λ^6, which can be neglected. Here we follow the same procedure which was used in obtaining Eq. (5-98). Then we have $\langle n_{k_0}(t)\rangle_{\Pi^{(1k)}}$ up to $O(\lambda^2)$,

$$\begin{aligned}\langle n_{k_0}(t)\rangle_{\Pi^{(1k)}} &\approx nL_{21}\Phi_{k_0}\Phi^*_{k_0}\langle\langle k_0;k_0|\lambda\mathcal{C}_1^{(1k)}e^{-i\theta^{(1k_0)}t}\lambda\mathcal{D}_1^{(1k_0)}|k_0;k_0\rangle\rangle \\ &= -n\frac{L}{\Omega}\frac{v_k^2}{(\omega_{k_0}-\omega_l+i\epsilon)^2}e^{i(\omega_k-\tilde{\omega}_1)t-\gamma t} \qquad \text{(H-6)}\end{aligned}$$

Again in this subspace, $\langle n_{k\neq k_0}(t)\rangle_{\Pi^{(1k)}} \sim \lambda^4$ is higher order effect.

Appendix I

Numerical simulation

In this appendix, we shall show the numerical simulation method we used in Section 5.7.

We first construct the numerical model corresponding to the Hamiltonian in Eq. (5-1). We confine our system inside a $1-D$ box with the size L with periodic boundary condition. The x-space is discretized into $2N+1$ points with the resolution $\delta x = L/(2N)$. The periodic condition gives the discretized wavevector $k_j \equiv 2\pi j/L$ with $j \in \{-N, ...N\}$. Under these considerations, the Hamiltonian we shall work numerically is

$$H = \omega_1 a_1^+ a_1 + \sum_{j=-N}^{N} \omega_{k_j} a_{k_j}^+ a_{k_j} + \lambda \sum_{j=-N}^{N} V_{k_j}(a_1^+ a_{k_j} + a_1 a_{k_j}^+) \tag{I-1}$$

According to our dispersion relation $\omega_{k_j} = |k_j|$, we have N 2-fold degeneracies in unperturbed spectrum. This enable us to rewrite the hamiltonian in another form, i.e

$$H = \omega_1 a_1^+ a_1 + \sum_{j=0}^{N} \omega_{k_j} u_{k_j}^+ u_{k_j} + \sum_{i=1}^{N} \omega_{k_i} s_{k_i}^+ s_{k_i} + \lambda \sum_{j=0}^{N} W_{k_j}(a_1^+ s_{k_j} + a_1 s_{k_j}^+) \tag{I-2}$$

with the new canonical coordinates

$$u_{k_j} \equiv \begin{cases} a_{k_j} & , \quad j = 0 \\ \frac{V_{k_j} a_{k_j} + V_{-k_j} a_{-k_j}}{\sqrt{|V_{k_j}|^2 + |V_{-k_j}|^2}} & , \quad j = 1, ..N \end{cases} \tag{I-3}$$

$$s_{k_i} \equiv \frac{1}{\sqrt{|V_{k_i}|^{-2} + |V_{-k_i}|^{-2}}} \left(\frac{a_{k_i}}{V_{k_i}} - \frac{a_{-k_i}}{V_{-k_i}} \right) \quad , \quad i = 1, ..N \tag{I-4}$$

and the modified potential

$$W_{k_j} = \begin{cases} V_{k_j} & , \quad j = 0 \\ \sqrt{V_{k_j}^2 + V_{-k_j}^2} & , \quad j = 1, ..N \end{cases} \tag{I-5}$$

In this form it is clearly $s_{k_i}^+ s_{k_i}$ form N invariants of motion with the same frequency $w_{k_i} = |k_i|$. The rest of the bilinear Hamiltonian is diagonalized by linear transforming $\{a_1, u_{k_j}\}$ to a new set of canonical variables $\{A_\alpha\}$, i.e.,

$$H = \sum_{\alpha=0}^{N} \tilde{\omega}_\alpha A_\alpha^+ A_\alpha + \sum_{i=1}^{N} \omega_{k_i} s_{k_i}^+ s_{k_i} \tag{I-6}$$

where the renormalized frequencies $\{\tilde{\omega}_\alpha\}$ are given by the solutions of the characteristic equation,

$$\omega_1 - \tilde{\omega}_\nu + \lambda^2 \sum_{j=0}^{N} \frac{|W_{k_j}|^2}{\tilde{\omega}_\nu - \omega_{k_j}} = 0 \tag{I-7}$$

Under the weak coupling condition $\lambda^2 \sum_{j=0}^{N} \frac{|W_{k_j}|^2}{\omega_{k_j}} < \omega_1$, one can show Eq. (I-7) has $N+2$ real solutions[1] which are different from the unperturbed frequency ω_{k_j}. The interaction removes all degeneracies in the original spectrum. The eigenvectors correspond to these new frequencies are,

$$A_\alpha = c_\alpha a_1 + \sum_{i=0}^{N} c_{\alpha,k_i} u_{k_i} \quad \alpha = 0, ...(N+1) \tag{I-8}$$

where the relation of these coefficients are given by

$$c_{\alpha,k_j} = \frac{\lambda W_{k_j}}{\tilde{\omega}_\alpha - \omega_{k_j}} c_\alpha \tag{I-9}$$

with

$$|c_\alpha|^2 = \left[1 + \lambda^2 \sum_{j=0}^{N} \frac{|W_{k_j}|^2}{(\tilde{\omega}_\alpha - \omega_{k_j})} \right]^{-1} \tag{I-10}$$

[1]For the case where $V_{k_j=0} = 0$, there is only $N+1$ real solutions of this transcendental equation. Then the $u_{k_j=0}^+ u_{k_j=0}$ becomes invariant of motion in this case.

Due to the completeness, and orthonormal properties of the new canonical variables $\{p_{k_j}, b_\alpha\}$, we obtain

$$\sum_{\alpha=0}^{N+1} c_\alpha^2 = 1 \tag{I-11a}$$

$$\sum_{\alpha=0}^{N+1} c_\alpha c_{\alpha,k_j} = 0 \tag{I-11b}$$

$$\sum_{\alpha=0}^{N+1} c_{\alpha,k_j} c_{\alpha,k_{j'}} = \delta_{j,j'} - \bar{\delta}_{j,0} \frac{V_{-k_j}^2 \delta_{j,j'} + V_{k_j} V_{-k_j} \delta_{j,-j'}}{V_{k_j}^2 + V_{-k_j}^2} \tag{I-11c}$$

where $\bar{\delta}_{j,0} \equiv 1 - \delta_{j,0}$. The time evolution is simply

$$A_\alpha(t) = e^{-i\tilde{\omega}_\alpha t} A_\alpha(0) \quad , \quad \alpha = 0, 1...N+1 \tag{I-12}$$

$$s_{k_i}(t) = e^{-i\omega_{k_j} t} s_{k_i}(0) \quad , \quad i = 1, 2...N \tag{I-13}$$

In order to express the time evolution of the original variables, we derive the inverse transformation.

$$a_1 = \sum_{\alpha=0}^{N+1} c_\alpha A_\alpha \tag{I-14}$$

$$a_{k_j} = \sum_{\alpha=0}^{N+1} c_{\alpha,k_j} A_\alpha + \frac{V_{-k_j}}{\sqrt{V_{k_j}^2 + V_{-k_j}^2}} \sum_{i=1}^{N} (\delta_{i,j} - \delta_{-i,j}) s_{k_i} \quad , j = -N...N \tag{I-15}$$

Combining Eq. (I-8) and Eq. (I-15), we obtain the exact solution in terms of the original variables.

$$a_1(t) = \sum_{\alpha=0}^{N+1} c_\alpha^2 e^{-i\tilde{\omega}_\alpha t} \left(a_1(0) + \lambda \sum_{i=-N}^{N} \frac{V_{k_i}}{\tilde{\omega}_\alpha - \omega_{k_i}} a_{k_i}(0) \right) \tag{I-16}$$

$$\begin{aligned} a_{k_j}(t) = {} & V_{k_j} \sum_{\alpha=0}^{N+1} \frac{c_\alpha^2 e^{-i\tilde{\omega}_\alpha t}}{\tilde{\omega}_\alpha - \omega_{k_j}} \left(a_1(0) + \lambda \sum_{i=-N}^{N} \frac{\lambda V_{k_i}}{\tilde{\omega}_\alpha - \omega_j} a_{k_i}(0) \right) \\ & + e^{-i\omega_{k_j} t} \frac{V_{-k_j}}{V_{k_j}^2 + V_{-k_j}^2} \left(V_{-k_j} a_{k_j}(0) - V_{k_j} a_{-k_j}(0) \right) \end{aligned} \tag{I-17}$$

Hence we obtain the explicit expression of the exact solution of this system. Given the interaction potential V_k, we solve numerically the renormalized frequencies $\tilde{\omega}_\alpha$ for once. Then we just substitute them together with the initial conditions into Eq. (I-16) and Eq. (I-17), to evaluate the time evolution of the system. For the case of a pure state such as rectangular wavepacket, we have the the time evolution of k_ith mode photon number density,

$$\langle n_{k_i}(t)\rangle = nL_{21}\left| e^{-i\omega_{k_i}t}\frac{\Phi_{k_i}-\Phi_{-k_i}}{2} + \lambda V_{k_i}\sum_{\alpha=0}^{N+1}\frac{c_\alpha^2 e^{-i\tilde{\omega}_\alpha t}}{\tilde{\omega}_\alpha-\omega_{k_i}}\sum_{k=-N}^{N}\frac{\lambda V_{k_j}\Phi_{k_j}}{\tilde{\omega}_\alpha-\omega_{k_i}}\right|^2 \quad \text{(I-18)}$$

with Φ_{k_j} given in Eq. (5-86). Notice there is no iterations of time in our method. Therefore we can obtain the asymptotic result of large t without iteration.

Bibliography

[1] J. J. Halliwell et al. *Physical Origins of Time Asymmetry.* Cambridge University Press, 1994.

[2] R. Peierls. *Surprises in Theoretical Physics.* Princeton, N.J., 1979.

[3] H. Poincaré. *Les Méthodes Nouvelles de la Mécanique Céleste (1892)*, volume 1. Dover, New York, 1957.

[4] T. Petrosky and I. Prigogine. Poincarés theorem and unitary transformations for classical and quantum systems. *Physica A*, 147:461, 1988.

[5] K. O. Friedrichs. On the perturbation of continuous spectra. *Communication of Pure Appplied Mathematics*, 1:361, 1948.

[6] E. C. G. Sudarshan. *Structure of Dynamical Theories.* 1961 Brandeis Lectures in Physics. W. A. Benjamin, NY, 1962.

[7] G. Ordonez T. Petrosky and I. Prigogine. Quantum transitions and nonlocality. *Phys. Rev. A*, 62:042106, 2000.

[8] T. Petrosky E. Karpov, I. Prigogine and G. Pronko. Friedrichs model with virtual transitions: Exact solution and indirect spectroskcopy. *J. Math. Phys.*, 41(1):118, 2000.

[9] T. Petrosky G. Ordonze and I. Prigogine. Quantum transition and dressed unstable states. *Phys. Rev. A*, 63:052106, April 2001.

[10] G. Ordonze T. Petrosky and I. Prigogine. Space-time formulation of quantum transitions. *Phys. Rev. A*, 64:062106, Nov 2001.

[11] J. D. Jackson. *Classical Electrodynamics*. John Wiley & Sons, second edition, 1990.

[12] L. D. Landau and E. M. Lifshitz. *The classical theory of fields*. Addison-Wesley, Reading, Mass., 3rd edition, 1971.

[13] I. Prigogine T. Petrosky and S. Tasaki. Quantum theory of non-integrable systems. *Physica A*, 173:175, 1991.

[14] E. C. G. Sudarshan and B. Misra. The zeno's paradox in quantum theory. *J. Math. Phys.*, 18:756, 1977.

[15] W. G. Unruh and W. H. Zurek. Reduction of a wave packet in quantum brownian motion. *Phys. Rev. D*, 40:1071, 1989.

[16] D. Giulini. *Decoherence and the appearance of a classical world in quantum theory*. Springer-Verlag, 1996.

[17] A. O. Caldeira and A. J. Leggett. Path integral approach to quantum brownian motion. *Physica A*, 121:587, 1983.

[18] J. P. Paz B. L. Hu and Y. Zhang. Quantum brownian motion in a general environment: Exact master equation with nonlocal dissipation and colored noise. *Phys. Rev. D*, 45:2843, 1992.

[19] J. P. Paz B. L. Hu and Y. Zhang. Quantum brownian motion in a general environment. (nonlinear coupling and perturbative approach). *Phys. Rev. D*, 47:1576, 1993.

[20] C. Chiu E. C. G. Sudarshan and V. Gorini. *Phys. Rev. D*, 18:2914, 1978.

[21] A. Böhm and M. Gadella. *The Rigged Hilbert Space and quantum mechanics*, volume 78. Springer, New York, 1978.

[22] J. Kumicak and E. Brändas. *Int. J. Quantum Chem.*, 32:669, 1987.

[23] T. Petrosky, C. O. Ting, and V. Barsegov. Decoherence in a field and time symmetry breaking. *Chaos, Soliton and Fractals*, 16:381, 2003.

[24] T. Petrosky and C. O. Ting. Propagation of decoherence in a field and complex spectral representation. *Proceedings of XXII International Solvay Conference in Physics*, 2001.

[25] H. Spohn. *Europhys. Lett.*, 50(3):287, 2000.

[26] F. Rohrilich. *Physics Letter A*, 283:276, 2001.

[27] C. Compgano, G. M. Palma, R. Passante, and F. Persico. Atoms dressed and partially dressed by the zero-point fluctuations of the electromagnetic field. *J. Phys. B*, 28:1105, 1995.

[28] D. A. McQuarrie. *Quantum Chemistry*. University Science Books, California, 1983.

[29] C. Compgano, R. Passante, and F. Persico. *Atom-Field interactions and Dressed Atoms*. Cambridge University Press, 1995.

[30] I. S. Gradshteyn and I. M. Ryzhik. *Table of Integrals, Series and Products*. Academic Press, fifth edition, 1994.

[31] A H. Nayfeh. *Introduction to perturbation techniques*. John Wiley and Sons, 1993.

[32] T. Petrosky and I. Prigogine. Poincare resonances and the extension of classical dynamics. *Chaos, Soliton and Fractals*, 7(4):441, 1996.

[33] T. Petrosky and I. Prigogine. The liouville space extension of quantum mechanics. In *Adv. Chem. Phys.*, volume 99, page 1. 1997.

[34] C. C. Tannoudji. *Atom-Photon interactions*. John Wiley & Sons, 1998.

[35] T. Petrosky and V. Barsegov. Quantum decoherence and time symmetry breaking. *Phys. Rev. E*, 65:046102, 2002.

[36] E. C. G. Sudarshan. Relativistic particle interactions, 1962.

[37] I. Prigogine. *Non-Equilibrium statistical mechanics*. Wiley, New York, 1962.

[38] T. Petrosky and V. Barsegov. In *Advanced studies in Astrophysics and Cosmology: The chaotic universe*. World Scientific, Singapore, 1999.

[39] P. Facchi and S. Pascazio. Deviations from exponential law and van hove's $\lambda^2 t$ limit. *Physica A*, 271:133, 1999.

[40] H. A. Bethe. The electromagnetic shift of energy levels. *Phys. Rev.*, 72:339–341, 1947.

Vita

Chu Ong Ting was born in Sibu, Malaysia on 23rd December 1975, the son of Diu Kiong Ting and Ing Kiew Tang. He received the Bachelor of Science degree in Physics from the National Cheng Kung University at Taiwan in 1997. He then started graduate studies at Unversity of Texas at Austin in August, 1997. Since then he has been employed as a teaching assistant at the Physics department, University of Texas at Austin. In June 2001 he married Yue Ma as his wife. In September 2002, his son, Daniel Ze-Chuan Ting was born in North Austin Medical Hospital in Texas.

Permanent address: 12 Brooke Drive 4, 96000 Sibu
Sarawak, Malaysia

This dissertation was typeset with LaTeX[†] by the author.

[†]LaTeX is a document preparation system developed by Leslie Lamport as a special version of Donald Knuth's TeX Program.